ASEMS:
AUTONOMOUS-SPECIFIC ENERGY MANAGEMENT STRATEGY

ASEMS: AUTONOMOUS-SPECIFIC ENERGY MANAGEMENT STRATEGY

BY

SAEED AMIRFARHANGI BONAB, B.A.SC.

A Thesis Submitted to the Department of Mechanical Engineering and the School of Graduate Studies in Partial Fullfilment of the Requirements for the Degree of Master of Applied Science

McMaster University MASTER OF APPLIED SCIENCE (2019) (Mechanical Engineering)
Hamilton, Ontario, Canada
TITLE: ASEMS: Autonomous-specific Energy Management Strategy
AUTHOR: Saeed Amirfarhangi Bonab, B.A.Sc. (McMaster University)
SUPERVISOR: Professor Ali Emadi
NUMBER OF PAGES: ix, 160

Lay Abstract

The automotive industry is on the verge of groundbreaking transformations as a result of electrification and autonomous driving. Electrified autonomous car of the future is sustainable, energy-efficient, more convenient, and safer. In addition to the advantages of electrification and autonomous driving individually, the intersection and interaction of these mainstreams provide new opportunities for further improvements on the vehicles. Autonomous cars generate an unprecedented amount of real-time data due to excessive use of perception sensors and processing units. This thesis considers the case of an autonomous hybrid electric vehicle and presents the novel idea of autonomous-specific energy management strategy. Specifically, this thesis is a proof-of-concept, a trial to exploit the motion planning data for a self-driving car to improve the fuel economy of the hybrid electric power unit by adopting a more efficient energy management strategy. With the ever-increasing number of autonomous hybrid electric vehicles, particularly in the self-driving fleets, the presented method shows an extremely promising potential to reduce the fuel consumption of these vehicles.

Abstract

This thesis addresses the problem of energy management of a hybrid electric power unit for an autonomous vehicle. We introduce, evaluate, and discuss the idea of autonomous-specific energy management strategy. This method is an optimization-based strategy which improves the powertrain fuel economy by exploiting motion planning data. First, to build a firm base for further evaluations, we will develop a high-fidelity system-level model for our case study using MATLAB/Simulink. This model mostly concerns about energy-related aspects of the powertrain and the vehicle. We will derive and implement the equations for each of the model subsystems. We derive model parameters using available data in the literature or online. Evaluation of the developed model shows acceptable conformity with the actual dynamometer data. We will use this model to replace the built-in rule-based logic with the proposed strategy and assess the performance.

Second, since we are considering an optimization-based approach, we will develop a novel convex representation of the vehicle and powertrain model. This translates to reformulating the model equations using convex functions. Consequently, we will express the fuel-efficient energy management problem as the convex optimization problem. We will solve the optimization problem using dedicated numerical solvers. Extracting the control inputs using this approach and applying them on the high-fidelity model provides similar results to dynamic programming in terms of fuel consumption but in substantially less amount of time. This will act as a pivot for the subsequent real-time analysis.

Third, we will perform a proof-of-concept for the autonomous-specific energy management strategy. We implement an optimization-based path and trajectory planning for a vehicle in the simplified driving scenario of a racing track. Accordingly, we use motion planning data to obtain the energy management strategy by solving an optimization problem. We will let the vehicle to travel around the circuit with the ability to perceive and plan up to an observable horizon using the receding horizon approach. Developed approach for energy management strategy shows a substantial reduction in the fuel consumption of the high-fidelity model, compared to the rule-based controller.

Acknowledgements

This research was undertaken, in part, thanks to funding from the Canada Excellence Research Chairs Program.

I want to sincerely thank my supervisor and mentor, Professor Ali Emadi, for trusting, motivating, and empowering me throughout my graduate studies. Thanks to all researchers at McMaster Automotive Resource Centre for contributing to building an outstanding work environment.

I would like to offer my special thanks to Fiat Chrysler Automobiles team, specifically those involved in the leadership in automotive powertrain (LEAP) project.

I would like to acknowledge all the people that I have collaborated with, specifically my colleagues in room 218. Thanks to Giuseppe for making the room culture more friendly. Thanks to Iman for exploiting the multilingual potential of the room to the maximum. Thanks to Lucas for the lunchtime discussions. Thanks to Carin for being a car enthusiast. Thanks to Atriya for the homemade snacks. Thanks to Diego for possessing a good sense of humor. Thanks to Peter for teaching me the work-life balance. Thanks to Jeremy for the dynamic programming. And thanks to Sumedh for his research.

The last but definitely not the least, I cannot find the words to express my deep appreciation to my beloved family and my wife, Nayereh, for believing and supporting me throughout my life. This would not have been possible without you.

Notation and Abbreviations

A-HEV Autonomous Hybrid Electric Vehicle

ABS Anti-Lock Brake

ACC Adaptive Cruise Controller

ADAS Advanced Driver-Assistant Systems

AI Artificial Intelligence

ASEMS Autonomous-Specific Energy Management Strategy

AV Autonomous Vehicle

AWD All Wheel Drive

BEV Battery Electric Vehicle

CAFE Corporate Average Fuel Economy

CNN Convolutional Neural Network

DP Dynamic Programming

ECMS Equivalent Consumption Minimization Strategy

EMS Energy Management Strategy

EPA Environmental Protection Agency

ESS Energy Storage System

F1 Formula 1

FC Fuel Consumption

FCA Fiat Chrysler Automobiles

FIA Federation Internationale de l'Automobile

GHG Greenhouse Gas

GPS Global Positioning System

HEV Hybrid Electric Vehicle

ICE Internal Combustion Engine

ITS Intelligent Transportation System

KKT Karush-Kuhn-Tucker

LDV Light-duty Vehicle

LMI Linear Matrix Inequality

LP Linear Programming

M/G Motor/Generator

MPC Model Predictive Control

NEDC New European Driving Cycle

OCV Open Circuit Voltage

OEM Original Equipment Manufacturer

PGS Planetary Gear Set

PHEV Plug-in Hybrid Electric Vehicle

PMP Pontryagin Minimum Principle

QP Quadratic Programming

SDP Semidefinite Programming

SOC State of Charge

SOH State of Health

UDDS Urban Dynamometer Driving Schedule

VMT Vehicle Miles Traveled

VTTS Value of Travel Time Saving

ZEV Zero Emission Vehicle

Contents

Chapter 1

Introduction

The automotive industry is a quintessential combination of art, technology, and business. Originated in the late 1800s, this industry has seen the fascinating achievements, rivalries, and products. The scale of the modern automotive industry is colossal with significant economic and social impacts. Thanks to the intensive investments and research on automotive technologies worldwide in the last century, current vehicles are complicated technical systems with multiple function-specific subsystems. A modern car is a meticulously designed and assembled combination of thousands of components, equipped with highly advanced technologies. Current automotive technologies are results of the evolution of previously existing technologies. The improvements are also due to new emerging achievements in electronics, materials science, and computer science. The passion of engineers, the desire of designers, the demand of customers, and legislation have consistently expanded the borders of the automotive industry to produce more efficient, practical, safer, and attractive cars.

Among the most important advances in vehicular technologies, we primarily focus on the powertrain electrification and autonomous driving in this work. Most other automotive technologies usually end up integrating with the existing vehicle to improve an aspect or aspects of the transportation such as fuel economy, emissions, performance, and safety. For instance, anti-lock brake systems (ABS) replaced the conventional brakes since they showed the potential to improve the safety of the vehicles while barking by employing threshold braking and cadence braking. Similarly, widespread adoption of fuel injection systems instead of conventional carburetors has resulted in more powerful and efficient engines with a reduction in undesirable emissions.

Turbocharging has also helped to increase the performance and drivability or to downsize the engine while getting the same output power. Although these technologies are the crucial elements of modern cars, the overall impact is not comparable to the potentials of electrification and autonomous mobility at all.

1.1 Motivation

The internal combustion engine has been an inseparable component of the cars of the 20th century. As a result of extensive long-term research and development, modern engines are highly complex and advanced. However, they all share fundamental drawbacks. ICEs are essentially heat engines, restricted to the maximum of Carnot efficiency. Considering reasonable temperatures for the hot and cold source, Carnot efficiency of an ICE might be around 75%. Practically, efficiency tends to be much lower due to reasons such as friction and imperfect combustion. Peak efficiency for the majority of the modern operating engines is around 30-35%. Besides unacceptable efficiency, emissions is another major environmental concern. The large-scale negative impact of greenhouse gas (GHG) emissions is well-known. According to the environmental protection agency (EPA), almost 29% of the U.S. GHG emissions of the economic sector is from transportation in 2017 [1]. Following table shows a comparison between conventional and electric vehicles, for a Toyota Prius sized family car [2].

While current transportation depends heavily on fuel-powered vehicles, there is an intensive global competition toward prototyping and developing the next generation of vehicles. This generation of vehicles should be sustainable. The most promising solution is the electrified transportation - transportation 2.0 [3]. Apart from sporadic trials to prototype electric vehicles in the 20th century, the project such as GM EV1 for instance, it is the modern advances in battery technology, electric machines, and the power electronics that have made widespread adoption of the electric vehicles feasible.

In the battery section, there is a promising trend toward the next generation of battery packs, which are lighter and more power and energy-dense. Advantages of lithium-metal-polymer and lithium-ion batteries over the conventional lead-acid counterparts made the concept of EV feasible in this century. Lithium-silicon, solid state, and lithium-air batteries promise an even brighter future for dominance of battery electric vehicles.

Table 1.1: Conventional vs. EV

	Conventional vehicle	Electric vehicle
Power supply components	Fuel tank + ICE	Battery + Inverter + AC machine
Tank-to-wheel efficiency	$\approx 20\%$ 1.2 kWh/mile or 28 MGP	$\approx 85\%$ 0.17 kWh/mile or 200 MGP
Energy storage	12.3 kWh/kg Gasoline energy content	0.1 kWh/kg $LiFePO_4$ Battery
Refueling	11 MW or 140 miles/minute	6 kW ac charger: <32 miles/hour 100 kW dc charger: <9 miles/minute
Cost	12 ¢/mile at \$ 3.50/gallon	2 ¢/mile at \$ 0.12/kWh
CO_2 emissions	300-350 g/mile	0 g/mile at tailpipe $\approx$ 120 g/mile well-to-wheel at current U.S. electricity mix
Regenerative braking	No	Yes

EVs rely on the electric machines as the propulsion means. Two main types of electric motors in EVs, AC induction motors and permanent magnet synchronous motors, are getting more efficient and power-dense as a result of intensive research on these motors. Besides, researchers and engineers aim to develop more desirable electric motors for traction purposes such as switched reluctance motors, which have shown outstanding propulsion and manufacturing characteristics [4–6].

Power electronics provide the opportunity to seamlessly convert the different forms of electric power into each other with the ability to modify the output voltage and current. Power electronic converters consist of AC-AC converter, DC-AC inverter, AC-DC rectifier, and DC-DC choppers [3].

Electrification in the lower level for the powertrain results in a hybrid electric vehicle (HEV), a vehicle which takes advantage of both fuel energy in an internal combustion engine (ICE) and electric energy from batteries to electric machines. As the share of the electric power increases in the propulsion and vehicle offers all-electric drive with ICE off, we achieve to plug-in hybrid electric vehicles (PHEV). The ultimate form of powertrain electrification is in the battery electric vehicles (BEV) with only electric power to propel the vehicle.

Besides discussed ongoing concerns regarding conventional vehicles, governmental legislation also play into the hands of electrification. In Canada, for instance, effective 2018, regulations push automakers toward selling more zero-emission vehicles (ZEV) [7]. Moreover, in British Columbia, all new vehicles should be emission-free by 2040 [8]. This would significantly ramp up the current trend in new electric car sales, shown in Figure 1.1. Although BEVs are promising solutions to address the environmental

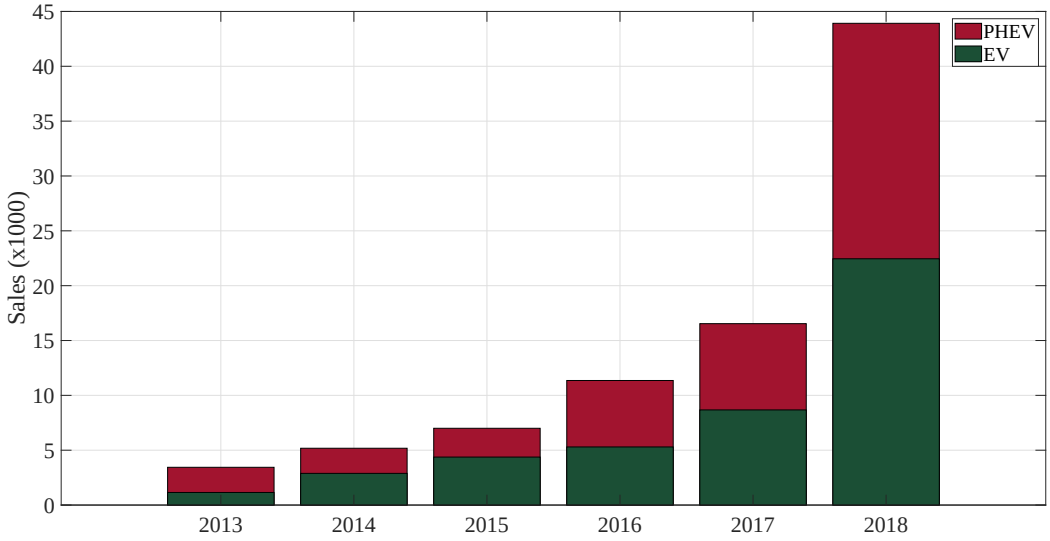

Figure 1.1: Number of new EV/PHEV car sales in Canada for 2013-2018. (adapted from [9])

problems and energy concerns regarding conventional transportation, widespread employment of battery electric vehicles have a few challenges to tackle. Besides immature infrastructure in the electricity grid and charging stations, safety issues, extended charging time, high manufacturing cost, the rare material intensity of the manufacturing, and undesirable driving range constitute other challenges for BEVs [10]. These problems would be tackled as technologies in battery manufacturing and power electronics are expanding, and up to that point, PHEVs, HEVs, and mild hybrids

would be the alternatives.

The other mainstream in automotive with a substantial impact not only on the automotive industry, but on any other related field (e.g., delivery, public transit, logistics, robotics), is autonomous driving. This time, autonomous vehicles (AV) are not just science projects, and they are only steps away from commercialization. Major automotive companies are investing an incredible amount of effort and money on autonomous vehicle programs and real-life testing. In the large-scale, the market for autonomous driving is anticipated to grow up to $173.15 B by 2030 [11]. Figure 1.2 shows the anticipated contribution of different levels of autonomy (discussed later) in North America. Concludingly, autonomous mobility and electrification are essential

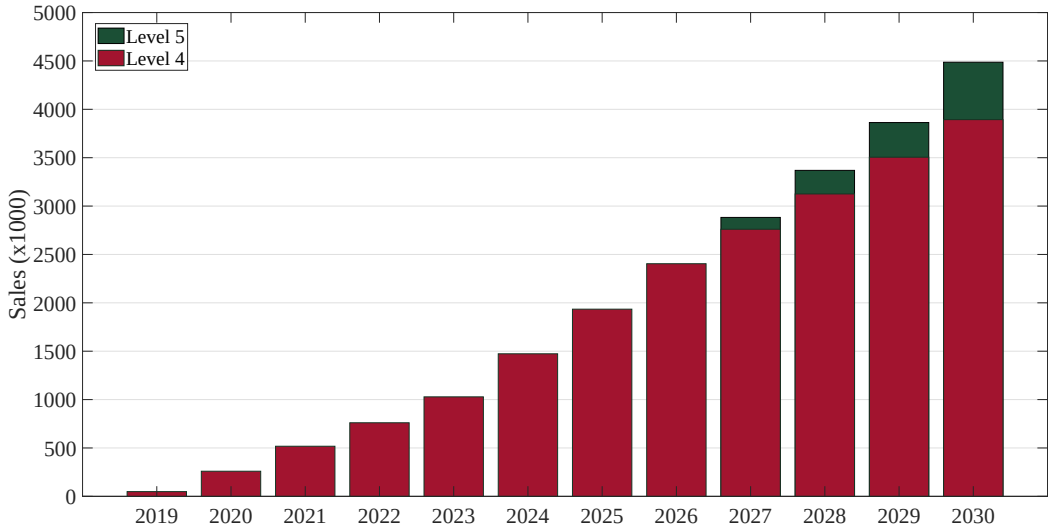

Figure 1.2: Number of new car sales with autonomous driving features in North America for 2019-2030. (adapted from [11])

elements of next-generation transportation. Car of the future is hybrid/electric (HEV, PHEV, and BEV) and autonomous. In the car of the future, technologies in both fields of autonomous driving and electrification should interact effectively, to bolster up the overall advantages while minimizing the drawbacks. For instance, autonomous driving provides an unprecedentedly overwhelming amount of data about driving scene, objects, and vehicle motion, as a result of perception and processing units. This data can be efficiently employed to design and control the electrified power unit. While the effect of the available data on control of different systems within the powertrain is highly extensive, we consider a niche but critical application in this work. In a hybrid electric vehicle, the powertrain control unit is managing the power flow among different

components to satisfy the power demand within the powertrain constraints. Different strategies to manage power flow result in a particular fuel economy, performance, and emissions. These strategies are known as energy management strategies (EMS) and are a crucial element of any hybrid system. In this work, we present autonomous-specific energy management strategies (ASEMS). ASEMS is a strategy, specifically designed to integrate with autonomous mobility modules, to provide improved efficiency, performance, and emissions. In this work, we have only focused on the performance and fuel economy side. We also provide a proof-of-concept of an optimization-based ASEMS, based on model predictive control (MPC) approach in this work.

We believe ASEMS has an immense potential to make the autonomous hybrid electric (A-HEV) car of the future more efficient. Just considering the announced partnerships, Waymo is going to add 62,000 more Chrysler Pacificas to the current 600 sized fleet [12]. Pacifica has almost the similar HEV architecture that we examine in this work. Additionally, Uber has a plan to add 24,000 Volvo XC90 to its self-driving fleet [13]. This vehicle has a T8 twin-engine plug-in hybrid powertrain [14]. Also, Argo AI has a partnership with Ford and currently has a fleet of self-driving Ford Fusion sedans. Toyota is also working on the autonomous prototype of Lexus GS 450h, which also has a similar architecture, used in this work. The mentioned cases are just examples of HEVs in self-driving fleets, and we expect this amount to increase significantly in the upcoming years. We also note that beside ever-increasing growth in total number, A-HEVs in self-driving fleets operate significantly more than a conventional family car. Conservatively, for even very short prediction horizons (100 m and 200 m), as presented later, our work shows the potential of improving the fuel economy by about 3.2%. Roughly, this conservative assumption results in gasoline saving of about 30,000,000 liters per year, in the upcoming Waymo and Uber fleets combined. This amount of saving would be much more notable if longer horizon is available and the introduced approach (ASMES) has been investigated comprehensively.

1.2 Thesis Outline and Contributions

In this section, we will outline the thesis by introducing the chapters. In each part, we will also explain our contributions.

1.2.1 Chapter 2: Hybrid Electric Powertrains

We discuss the state-of-the-art in hybrid electric powertrains in the second chapter. We start by explaining the electrification level and illustrating the common hybrid power unit architectures. We will also designate the architecture we are considering in this work and how it can be applied for other cases with a few modifications. Next, we discuss the main advantages of electrified powertrains in great details in terms of fuel economy, performance, and emissions. Finally, we discuss the feasible future trends for the electrification. This chapter contributes to providing a brief tour of the electrification, which is crucial for the next chapters.

1.2.2 Chapter 3: Autonomous Driving

Although the extent of autonomous driving technologies and applications is vast, again, our purpose is to present a short but valuable introduction over the technology. Since our work is at the intersection of electrification and autonomous driving, this chapter is necessary to realize how these two mainstreams in automotive interact. Next, we discuss the global impact of achieving autonomous transportation. Later, we categorize the vehicles based on the level of autonomy and explain which levels do we target in this work. Finally, we shortly discuss different modules within the autonomous driving.

1.2.3 Chapter 4: Fundamentals of Energy Management Strategies

We elaborate on the fundamentals of various energy management strategies in this chapter. This includes rule-based, fuzzy logic-based, equivalent consumption minimization strategy, dynamic programming, Pontryagin's minimum principle, convex optimization, and model predictive control. This chapter contributes to show the canonical mathematical format for each of these methods rather than discussing implemented results in the literature. This is the last chapter of the literature review.

1.2.4 Chapter 5: High-fidelity Model

Since any designed or newly developed control strategy should be evaluated first on a high-fidelity model and ultimately on the actual system, developing the high-fidelity

model is crucial in our work. In this chapter, we choose the Toyota Prius 2010 as our case study. We also use MATLAB/Simulink programming and modeling language to develop a system-level high-fidelity model of the vehicle with the powertrain inside. The model consisted of a driver, control unit, and vehicle subsystems. We explain the components within each of these subsystems in great details. We obtain the required data for the model using the available online sources and also taking the reverse-engineering approach to identify the model parameters, given the vehicle dynamometer data. The contribution in this chapter, as shown in the evaluation section, is achieving an accurate model in capturing the actual vehicle energy-related details without getting obsessed in irrelevant model dynamics.

1.2.5 Chapter 6: Fast Offline Energy Management Strategy

In the context of EMS, offline translates to having access to the velocity profile in the form of established driving cycles in advance. The offline analysis is highly critical for design and dimensioning purposes. In this chapter, we present a first of its kind convex representation of a power-split powertrain. This includes deriving a convex model for the component (some are novel) and expressing the overall fuel-efficient control strategy problem in the canonical convex optimization format. We show that the developed convex model differs acceptably with the high-fidelity model. Advantage of facing a convex optimization problem is having access to dedicated efficient numerical solvers. Finally, we discuss the results and compare the presented method with other established methods such as dynamic programming. We also accentuate the potentials of the developed method in real-time applications.

1.2.6 Chapter 7: Real-time Energy Management Strategy for an Autonomous Vehicle

In this chapter, we present the novel idea of autonomous-specific energy management strategy (ASEMS). ASEMS should integrate with the autonomous driving modules to use the motion planning data. To perform the proof-of-concept, first, we carefully simplify the driving scenario. Then, we employ an established optimization-based approach to apply the path planning and trajectory planning for the vehicle, considering the comfort and travel time as objectives. Later, we integrate the developed convex representation of the powertrain into the model, the integrated model. Finally, we

present the results and analyze the sensitivity on a few hyper-parameters. The fascinating result is that fuel consumption shows a potential decrease of between 3.2 - 13.5 % reduction, depending on the prediction horizon, or as we call, the observable horizon.

1.3 Publications

In the time of articulating this work, we have prepared the following publications. Some of the chapters are based on the following publications. These publications are either submitted or planned to submit to journals and conferences or accepted and officially published.

1. Saeed Amirfarhangi Bonab, Ali Emadi. "Fuel-optimal Control Strategy for a Power-split Powertrain via Convex Optimization", Submitted to *IEEE Access*.

2. Saeed Amirfarhangi Bonab, Ali Emadi. "Optimization-based Path Planning for an Autonomous Vehicle in a Racing Track", Submitted to *IEEE 45th Annual Conference of the Industrial Electronics Society*, To appear.

We have also planned to present the ASEMS with obtained results in the form of another journal paper.

Chapter 2

Hybrid Electric Powertrains

2.1 Introduction

Developing alternative powertrains with the ablility to incorporate more than a single fuel-based power source has a long tradition, comparable to the history of automotive industry itself. Lohner-Porsche Elektromobil, introduced in 1900, initially was an electric vehicle. Later on, Porsche included an internal combustion engine in the powertrain to run a generator to keep the batteries charged. Batteries then would supply power for two or four wheel hub electric motors. Also, it is intersting to note that by 1900, American companies had produced more EVs than gasoline cars [10]. However, the idea of electric or hybrid electric vehicle faded into the history, and just resurfaced few times with now practical impact in the following century. [15].

Interest in vehicles with alternative propulsion systems has been revived in the past decades as a development plan with large-scale global impact and there has been substantial growth in applied investments in research and development of technologies regarding these vehicles. Batteries, supercapacitors, and fuel cells combined with electric motors are examples of alternative power sources.

In this chapter, our main focus is on the vehicles with hybrid electric powertrains. Although by definition, a hybrid can be assumed as any sort of combining different power sources in the powertrain, we exclusively consider a hybrid electric powertrain to consist of an internal combustion engine (ICE), battery pack, and electric motors as the means power generation and propulsion. Hybrid electric powertrains are in different level of electrification with variety of architectures. Moreover, these powertrains provide

a reasonable trade-off between fuel economy, emissions, performance, and the driving range which makes them a suitable choice as a propulsion system, at least up to the point that battery and fuel cell technologies get mature enough to provide comparable performance. We will discuss these later in this chapter in more details.

2.2 Electrification Level and Architecture

As discussed, in a hybrid electric propulsion system, ICE operates accordingly with electrical units to provide the required propulsive power. Considering this, we can categorize the available powertrain technologies based on the electrification level, which is the share of each propulsion component in producing the total energy consumption for typical driving scenarios [16]. As shown in Figure 2.1, degree of electrification for hybrid electric vehicles (HEVs) falls in the spectrum with conventional vehicles and fully electric vehicles on both ends and directly contributes to the emissions reduction. Powertrain electrification is closely connected with powertrain architecture.

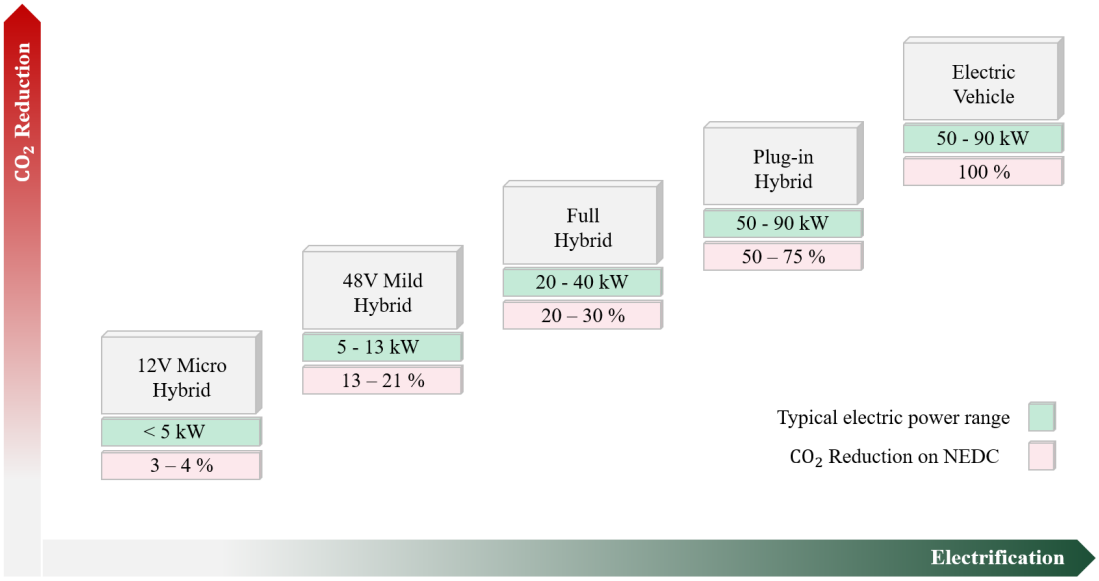

Figure 2.1: Degree of electrification for various electrified powertrains with resulted reduction in emissions on new european driving cycle (NEDC). (adapted from [17])

Architecture can be simply seen as the arrangement of propulsion systems in the powertrain, which imposes how components will interact to supply the demanded power. Figure 2.2 shows the arrangement of components in few common HEV architectures.

While various architectures deliver different operation conditions, we will focus mainly on the power-split architecture in this work. Power-splits are the most advanced hybrid powertrains which benefit from the redundant degree of freedom in planetary gear sets (PGS). This particular architecture offers complex operation conditions, wide electrification degree, and better fuel economy/performance. Examples of this kind has been successfully employed in vehicles such as Fiat-Chrysler Pacifica, Toyota Prius, and Chevrolet Volt.

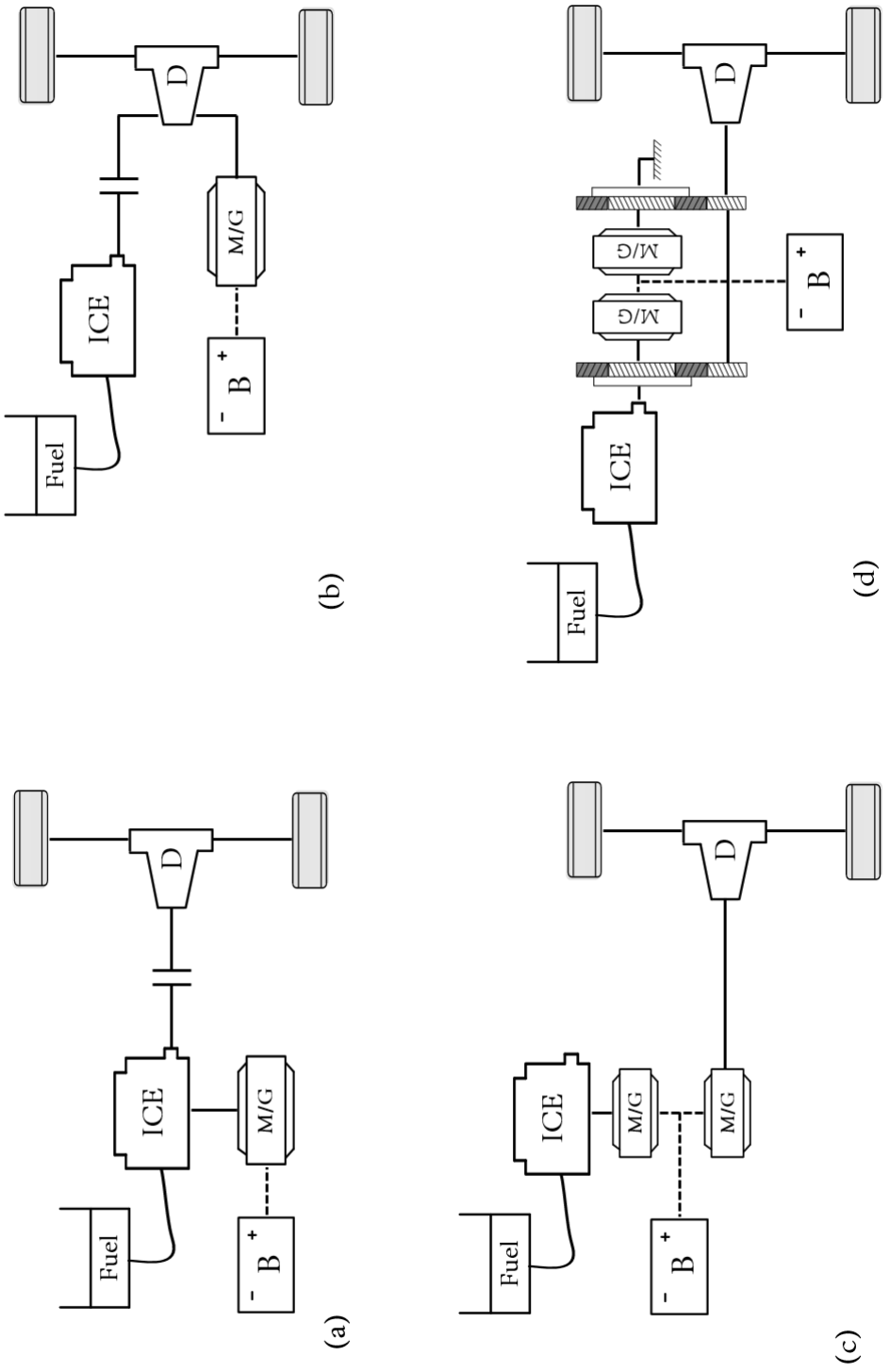

Figure 2.2: Common HEV architectures: (a) mild hybrid, (b) parallel hybrid, (c) series hybrid, and (d) power-split hybrid. Note that M/G, B, and D denote motor/generator, battery, and drivetrain respectively. Mechanical joints are shown with solid line, while dashed lines stand for electric connections.

2.3 Fuel Economy

The competition and the endeavor to achieve better fuel economy is highly intense in the automotive field. Less fuel consumption benefits customers financially and the world environmentally. In the course of their progress, vehicles are getting lighter, more aerodynamic, and they are using more efficient components to achieve better fuel economy while staying competitive on the performance side. The average fuel economy for all U.S. cars has improved 12 percent from 2010 to 2017 [18]. However, the fuel economy rate, imposed by governmental standards seems inapproachable with current rate of improvement in fuel economy. Corporate average fuel economy (CAFE) for instance, requires passenger vehicles to achieve fuel economy of 54.5 MPG by 2025 [19]. Figure 2.3 shows the previous trend and legislated trend for fuel economy of the vehicles by CAFE for different types of vehicles in more detail. The trend toward more fuel efficient vehicles is clear in each category.

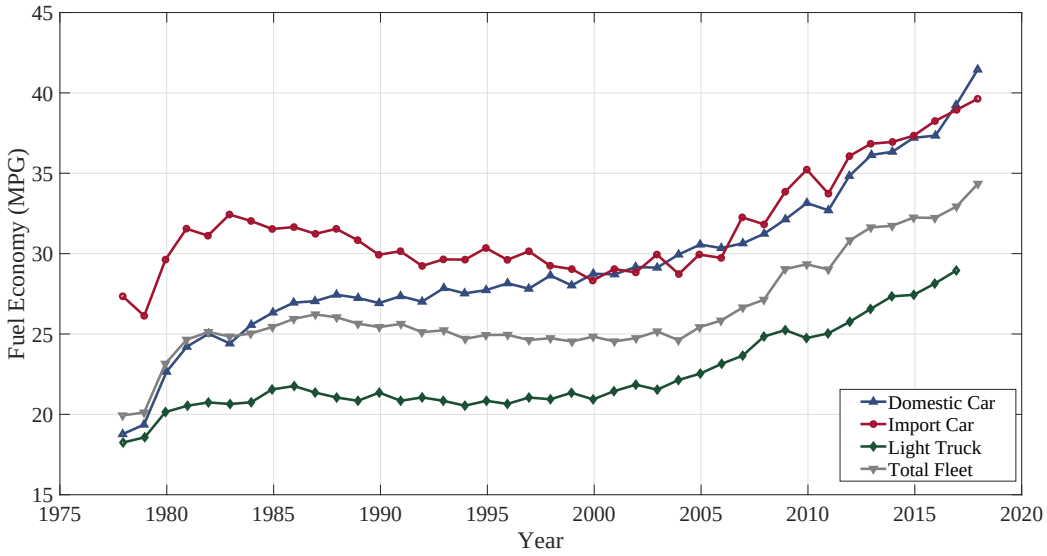

Figure 2.3: Required fuel economy standards for each model year by corporate average fuel economy (CAFE) standard. (adapted from [19])

Electrification of the powertrain is one of the most appealing solutions for automotive companies. According to Fiat-Chrysler Automobiles chief technical officer, "You won't get the 2025 standards without significantly higher penetration of electrification than we have today" [18]. Some of the benefits of an electrified powertrain, which especially significant for urban driving cases, is to help reduce the fuel consumption

by operating ICE in higher efficiency zone, avoiding total energy waste during braking by performing regenerative braking, and avoiding idling for ICE. The current trend suggests that electrification plans should be boosted up by automakers to meet the prospective standards.

2.4 Emissions

Fossil fuels are the major source of carbon dioxide production [20]. In addition to greenhouse gas emissions (GHG), other exhaust emissions such as CO and NO_x are among substantial environmental threats. Table 2.1 shows the incurred cost as a result of the vehicle emissions on the society, estimated by NHTSA in Final Regulatory Impact Analysis report [21]. Despite the effort of automotive companies to lower the

Table 2.1: Emissions Cost Estimate in 2010

Emissions Cost	Weighted Costs
Carbon dioxide (CO_2)	\$22/metric ton
Nitrogen oxides (NOx)	\$6,700/ton
Sulfur dioxide (SO_2)	\$39,600/ton
Volatile organic compounds (VOC)	\$1,700/ton
Particulate matter (PM)	\$306,500/ton
Economic benefits oil import reduction	\$0.197/gallon in 2025

emissions by deploying catalyst converters, advance A/F ratio control, choke operation, spark timing, and exhaust gas recirculation (EGR) [22], emission standards seem to be highly demanding to be met with the current progress. Beside market-based approaches such as emission penalties for motor vehicles and gasoline tax, produced vehicles are also restricted by strict emission standards. Euro VI emission standards, for instance, restricts light-duty vehicles (LDV) to producing 1 g/km of CO and 0.06 g/km for NO_x emissions for gasoline vehicles over NEDC driving cycle [23]. Also, as Figure 2.4 suggests, produced passenger vehicles should meet even more stringent CO_2 emissions performance in various countries in the near future. Electrification

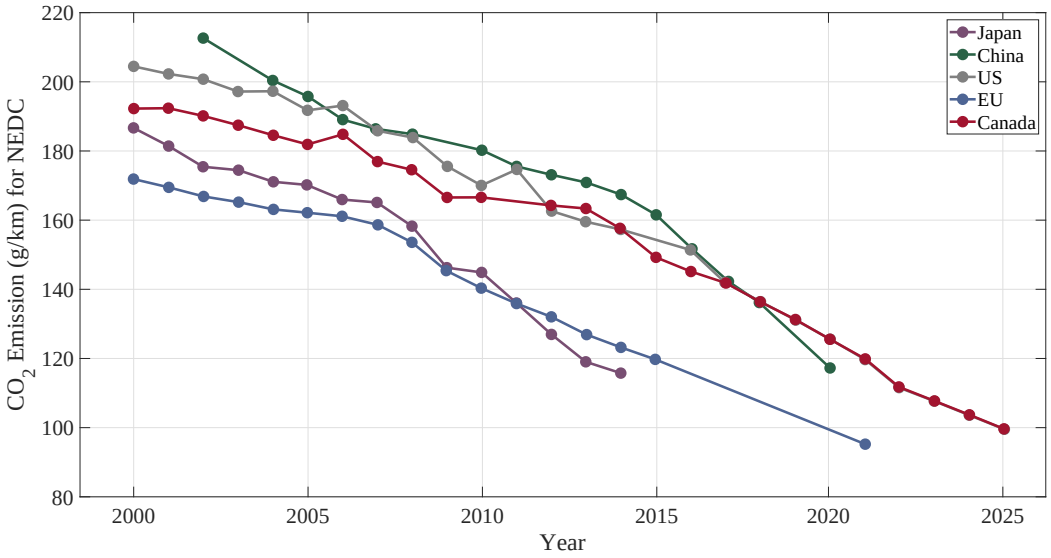

Figure 2.4: Future, current, and historical CO_2 emission performance for passenger car fleets. (adapted from [24])

of the powertrain, in any level, have shown a great potential for reducing vehicle exhaust emissions by first, improving the efficiency and decreasing fuel consumption, and second, avoiding the operational condition for ICE which is prone to producing undesirable emissions. In [25] for instance, Euro VI hybrid buses have shown 93% less NO_x emissions compared to Euro V ones. More noticeably, HEVs are better than PHEVs recharged by mixed electricity generation in case of GHG emissions [26]. Regardless, by moving toward sustainable electricity generation and nonfossil generation mix, power-split PHEVs have the potential to reduce the GHG emissions by 60% compared to gasoline ICE-powered vehicles [26]. Ultimately, BEVs are the most sustainable means of transportation in terms of emissions, if conditioned to be recharged by renewable electricity generation.

2.5 Performance

While discussed benefits of electrified powertrains guarantee better fuel economy and the fewer emissions, it is often the performance, or by other words the "coolness factor" [27], that makes vehicles attractive and marketable. In this context, there is a significant opportunity to utilize the available electric power in the HEV in harmony with ICE power to achieve unprecedented vehicle drivability in case of acceleration,

handling, stability, and braking. We will examine the methods of achieving better performance as a result of electrification in more detail in this section.

Turbocharging is helpful with increasing the engine efficiency and power to weight ratio. In fact, this is one of the current mainstreams in engine design that modern engines tend to be downsized and turbocharged. In the U.S. market, for example, 27.6 % of the cars and light trucks were produced with a turbocharged engine in 2017 [28]. Most significant disadvantage for a turbocharged engine from the performance point of view is the time gap for the turbocharger to spool up to provide a useful boost, known as turbo lag. Dynamic characteristics of these engines can be substantially improved by using an electric motor attached to the turboshaft [29]. Electrically-assisted turbochargers are more effective than conventional turbochargers in reducing the engine response time and providing instant power.

Electric motors can also compensate for the lack of available torque from engine at low speed. As it is well-known, electric motors can provide the maximum rated torque at low motor speed, which is highly desirable for traction and propulsion purposes. While ICEs can produce the peak torque around at least 1/3 of the maximum engine speed. As a result, a hybrid powertrain can provide better acceleration by providing electric boost. Figure 2.5 compares the performance of the ICE with an electric motor in terms of torque and power. In addition to better traction performance, the

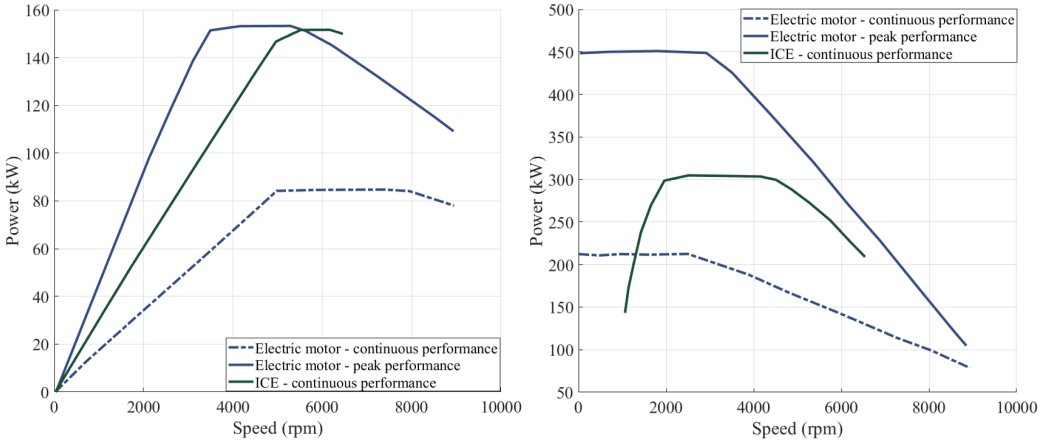

Figure 2.5: Different torque and power charactristics of an ICE and an electric motor. (adapted from [30])

possibility of regenerative braking imposes less pressure on the brakes and recovers free energy in braking zones which can be used as an electric boost later.

Finally, having an independent electric motor for each wheel provides all wheel drive (AWD) drivability and toque vectoring during cornering which would result in overall better stability and performance .

The recent trend in the motorsport supports the application of the electrified powertrains in the high-performance racing vehicles. Policies of Federation Internationale de l'Automobile (FIA) have pushed racing teams to be in the front line of developing faster, fuel-efficient, and sustainable. Taking Formula 1 (F1) competition as the case, regulations have progressively pushed powertrains toward utilization of smaller, efficient, and turbocharged engines since 2000. Electrification considered as the best option to keep the vehicles competitive compared to former F1 cars with giant naturally aspirated engines. This made a breakthrough in the history of F1 competition in 2014 by incorporating two motor generators in the powertrain, the period after which is known as the hybrid era. This enabled Mercedes AMG Petronas F1 engineering team to achieve a thermal efficiency of more than 50% for the powertrain for the first time [31]. The recent updates in the powertrain of F1 cars is captured in the following table.

Table 2.2: Formula One Powertrains

Specification	1995-2005	2006-2008	2009-2014	2014-Present
Engine Type	Naturally aspirated	Naturally aspirated	Naturally aspirated	Turbocharged
Engine Cylinders	V10 or V12	V8	V8	V6
Engine Power	650-965 hp	$<$ 740 hp	700-800 hp	700-800 hp
Engine Capacity	3000 cc	2400 cc	2400 cc	1600 cc
Electric System	n/a	n/a	KERS	MGU-K and MGU-H
Electric Power	n/a	n/a	81 hp	160 hp

2.6 Future Trend

Increasing fossil fuel cost, clean electricity generation, demand to achieve higher efficiency and performance, and environmental issues are the propellants of powertrain electrification stream. Electrification is the solution for most of the upcoming challenges in the automotive industry. Although research and development on internal combustion engines show potentials of improving efficiency and decreasing the emissions, they are naturally unable to meet the future standards. Therefore, powertrain electrification should be considered more seriously. Although technical issues have been investigated for the key hybrid electric powertrain components, the major challenge is the cost, regulations, and the infrastructure for electrified vehicles to dominate the market. However, one can safely state that "future drives electric" [30].

On the other hand, ICE has been considered as the primary power source in the HEVs with electric systems to compensate for the deficits of the internal combustion engine. However, as electrification becomes the dominant philosophy, we predict intensive research on re-designing engines in the near future to achieve a new generation of ICEs with characteristics suitable for compensating the deficits of electric drivetrain. New technologies for internal combustion engines can substantially prolong the existence of these propulsion systems in the market.

While fully electric vehicles are considered as the future of transportation, this will not happen abruptly. Definitely, there is a transition period, moving from ICE-powered vehicles to BEVs. The overall transition time depends on the customer feedback, original equipment manufacturers (OEMs) initiatives, and governmental regulations, but it would cover a few decades at least.

Although battery technology is growing fast toward the next-generation batteries that offer lower cost and higher better specific energy characteristic, but currently, the cost of a battery pack pushes the overall cost of the vehicle significantly. Also, manufacturing of the current batteries is aggressive on the rare earth materials. Other major challenges for the prevalence of the EVs are battery pack weight, offered range for a fully charged battery pack, availability of the public chargers, recharging time, and the impact on the power grid.

There is also a remarkable challenge regarding the charging time and the range of electric vehicles. While refueling of a 10-gallon fuel tank takes a few minutes, it provides about 360 kWh of energy and adds only 62 pounds to the vehicle mass. This

amount of fuel is enough for 300 miles, considering a vehicle with reasonable fuel economy of 30 MPG [30]. Competing with this luxury of conventional vehicles would be arduous for EVs.

As long as the mentioned challenges have not been addressed efficiently, OEMs should have an alternative for the transition period. A PHEV which offer a reasonable electric range with an ICE used to extend the overall range while avoiding the cost of a bulky battery pack, as well as providing the option of refueling to keep the vehicle operating continuously for a long period of time is a firm bridge from ICE-powered vehicles to full EVs. Besides, in spite of the fact that most of the different forms of full hybrid vehicles have a low benefit to cost rate, HEVs with power-split powertrain have shown outstanding efficiency, driving comfort, and customer feedback. From a different perspective, as discussed, electric systems in today's HEVs are considered and designed to account for flaws of ICE-powered powertrain. However, we believe this process can be reversed by changing the design language of ICEs, promoting the idea of designing ICEs in a way to compensate for the defects of the electrically powered powertrain. As a result, a power-split PHEV can be the best option for post-ICE and pre-EV era.

Chapter 3

Autonomous Driving

3.1 Introduction

It has been more than 80 years from "Futurama," an exhibit where General Motors seriously depicted the idea of autonomous mobility for the future transportation [32]. While the vision seemed to be over-ambitious for the time, but initiated a dream of smart and autonomous transportation. The dream seems to coming true now, thanks to recent advances in computing, sensors, and artificial intelligence.

The automotive industry is moving toward intelligent transportation systems (ITS) to improve the safety and efficiency. For the case of passenger vehicles, it is quite pleasant to imagine that cars are autonomous, sustainable, connected, and they are operating on the real-time supervised roads with intelligent infrastructures. Being autonomous is not restricted only to the case of passenger vehicles. Advances in this field can deeply impact other areas such as unmanned aerial, agricultural, and transport vehicles. Autonomous vehicles play a key role in the prospective scheme for transportation and they can revolutionize the concept of mobility we hold today.

Although the concept of autonomous mobility is fascinating, the implementation is technically complicated. Introduced technology should be able to outperform human performance in driving, while humans are not necessarily poorly under-performed drivers. As mentioned, one of the potentially significant benefits of autonomous vehicles (AVs) is better safety. While casualties in the car accidents are unfortunately a considerable number (more than 40000 reported traffic deaths in 2017 in U.S.[33]) and human errors are to blame for the 94% of the car crashes in U.S.[34], but human

fatal driving mistakes are likely to happen every 86 million miles for each individual in U.S. [35]. From the technological point of view, the difficulty arises from both scene perception aspect as well as the fact that operating artificial intelligence of an AV should function in any arbitrarily complex condition, and should reason and generalize for the unpredictable situations based on the available data. Moreover, this process should happen real-time with the obtained perception of computer vision systems.

Research on autonomous vehicles spans over the last decades. One of the important early examples is the Eureka Prometheus project (1986), which is also the largest R&D project ever held on the self-driving cars [36]. In recent years, competition between major vehicle manufacturers and technology giants to achieve the first commercial fully autonomous vehicle have heated up. As for now, Waymo self-driving cars and the Tesla Autopilot technology seem to lead the competition as a result of massive R&D effort and ever-increasing amount of available data from their autonomous fleets. Despite the current achievements, dated technologies for autonomous mobility have yet to face great challenges such as acceptance from customers, regulations, technology maturity, and the infrastructure. [37]

In the rest of this chapter, we will examine the large-scale impact of the autonomous mobility to appreciate the vast importance of this technology. Also, we will categorize the vehicles based on their degree of autonomy. Finally, we will illustrate how a modern autonomous vehicle operates to get the required helpful intuition for understanding the motivation of the presented work in the next chapters.

3.2 Global Impact

AVs have the potential to significantly influence the transportation aspects, including safety, traffic congestion, mobility, and efficiency. There are both individual and public level sides of these effects. In this section, we will explain some of the large-scale impacts that prevalence of autonomous mobility will bring along. The extent of each aspect of the autonomous vehicles' global impact depends on the prospective policies, customer acceptance, and the infrastructure. Although there are disadvantages for autonomous mobility as for any other technology, advantages generally outweigh the negative aspects by a large margin.

Safety has been served as the pinpoint of autonomous mobility implication. Social acceptance of the AVs highly depends on the safe performance of these vehicles. The

motivation behind this is quite clear. Statistics below, adapted from [38], shows the dramatic negative side of vehicular transportation. Apart from the dramatic effect

Year	Fatalities	Injuries	Fatality Rate
2017	1,841	154,886	0.75 per 10,000 motor vehicles 4.8 per billion vehicle-kilometers

of accident casualties on society, most of the accidents also incur property damage, medical costs, and lost earnings. Autonomous mobility and advanced driving assistant systems (ADAS) has great potential to improve the safety of available transportation by a large margin. Examples of such driving assistant safety systems are adaptive cruise controller, forward collision warning and avoidance, lane departure and lane keeping, lane change assistance, active steering and evasion assist, and proactive pedestrian protection. As it can be seen in Figure 3.1, although the potentials of passive safety systems have been exploited substantially, there is a plausible improvement in the vehicle safety by exploiting active safety technologies. In the context of safety, the

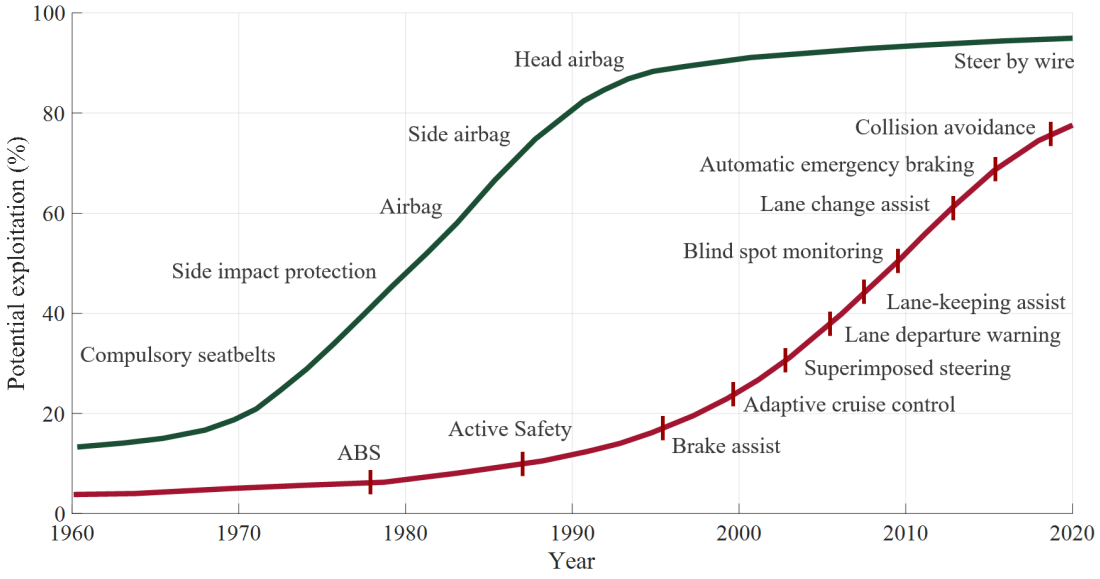

Figure 3.1: Active and passive safety systems exploitation in last decades. (adapted from [39])

current progress of the AVs is very promising. For instance, Waymo's self-driving cars finished five million miles of driving in U.S. up to February 2018 with 30 minor crashes [40]. However, these vehicles had caused just one of these accidents. According to [41],

the U.S. crash rate for an average human driver is 4.2 crashes per million miles, which means human drivers could have caused 20 more accidents if they were operating the Waymo's fleet.

Another beneficial aspect of autonomous driving can be seen from the value of travel time savings (VTTS) perspective. VTTS can be defined as the benefits of faster travel that saves time [42]. In large-scale, many governmental regulations and actions regarding transportation are designed to decrease the cost and the time of the traveling and commuting [43]. In fact, owning and driving an AV can potentially reduce the VTTS by almost 30% compared to driving a non-AV [44]. This can be as a result of providing the opportunity for passengers to perform more valuable activities while having a drive, less traffic congestion as a result of autonomous mobility, and using shared autonomous vehicles.

AVs can also substantially extend the application of automobiles for the vast majority of the population who cannot or are not permitted to drive a vehicle, including people with disability, children, and senior citizens. It is very probable to imagine on-demand services for impaired or injured individuals shortly, equipped with AVs, which are more comfortable and cost-effective than other alternatives. This aspect of autonomous mobility has been brilliantly showcased, as a legally blind man had a successful ride around Austin in 2015 in Waymo's self-driving car [45]. Similar services can be provided as mobility options for children, an AV as the school bus for instance. Moreover, a study shows that elderly people who give up driving, considerably travel less, far beyond to be justified by normal aging [46]. This shows the traumatic aspect of driving cessation and indicates that having access to AVs would potentially improve the well-being of these people.

Adoption of AVs can influence traffic congestion in at least three ways: affecting vehicle miles traveled (VMT) per capita, increasing vehicle throughput for the roads, and eliminating traffic delays, caused by crashes. Willingness to travel by vehicle is directly related to travel cost (fuel, insurance, parking, etc.) and drive comfort. Autonomous driving can encourage AV owners to drive more and thus increase the VMT by reducing travel costs and improving comfort by letting them engage in other activities. A significant jump in VMT can also be as a result of new transportation models such as car-sharing programs, autonomous transit lines, and autonomous taxi services [21]. Car-sharing programs have a two-sided effect on VMT. These programs can decrease the overall VMT since the availability of car-sharing would lead to a

reduction in the number of owned automobiles per household. On the other hand, existing AVs in car-sharing programs would operate significantly longer hours and distances if otherwise owned by a household. The net result of this is a more efficient transportation system. An excellent example of this is the Tesla Robotaxi program for 2020, introduced in Tesla autonomy day event [47], in which every customer can add or remove their vehicles to the network of Tesla Robotaxis. This has a substantial impact of increasing weekly vehicle operation hours five times, and also offsetting some of the monthly vehicle payments.

Fine-tuned sensors/actuators, inter-vehicular communication, and access to travel data would enable AVs to increase vehicle throughput on the roads. In this context, one study shows that vehicle throughput per lane (vehicles per lane per hour) can be increased by 500 percent as a result of AV platooning [48]. Moreover, there is an optimal point for traffic flow speed to produce maximum vehicle throughput. AVs can keep the traffic flow in the optimal condition by removing start-and-stop traffic conditions [49]. Additionally, traffic incidents, mainly vehicle crashes, account for 25 percent of all congestion delays [21]. Therefore, more fluent traffic can be expected by AVs which have far less chance of causing a collision compared to human drivers as discussed.

The final impact of AVs as a result of large-scale utilization that we discuss here and focus in more details in the following chapters is related to the energy consumption of AVs. As shown in Figure 3.2, the mainstream trend for vehicles since 1975 has been getting more efficient and powerful at the same time. NRC estimates that fuel economy improvements will fall between 130 to 250 percent for passenger vehicles in 2050, hybrid vehicles expected to have the 145 MPG fuel economy [21].

AVs can contribute to fuel economy improvement, first by providing optimal driving know as "eco-driving." This mode of driving avoids unnecessary acceleration/deceleration and incorporates the best driving habits to improve efficiency. Moreover, from the large-scale point of view, fuel economy can be improved as a result of the increased vehicle throughout and lane capacity and decreased traffic congestion. Cars that are connected can improve drive-cycle efficiency by reducing the idle time. Also, vehicle platooning provides the opportunity for AVs to travel efficiently in a way that resembles a train, which can lead to higher effective speeds and low aerodynamic drag on the vehicles [51]. Pod-car AVs, which can accommodate one or two passengers are also gaining attention, with great potential in improving the fuel economy. Overall,

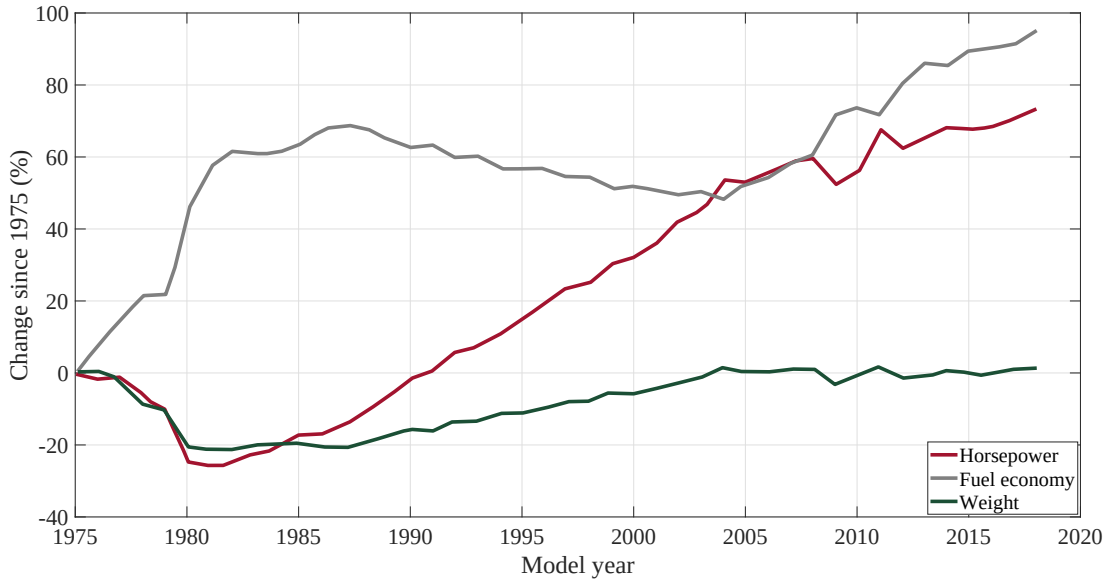

Figure 3.2: Estimated changes in maximum available power, real-world fuel economy, and weight of production vehicles since 1975. (adapted from [50])

Figure 3.3 summarizes the potentials of combining electrification and automation of vehicles in terms of fuel economy. In the context of improving fuel economy for AVs,

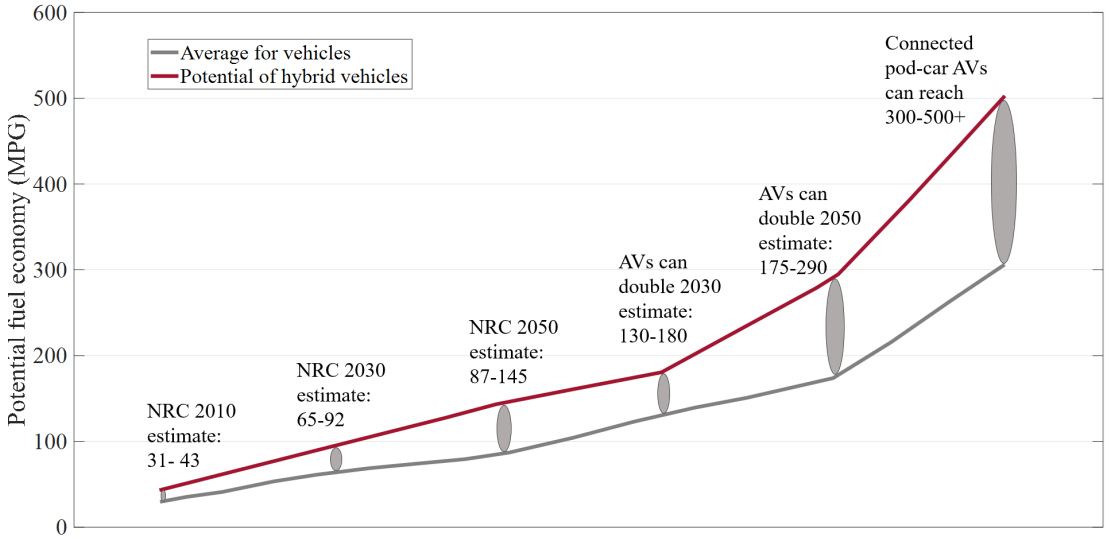

Figure 3.3: Potential influence of autonomous driving on fuel economy of conventional and hybrid electric vehicles. (adapted from [21])

we will focus on a very niche area in the following chapters. In summary, we will try to employ the potentials of journey mapping and motion planning data, produced

by perception and control system of AVs, to obtain the optimal energy management strategy of HEV or PHEV. It should be noted that although being niche, the effect of this would not be trivial by no mean. We predict a substantial improvement in fuel economy using autonomous-specific EMS and we will demonstrate this. To get to know the large-scale impact of this, in just a single case, the Alphabet unit have announced deploying further 62,000 minivans, made by Fiat Chrysler Automobiles, in Waymo's self-driving fleet [12]. Chrysler Pacifica has a power-split hybrid electric powertrain, very similar to the case we are considering. We will discuss benefits of our idea in great details later in this work.

3.3 Level of Autonomy

According to [52], an autonomous vehicle is a self-driving motor vehicle, being able to operate without human intervention using GPS, AI, and sensors. There is a broad variation in vehicles with zero autonomy to full autonomy. Hence, there are few well-known standards, tried to assign and define different levels of autonomy. Society of automotive engineers (SAE) has defined a level of autonomy in J3016 [53] document, which is summarized below.

Level 0 - No Automation In this level, the driver is performing all aspects of diving such as steering, monitoring the environment, and acceleration/deceleration at all the times.

Level 1 - Driver assistance Driver-assist systems can execute either steering or acceleration/deceleration. The human driver is solely responsible for safe operation and should keep full attention to the driving environment. Also, different functions of driving-assistance are operating independently in this level. Examples of these systems are adaptive cruise controller (ACC), lane assist, stability control, emergency brake, and parking assist.

Level 2 - Partial Automation Driving mode-specific can execute both of primary functions, steering and acceleration/deceleration. This can be seen as deploying lane centering and ACC modes at a same time. Driver is still fully responsible for monitoring

the driving environment, and should be available to intervene or regain the full driving operation immediately.

Level 3 - Conditional Automation While the driver should be able to intervene and respond appropriately, the vehicle can take control of performing all critical safe driving actions in specific conditions by monitoring the environment.

Level 4 - High Automation The vehicle can perform all aspects of driving, even without requiring the human driver to intervene or respond. However, in some conditions, such as adverse weather or environment, vehicle might ask the human driver to take over driving.

Level 5 - Full Automation There is no need for human supervision for this level of autonomy at all, considering that vehicle can perform all driving tasks at any time in any condition, even without human existence inside the vehicle. There is no definition of the human driver for the vehicle in this case, and everyone can be considered as a passenger.

The idea we are following in this research considers a vehicle to have a level of automation of three and above, mostly because in these vehicles, autonomous driving systems can provide rich information about the environment and design action plans for driving.

3.4 Autonomous Vehicle Modules

Autonomous driving is a result of multiple modules embedded in AVs, each responsible for specific tasks, but working coordinately. A generic overview of the autonomous system architecture is shown in Figure 3.4. We will explain each module in this figure in more details, highlighting information that would be useful for our purpose.

Route planning functions similar to the commercially available GPS navigation systems and produces a high-level journey plan. This might include the preferred path between the current location and the destination.

Perception module analyzes and fuses real-time data from sensors such as radar, lidar, and cameras to identify and track various objects within the driving scene. These objects can be pedestrians, traffic lights and signs, and other vehicles. Lidars (light

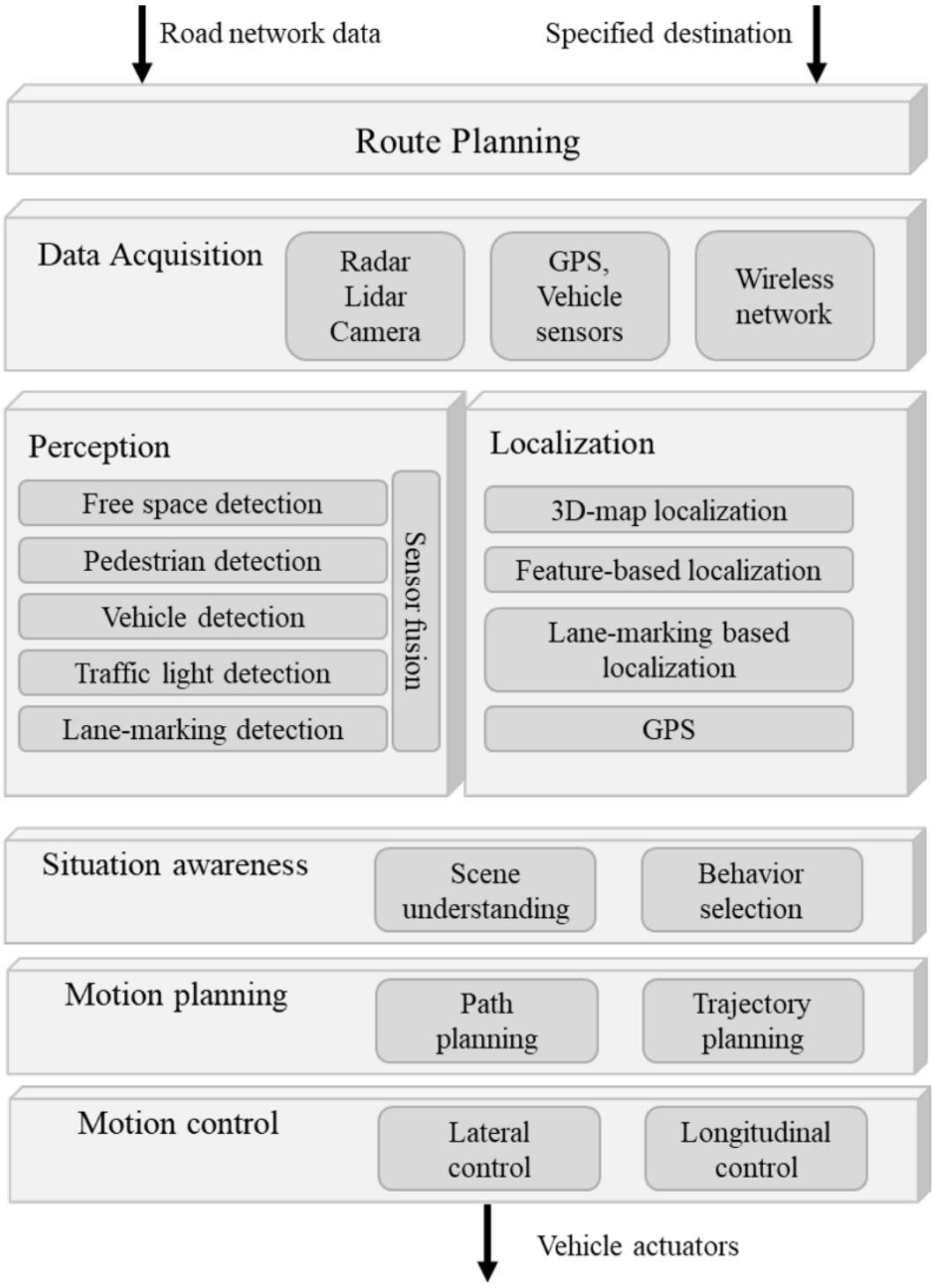

Figure 3.4: Schematic of autonomous vehicle modules. (adapted from [37] and [54])

detection and ranging) are laser-based sensors which can produce a high resolution 3D map of the environment. Besides, intensive application of convolutional neural networks (CNN) in the camera-based perception systems have achieved an incredible results in scene understanding and semantic segmentation of the environment [55]. 3D representation of the lidar can be fused with the semantic segmentation of the camera output to finally produce a 3D semantic segmentation of the driving scene.

To operate safely and efficiently, AV needs to localize itself with respect to other objects in the environment and identify the vehicle states (e.g., position, speed, and orientation). Localization module is responsible for this, employing the fusion of global location data (GPS) and local landmarks.

Scene understanding uses the data from perception and localization modules to represents the driving scene in a useful way for planning and decision making. In this context, the dynamic and static object would be differentiated, and occupancy grid is constituted at this level. Moreover, the prediction of dynamic objects behavior and interaction of vehicles on each other would be examined in this module.

Motion planning targets producing a feasible and ideally an optimal path and trajectory for the vehicle to execute, subjected to obstacles and vehicle dynamic constraints. Motion planning can take place in both structured and unstructured areas. Three main approached for motion planning is searching, sampling, and optimization-based algorithms [56]. In this work, we will focus on optimization-based motion planning in a structured area for the following reasons. First, optimization-based approaches can be implemented real-time and can handle constraints while generating non-jerky output. Dedicated embedded optimization problem solvers are achieving higher performance because of more competent hardware and more efficient implementation. Also, AVs are operating mostly in structured areas in terms of both driven distance and driven time. These factors justify our choice since our main target is employing motion planning data to improve fuel economy.

Finally, motion control is responsible for manipulating throttle, brakes, steering wheel, and other vehicle actuators to follow a given path or trajectory, obtained by motion planning module. This can be addressed using classical control, nonlinear control, model predictive control (MPC), etc.

In this work, we will consider that data from perception, localization, and situation awareness modules is provided for the vehicle in a structured path. Then we will develop and implement an optimization-based approach for motion planning. Generated

path/trajectory will be later used to improve vehicle efficiency using a real-time controller for the hybrid electric powertrain.

Chapter 4

Fundamentals of Energy Management Strategies

4.1 Introduction

Energy management strategy (EMS) can be seen as an action plan for deciding about power supply from different propulsion units (e.g., ICE, electric motor, fuel-cell) and ultimately energy sources (e.g., gasoline fuel tank, battery pack, hydrogen fuel tank) in a HEV to provide the demanded power from the powertrain. This is an integral part of powertrain supervisory control unit [57]. EMS decision should be near optimal and feasible. Various strategies result in different fuel economy, emissions, and drivability. It should be noted that the overall performance of a hybrid electric powertrain is linked to the implemented EMS. Performance of an EMS can be evaluated using software simulation, real-world driving [58], and vehicle simulators [59]. In order to best employ the additional degree of freedom in hybrid electric powertrains, energy and power flow among components should be meticulously determined. Therefore, defining EMS is one of the crucial elements in HEV powertrain design.

To better understand the embedded EMS responsibility, Figure 4.1 shows a simplified overview of how EMS functions with respect to other vehicle components in a HEV. EMS module takes vehicle data, feedback from propulsion and vehicle component (e.g. ICE, M/G, ESS), and demand from the driver as the input. EMS then decides about the power split between powertrain components and generates a reference output for components to follow. Implemented strategy or heuristic inside the EMS is considered

to guarantee optimal or near-optimal performance for the powertrain. In case of an AV, the signal from the driver is replaced by the output of the motion planning/control module.

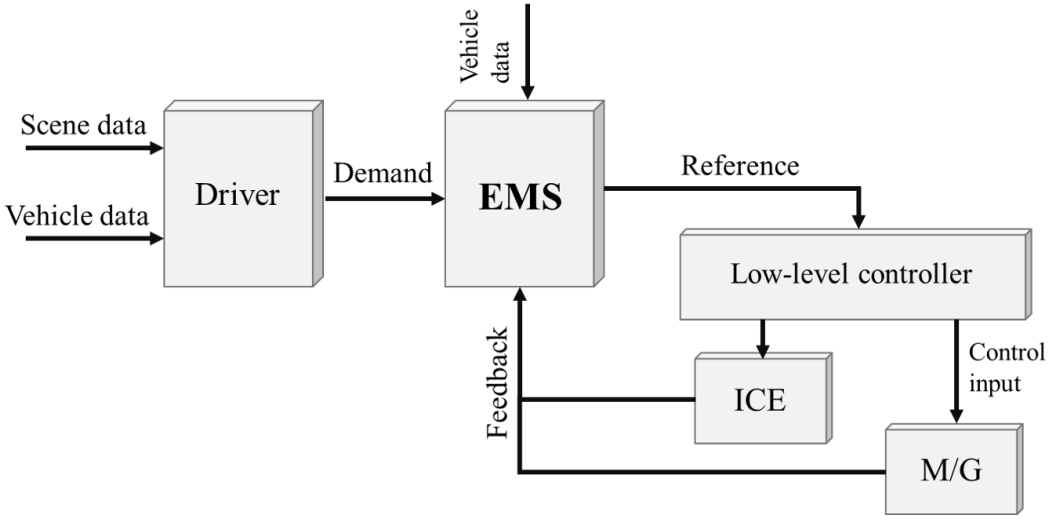

Figure 4.1: Overview of EMS operation in a HEV.

Defining EMS is essential both in real-time operation of HEV and also HEV design. There is a rich literature regarding EMS for HEVs or PHEVs, and this problem has been approached from various perspectives. In rest of this chapter, we will discuss the fundamentals of a few important approaches, comparing them in terms of optimality, the potential for real-time implementation, and required control horizon.

4.2 Rule-based and Fuzzy Rule-based

Rule-based EMS is the most applied strategy in the industry because of real-time capability and technical simplicity [60]. However, control design process is highly time-consuming and arduous [61]. Rule-based strategy can be simply viewed as having a pre-defined embedded rule book, written by control engineers, which generates a decisive action for different conditions. Majority of these rules are in the logical form of if-then format. For instance, one rule can be if the power demand from the powertrain is negative which signifies braking condition, the engine would be dismissed and the generator would try to recover as much as energy by performing regenerative braking. The main disadvantage of these controllers is that the performance can be significantly

deteriorated depending on the condition, because the rules are designed according to a typical set of experimental and simulation data.

Fuzzy logic-based EMS differs from rule-based strategies in a way that these controllers are easily adjustable and less sensitive to measurement errors and variations. The base is still sets of mostly if-then rules [62], with the addition of membership functions which can lead to better performance. There is no prediction horizon needed for these controllers and the performance in real-time can be acceptable if calibrated accurately.

4.3 Equivalent Consumption Minimization Strategy

These strategies are among the highly investigated strategies in the literature. The initial idea is to convert the electrical energy consumption to an equivalent amount in actual fuel consumption using the average efficiency of the components [63]. However, the idea can be extended to a broader point of view, trying to minimize the instantaneous cost, expressed in the following equation

$$u^* = \arg\min_{u \in \mathcal{U}} \dot{m}_{fuel}(u) + \mu_1 P_{elec}(u) + \mu_2 \dot{m}_{em}(u) \tag{4.1}$$

where μ_1 and μ_2 are tuning factors. The overall cost is a scalarization between fuel mass flow rate, $\dot{m}_{fuel}$, consumed electric power, P_{elec}, and mass flow rate of emissions, $\dot{m}_{em}$. Moreover, $\mathcal{U}$ is the set of all feasible control inputs at the moment. The potential of real-time implementation is very clear in this formulation [64]. To move toward optimality, however, tuning factors should be meticulously defined. This can be done by considering an average operation for components, employing historical data and make predictions, or considering available future data. Moreover, the sensitivity of the final solution on the tuning factors should be considered as well. As a result, required horizon depends on the implementation. Based on this concept, more advanced heuristics for defining the energy management strategy can be designed [65].

4.4 Dynamic Programming

It is a numerical optimization strategy to find the global optimal solution, introduced for a first time in [66]. The theory is based on the principle of optimality, expressed in following equation

$$J^*(x(t),t) = \min_{u(t)\in\mathcal{U}} \left(J^*(x(t+\Delta t), t+\Delta t) + \int_t^{t+\Delta t} g(x(\tau),u(\tau),\tau)d\tau \right) \tag{4.2}$$

Note that this criterion is necessary and sufficient for optimality, and which enables DP to obtain the globally optimal solution. In this equation, $J^*()$ is the optimal cost-to-go function. DP is the discrete numerical implementation of this equation, based on two concepts in computer science, recursion and memoization. If states are discretized in N points with an index of i in $1, 2, ..., N$ and time is discretized in M points with the index of k, this equation can be re-written as

$$J^*(x^i,k) = \min_{u(k)\in\mathcal{U}(k)} \{J^*(x^{i+1}, k+1) + g(x^i, u(k), k)\} \tag{4.3}$$

where $x^{i+1} = F(x^i, u(k), k)$ with F representing the nonlinear time variant model. DP can handle nonlinear dynamical systems with any cost function, $g(x,u)$ in equation above, and any constraints on control inputs and states. However, this comes with the price of extensive computation burden. In practice, the optimality of final results rely considerably on the discretization of numerical implementation. This makes the computation time to grow rapidly as problem dimension and resolution increases. Also, for the case of obtaining EMS, DP needs a prior knowledge about the driving cycle. As a result, DP is neither an option for real-time applications, nor the powertrain design cases with broad design space. Nevertheless, DP can provide the benchmark solution to assess the performance of other proposed techniques for EMS [67–69].

4.5 Pontryagin's Minimum Principle

For the general case of optimal control problems, PMP [70] as a generalization of the Euler-Lagrange equations can define the necessary but not sufficient conditions for a trajectory to be optimal, using the Hamiltonian mathematical formulation. Since PMP algorithm finds the control input based on minimizing the instantaneous Hamiltonian,

real-time implementation is feasible. For instance, for an unconstrained nonlinear time-invariant system of $\dot{x} = f(x, u)$ with initial condition of $x(t_0) = x_0$ and fixed final state of $x(t_f) = x_f$, if we try to minimize the following cost function

$$J = \Phi(x(t_f)) + \int_{t_0}^{t_f} g(x(t), u(t))dt \tag{4.4}$$

For this case Hamiltonian is defined as

$$H(x, u, p) = g + p^\top f \tag{4.5}$$

where p is the costate vector. Based of PMP, the necessary condition for $u \in \mathcal{U}$ to minimize (4.4) is

$$\dot{p} = -\left(\frac{\partial H}{\partial x}\right)^\top \tag{4.6}$$

and

$$u^* = \arg\min_{u \in \mathcal{U}} H(x, u, p) \tag{4.7}$$

While PMP has a less computation burden compared to DP, it produces just the necessary condition for optimality. Hence, the final output would be sub-optimal. Moreover, the solution of the PMP become more complex while handling numerous constraints on states and control inputs.

For the real-time purposes, again costate vector remains as the tunable parameter, influences directly on the overall performance of the controller. Interestingly, a study shows that PMP and ECMS approaches for EMS are equivalent in essence [71], showing that costate vector and ECMS tunable parameters are correlated.

4.6 Convex Optimization

Convex optimization problems is the set of optimization problems with in following form [72]

$$\begin{aligned} &\text{minimize } f_0(x) \\ &\text{subject to } f_i(x) \leq 0 \qquad i = 1, 2, ...n \\ &\qquad\qquad h_i(x) = 0 \qquad i = 1, 2, ...m \end{aligned} \tag{4.8}$$

where all functions are $\mathbb{R}^n \rightarrow \mathbb{R}$. Objective function $f_0(x)$ as well as functions in inequality constraints, $f_i(x)$, are convex functions in x. Moreover, functions in equality constraints, $h_i(x)$, are affine functions in x. Convex function is a function with a convex set as the domain which satisfies the following equation

$$f_i(\theta_1 x_1 + \theta_2 x_2) \leq \theta_1 f_i(x_1) + \theta_2 f_i(x_2) \tag{4.9}$$

for all $x_1, x_2 \in \text{dom} f$. Also, $\theta_1, \theta_2 \geq 0$ and $\theta_1 + \theta_2 = 1$. Convex optimization relies on dedicated solvers to find the optimal solution. Convex optimization is a generic name for the problems in a variety of formats including linear programming (LP), quadratic programming (QP), general conic programming, and semidefinite programming (SDP). Moving from LP to more complex forms of convex optimizaiton problems makes using more complex convex functions feasible. However, same in the size of variables and constraints, LP problems are the easiest to solve.

Convex optimization is gaining remarkable attention in various engineering and science fields such as optimal control, image processing, signal processing, and machine learning as a rapid and reliable approach for solving optimization problems. It has been noted that some of the major engineering problems in different fields are indeed convex optimization problems [73]. Convex optimization has also been employed in automotive research fields such as real-time powertrain optimal energy management [74] and component dimensioning [75]. Another application is also provided in [76], which is useful for finding the time-optimal control strategy for a racing car.

To be able to use the convex optimization in these problems, the first challenge is to express the model and components within the convex format. This would probably introduce some uncertainties to the model due to the inaccuracy of convex approximations. The second challenge is handling discrete parameters such as gear decision or clutch state. This problem arises from the fact that minimizing a convex function over a mixed-integer set is an NP-hard problem. Currently, intesive research and developement effort is going on in the field of convex optimization to tackle these problem by developing new convex functions and also heuristics to handle mixed-integer convex optimization problems [77], [78].

The first part of our contribution in this work will be dedicated to develop a convex model for a power-split hybrid electric powertrain, analyze the computational time, and evaluate the optimality of the final solution. Although employing convex optimization

needs a prior knowledge of the driving cycle in advance, we will discuss that how proposed model can be used effectively to improve the powertrain performance.

4.7 Model Predictive Control

MPC is an advanced control technique, very suitable for control problems with higher order dynamics and response delays while having strict constraints on states and control inputs. Figure 4.2 shows a simple schematic of MPC-based controller. The philosophy of MPC is to iteratively find the optimal control policy up to a horizon. Optimal policy is a result of solving an optimization problem using the predictions of the embedded system model and estimated state. [79]. For the simple case of LTI with

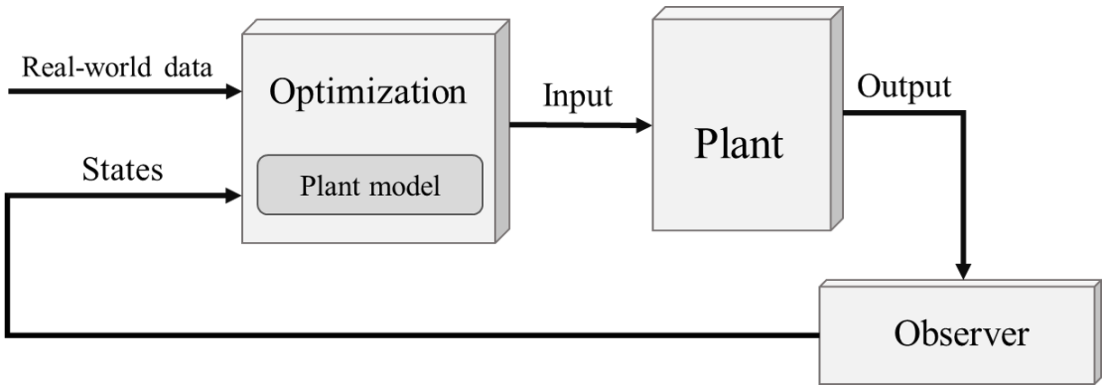

Figure 4.2: Overview of model predictive control operation.

no disturbance and model uncertainties, MPC can be seen as solving the following problem iteratively in time

$$\begin{aligned} \text{minimize } & \sum_{k=0}^{N-1} g(x(k), u(k)) \\ \text{subject to } & x(k) \in \mathcal{X},\ u(k) \in \mathcal{U} \qquad k = 0, 1, ..., N-1 \\ & x(k+1) = Ax(k) + Bu(k) \qquad k = 0, 1, ..., N-1 \\ & x(0) = x_0,\ x(N) = x_f \end{aligned} \tag{4.10}$$

Where N is the controller horizon and keeps receding as optimization moves to the next iteration.

MPC would be our primary approach for developing a real-time EMS in the last

chapters, and we will demonstrate the advantages of MPC in autonomous mobility applications.

4.8 Comparison

We end this chapter by a comparison of the discussed methods for addressing the energy management problem. Figure 4.3 shows an illustrative comparison of the rule-based, equivalent fuel consumption minimization, Pontryagin's minimum principle, model predictive control, dynamic programming, and convex optimization in terms of optimality, real-time implementation, and having access to the control horizon. Comparative analysis of these strategies is investigated in [80]. For the rest of this work, we will focus mainly on the convex optimization and model predictive approaches.

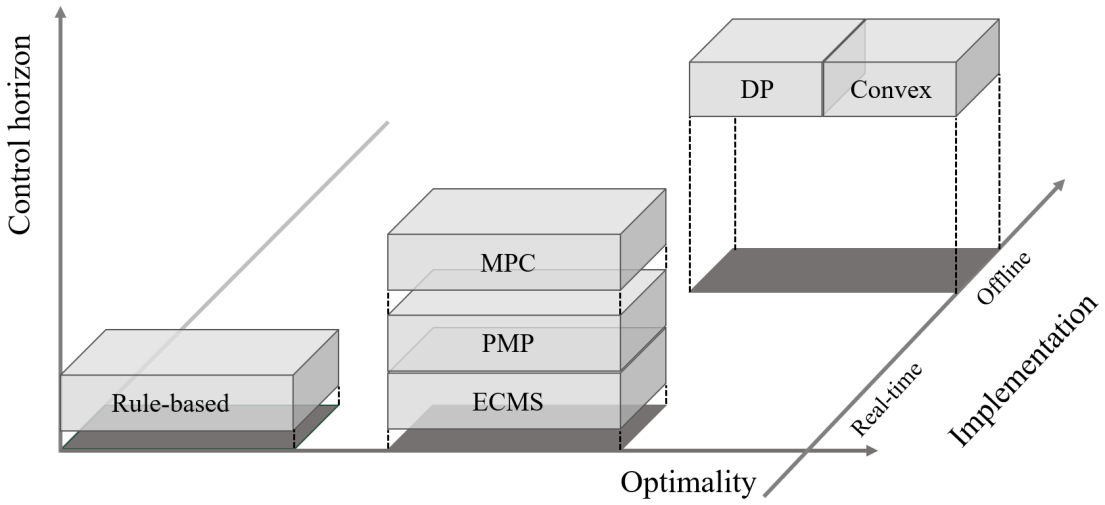

Figure 4.3: Comparison of various energy management strategies. (adapted from [81])

Chapter 5

High-fidelity Vehicle Model

5.1 Introduction

Developing a high-fidelity model in any application regarding design and control is crucial. Particularly in control applications, any modification or a new control strategy should be first evaluated on the model and then implemented in the actual system. Having a high-fidelity vehicle model which can reproduce the behavior of the actual vehicle for the energy-related metrics will help us to observe the performance of developed strategies and to increase the probability of obtaining similar performance from the actual vehicle.

We use MATLAB/Simulink programming and modeling language to develop a high-fidelity model considering the Toyota Prius 2010 as the case study. Our objective is to develop a system-level model which simulate the power flow between the components in the actual vehicle. The developed model is not case-specific and can be readily extended for other vehicles with power-split powertrain such as Chrysler Pacifica.

As the model organization, to have same framework comparing different strategies, we assume that the driving cycle is provided for the driver in advance. Driving cycle data includes the vehicle velocity, $v(t)$, for time scope of 0 to T. Example of a driving cycle is provided in Figure 5.1. In the case of non-flat path, road slope, $\theta(t)$, is also provided in the driving cycle. Based on the driving cycle, the driver then requests a necessary torque to follow the given velocity. This demanded torque then is fed to the control unit to decide about splitting the torque and power among components and generates a control input for powertrain components. Finally, the torque passes the

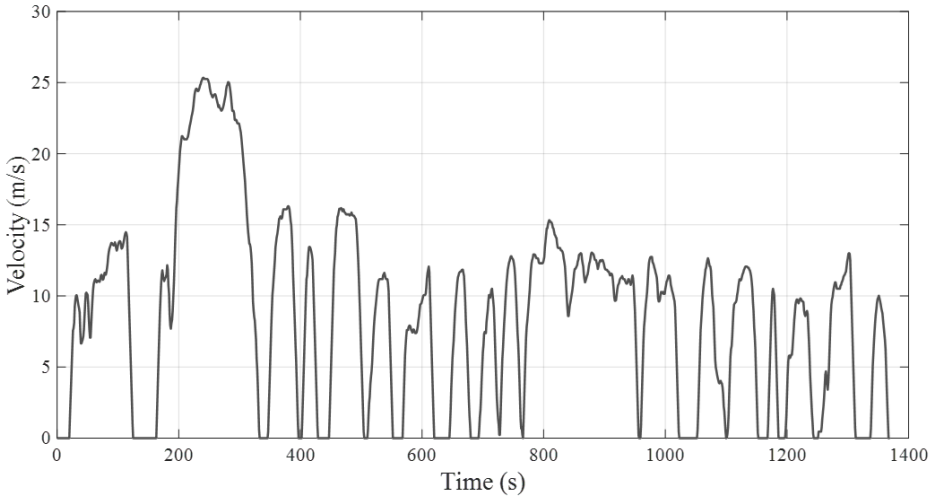

Figure 5.1: Urban Dynamometer Driving Schedule (UDDS).

drivetrain and reaches the wheel to provide acceleration/deceleration. Consequently, vehicle speed forms feedback to the vehicle and the driver. The structure is shown in Figure 5.2. Our model comprises three main components of a driver, control unit,

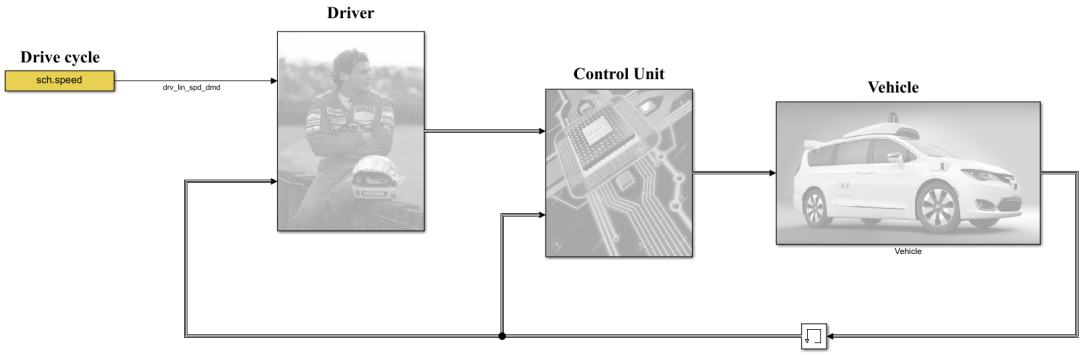

Figure 5.2: Main subsystems of the model: driver, control unit, and the vehicle.

and the vehicle model. We obtain the required data for the model using available publications, technical reports, and software packages such as Autonomie. Also, we will take a reverse-engineering approach to acquire some parameters from the available vehicle dynamometer data. We will also evaluate the fidelity of the developed model using dynamometer data. For these data, we use publicly available data of Argonne National Laboratory [82].

5.2 Vehicle Model

Figure 5.3 shows the schematic of the vehicle components. Naturally-aspirated gasoline internal combustion engine provides propulsion power by converting fuel chemical energy to the mechanical energy. First motor generator (MG1) unit engages directly to the engine in the first planetary gear set (PGS1) and mostly acts as a generator, converting a portion of the engine power to the electrical power and helps to crack the engine. Second motor generator (MG2) unit is placed in the second planetary gear set (PGS2) and is considered mostly for traction and propulsion purposes. MG2 is also responsible for regenerative braking. It worth mentioning that these applications for MG1 and MG2 are not definite. In other words, the design of the powertrain is in a way which provides a possibility to use MG1 in regenerative braking and MG2 to generate electrical power from the engine. Energy storage system (ESS) for the powertrain is a Nickel-metal hydride battery pack, which provides or captures dc electrical energy within some limitations. ESS also provides required power for auxiliary devices. Parameters for vehicle components are summarized in Table 5.1. We will examine each component in more details and explain the applied model for each of these components.

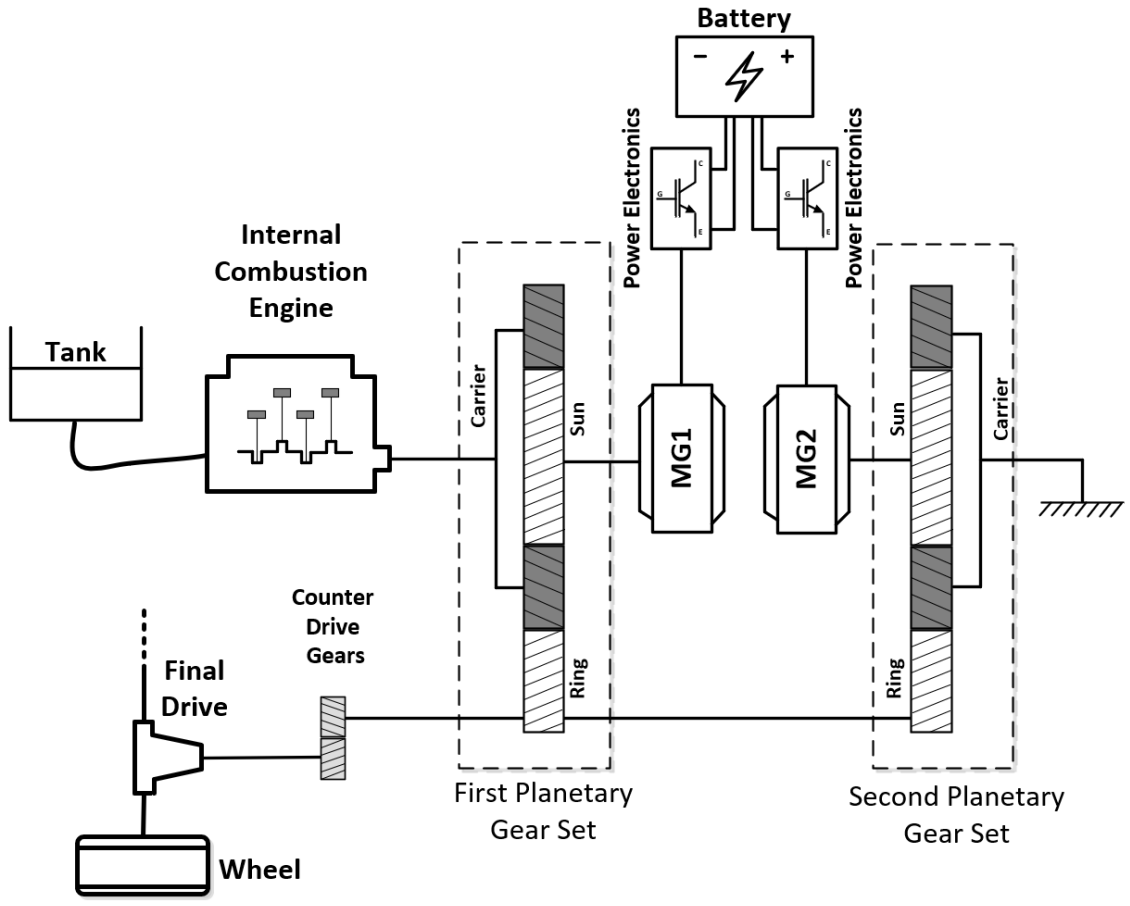

Figure 5.3: Main powertrain components.

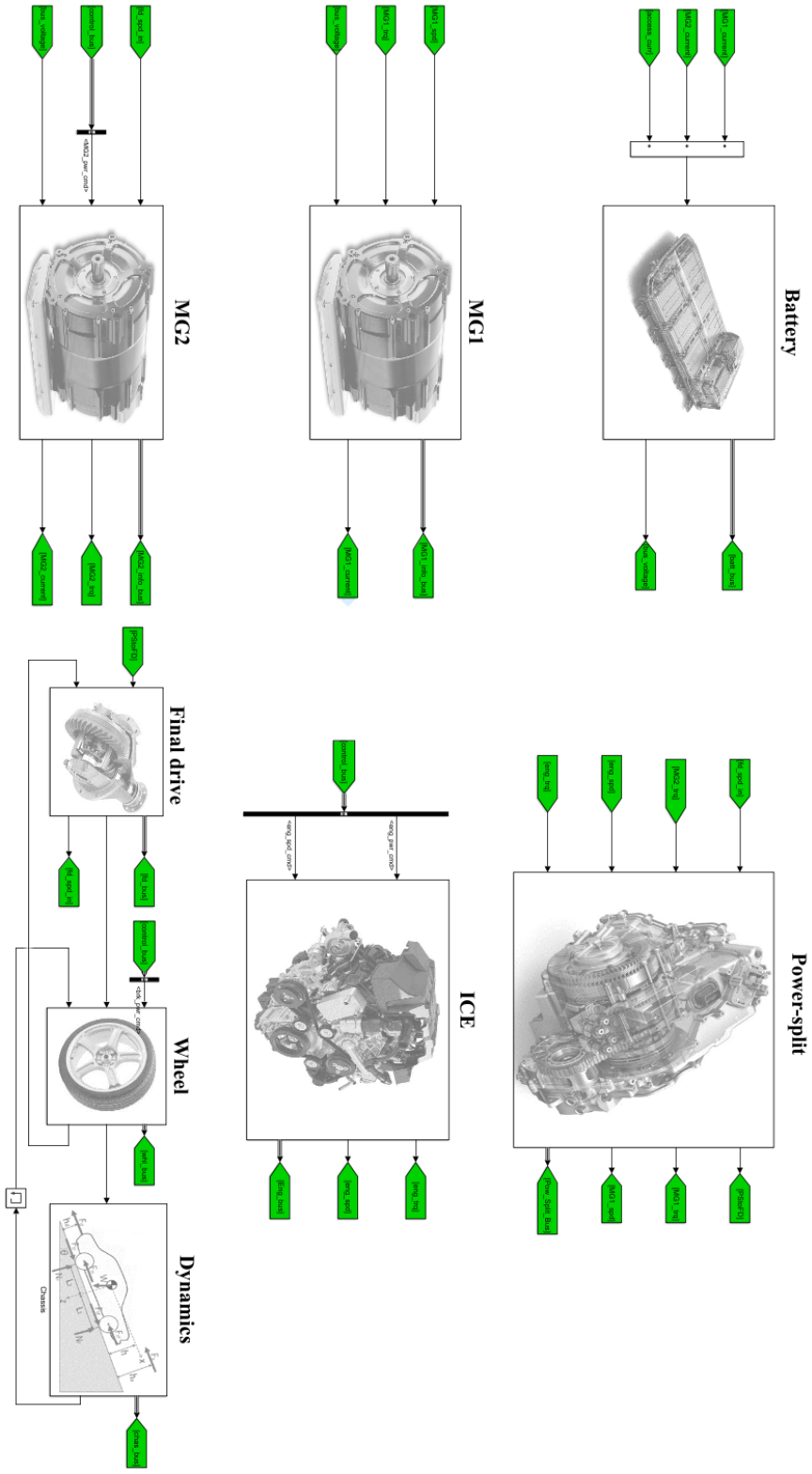

Figure 5.4: Simulink model for the vehicle, consisting battery, MG1, MG2, ICE, power-split device, final drive, wheel, and vehicle dynamics.

Table 5.1: Vehicle Component Parameters

Category	Parameter	Symbol	Value
Wheel	Dynamic radius	r_w	0.31 m
	Efficiency	η_w	.98
	Moment of inertia	J_w	0.8 kgm^2
Power-split	PGS1 ratio	r_1	78/30
	PGS2 ratio	r_2	58/22
Drivetrain	Gear ratio	r_d	3.268
	Efficiency	η_d	0.95
	Moment of inertia	J_d	0.1 kgm^2
MG1	Max. Torque	$T_{mg1,max}$	45 $N.m$
	Max. Power	$P_{mg1,max}$	42 kW
	Moment of inertia	J_{mg1}	0.02 kgm^2
MG2	Max. Torque	$T_{mg2,max}$	207 $N.m$
	Max. Power	$P_{mg2,max}$	60 kW
	Moment of inertia	J_{mg2}	0.05 kgm^2
Battery	Capacity	C_b	6.5 Ah
	Rated power	$P_{b,max}$	27kW
	Nominal battery voltage	$V_{b,nom}$	202 V
Engine	Max. Power	$P_{e,max}$	73 kW
	Max. Torque	$T_{e,max}$	142 $N.m$
	Moment of inertia	J_e	0.18 kgm^2

5.2.1 Internal Combustion Engine

We use a quasi-static model for ICE, ignoring the dynamics of the engine and complex losses. The static model is embedded in the ICE block of our Simulink model, using the 2-D lookup table. This map is shown using contour plot in Figure 5.5. Note that the solid black curve shows the engine maximum torque curve. This curve in addition to maximum speed and minimum idle speed for engine are considered in the model to avoid infeasible operation for the engine. As a result, we can write

$$P_{e,fuel} = \frac{P_e}{F_1(T_e, \omega_e)} \tag{5.1}$$

$$P_e = T_e \cdot \omega_e \tag{5.2}$$

Where $P_{e,f}$ and P_e are the fuel and mechanical power of ICE and F_1 is the 2-D lookup table.

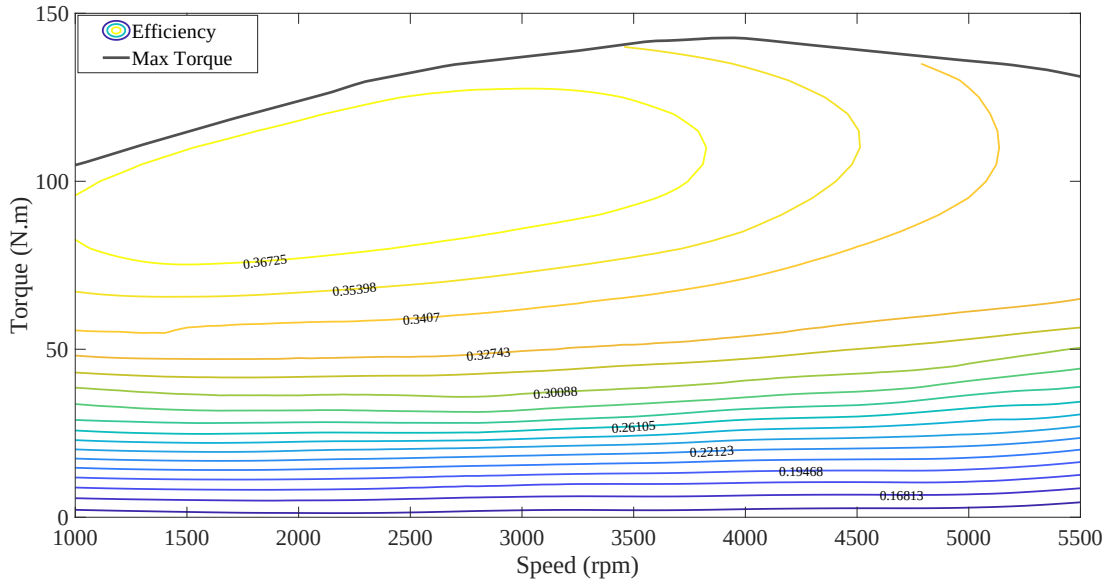

Figure 5.5: Contour map for the ICE with maximum toque curve.

5.2.2 Motor Generator Units and Power Electronics

Similar to ICE, we use a quasi-static model with efficiency maps for M/Gs and their related power electronics. Figure 5.6 and 5.7 show these maps in terms of contours for MG1 and MG2. We also consider the maximum available torque, maximum power,

and maximum speed for each of motor generator units to avoid infeasibilites. As a result, we can write

$$P_{mg1,elec} = P_{mg1} \cdot F_2(T_{mg1}, \omega_{mg1})^{-sgn(P_{mg1})} \tag{5.3}$$

$$P_{mg1} = T_{mg1} \cdot \omega_{mg1} \tag{5.4}$$

$$P_{mg2,elec} = P_{mg2} \cdot F_3(T_{mg2}, \omega_{mg1})^{-sgn(P_{mg1})} \tag{5.5}$$

$$P_{mg2} = T_{mg2} \cdot \omega_{mg2} \tag{5.6}$$

Where F_2 and F_3 are the 2-D lookup tables.

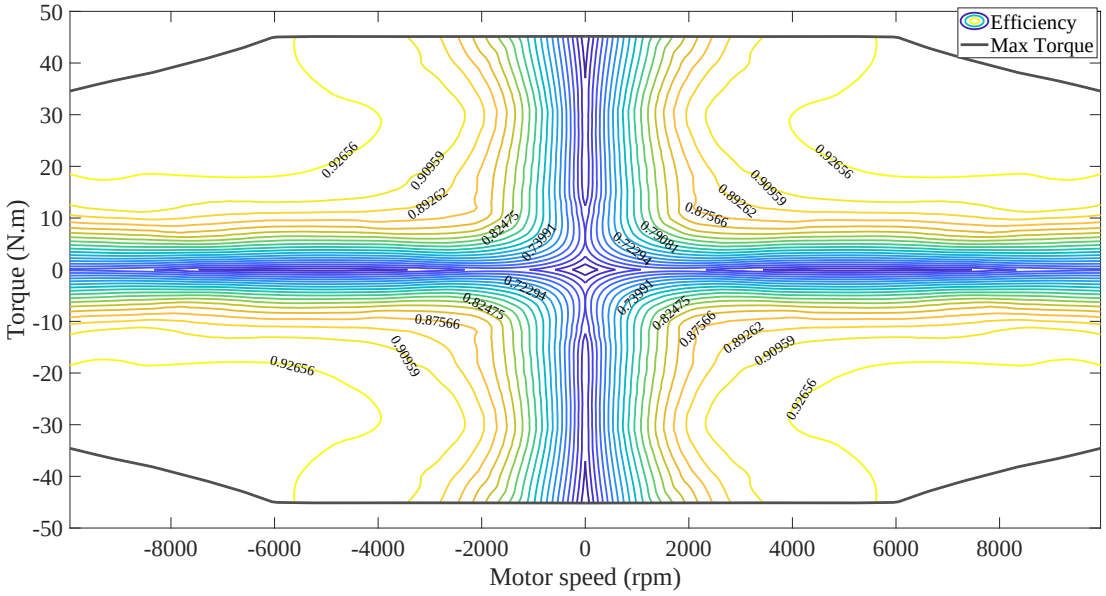

Figure 5.6: Efficiency map shown in contours for the MG1. Solid black line indicates the maximum available torque in absolute value.

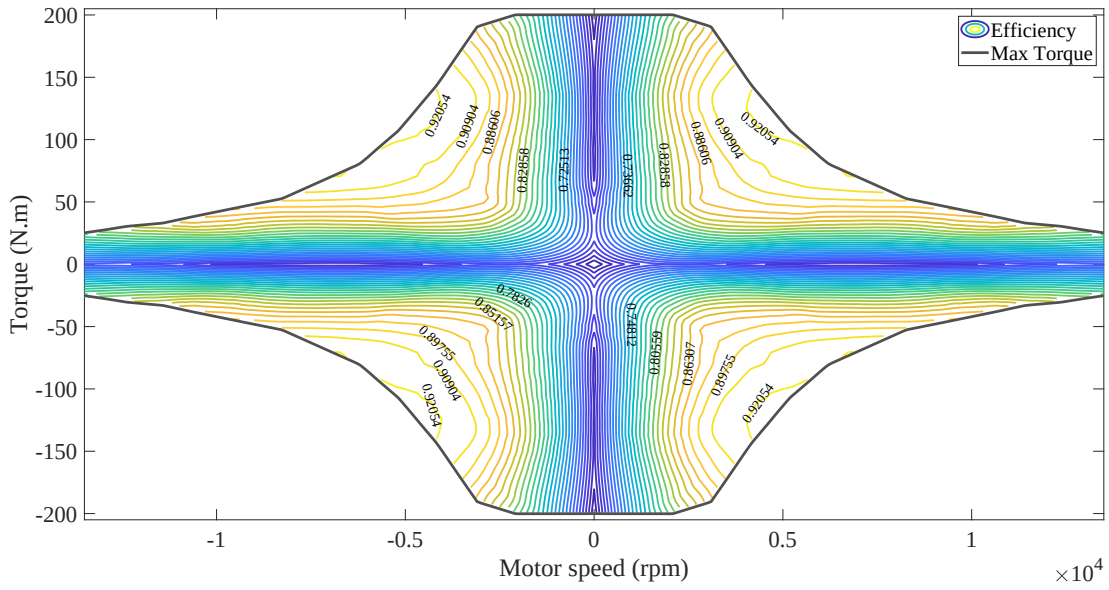

Figure 5.7: Efficiency map shown in contours for the MG2. Solid black line indicates the maximum available torque in absolute value.

5.2.3 Battery

We model battery using an equivalent circuit model. While we can use higher order battery model with a few RC branches, for our analysis, a complex battery model which is able to replicate the highly dynamic behavior of the battery is redundant. We use a simple equivalent circuit model for the battery, shown in Figure 5.8. We believe this level of abstraction is sufficient for our application as we will discuss in the evaluation section. This model uses a single voltage source, known as battery open circuit voltage (OCV), and resistance, known as battery's internal resistance. These parameters are dependent on temperature, battery state of health (SOH), and battery state of charge (SOC). For our analysis, we have considered a constant internal resistance with a SOC-dependent OCV. We have derived the resistance from the test data to be $R_0 = 0.32\,\Omega$, and the SOC-OCV curve is shown in Figure 5.9. Based on assumed battery model, we can write following equations

$$V_b = V_{oc} - R_0 \times I_b \tag{5.7}$$

$$P_b = V_b \times I_b \tag{5.8}$$

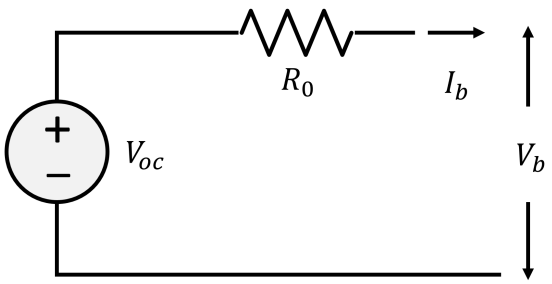

Figure 5.8: Equivalent circuit model for battery with a voltage source and a resistance.

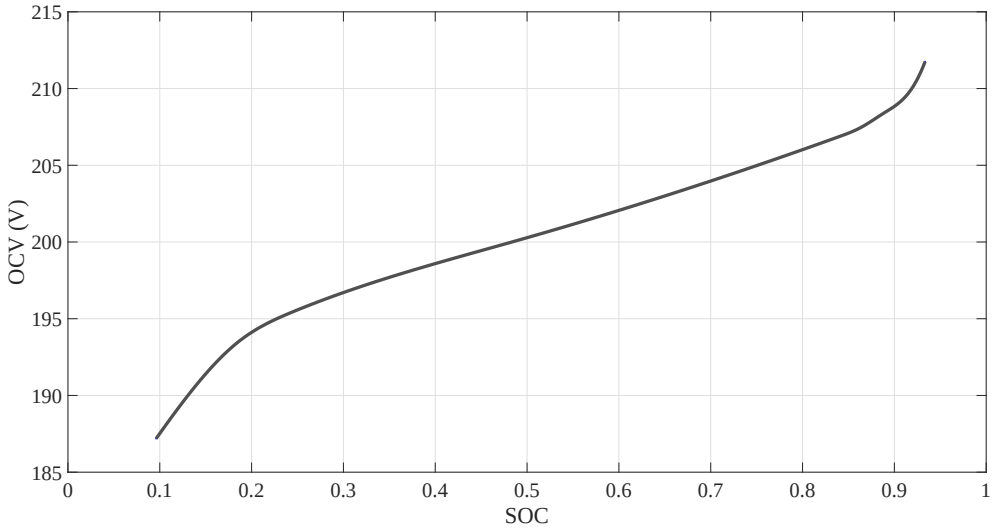

Figure 5.9: Open circuit voltage as a function of state of charge for an equivalent circuit model.

Combining these two equations, we can derive

$$I_b = \frac{V_{oc} - \sqrt{V_{oc}^2 - 4R_0P_b}}{2R_0} \tag{5.9}$$

Also, for the battery SOC, following equation holds

$$\frac{d\,\mathrm{SOC}}{dt} = \frac{1}{C_b}\frac{d\,Q_b}{dt} = -\frac{I_b}{C_b} \tag{5.10}$$

where Q_b is the amount of electric charge stored in battery, and C_b is the battery capacity, shown in Table 5.1. Throughout this work, we will consider positive sign for consuming power and discharging battery and vice versa. We also note the following

equation for energy balance at battery terminal

$$P_b = P_{mg1,elec} + P_{mg2,elec} + P_{aux} \tag{5.11}$$

We also consider a constant auxiliary load of $P_{aux} = 500\,W$.

5.2.4 Power-split

The power-split device provides a more complex operation for powertrain compared to conventional series or parallel hybrid electric powertrains. This is the result of employing planetary gear sets. The powertrain for our case study, as seen in Figure 5.3, includes two planetary gear sets. Internal combustion engine connects to the carrier of the first set. Planet gears of carrier engage with the sun gear and ring gear. In the first set, the sun gear is connected to MG1 and ring gear is coupled to the ring gear of the second set. In the second set, the carrier is held stationary through a coupling and MG2 is connected to the sun gear. Both ring gears are connected to counter drive gears, which make input direction of rotational speed for the final drive in the same direction of the engine rotational speed. Last connections for drivetrain are final drive and wheel. We use a quasi-static model for two existing PGSs in the power-split. For the first PGS, we can write

$$-T_{R_1} = \frac{r_1 \cdot T_e}{1 + r_1} = -r_1 \cdot T_{mg1} \tag{5.12}$$

$$r_1 \cdot \omega_{R_1} + \omega_{mg1} = (1 + r_1) \cdot \omega_e \tag{5.13}$$

T_{R_1}, T_e, and T_{mg1} denote torque for the first ring gear, engine, and MG1 respectively. ω also indicates the rotational speed of the components. Moreover, r_1 is the gear ratio for PGS1, which is shown in Table 5.1. Using the same approach, following equations has been considered for the PGS2

$$T_{R_2} = r_2 \cdot T_{mg2} \tag{5.14}$$

$$\omega_{mg2} = r_2 \cdot \omega_{R_2} \tag{5.15}$$

5.2.5 Final Drive and Wheel

We use a constant efficiency of $\eta_d = 0.95$ and $\eta_w = 0.98$ for the final drive and wheel efficiency (due to slip), respectively. Overall drivetrain gear ratio, combining final drive and counter-drive gears is $r_d = 3.268$. Dynamic rolling radius of the wheel is also $r_w = 0.31\,m$.

5.2.6 Longitudinal Dynamics

For design, component dimensioning, and EMS analysis, full 3D vehicle dynamics model is unnecessary and just a longitudinal vehicle dynamics will provide sufficient accuracy.

We model the load on vehicles to consist of aerodynamics, rolling resistance, intertia, and gravitational load. We have also summarized the required parameters in Table 5.2. For the aerodynamic drag force, we consider the following approximation

Table 5.2: Parameters for Longitudinal Dynamics

Parameter	Symbol	Value
Frontal area	A	2.5 m^2
Air density	ρ	1.23 kg/m^3
Drag coefficient	c_d	0.25
Total vehicle mass	m	1480 kg
Equivalent vehicle mass	m_{eq}	1557 kg
Gravity constant	g	9.81 m/s^2
Rolling resistance coefficient	c_r	0.02

$$F_a = \frac{1}{2}\rho\, c_d\, A\, v^2 \tag{5.16}$$

where ρ is the air density, c_d is coefficient of drag, and A is the projected frontal area for the vehicle. Following approximation is considered for rolling resistance force

$$F_r = c_r\, m\, g\, \cos(\theta) \tag{5.17}$$

in which c_r denotes coefficient of rolling resistance. Gravitational drag force is also considered as

$$F_g = m\, g\, \sin(\theta) \tag{5.18}$$

As a result, the overall force load on the vehicle is

$$F_l = F_a + F_r + F_g \tag{5.19}$$

We can derive the vehicle acceleration/decceleration using following equation

$$m_{eq}\, \frac{dv}{dt} = F_p - F_l \tag{5.20}$$

Where F_p is the propulsion force, supplied by the powertrain at the wheel. Also m_{eq} is the equiavalent vehicle mass, which is combination of vehicle mass and moment of inetria for rotational components, obtained by following equation

$$J_{total} = \left(r_1^2 J_{mg1} + \left(\frac{r_1}{1 + r_1} \right)^2 J_e + r_2^2 J_{mg2} \right) r_d^2 + J_d + 4 J_w$$

$$m_{eq} = m + \frac{J_{total}}{r_w^2} \tag{5.21}$$

Figure 5.10 shows the free body diagram for the longitudinal dynamics of the vehicle. To evaluate the considered model for longitudinal dynamics, we use the tractive effort

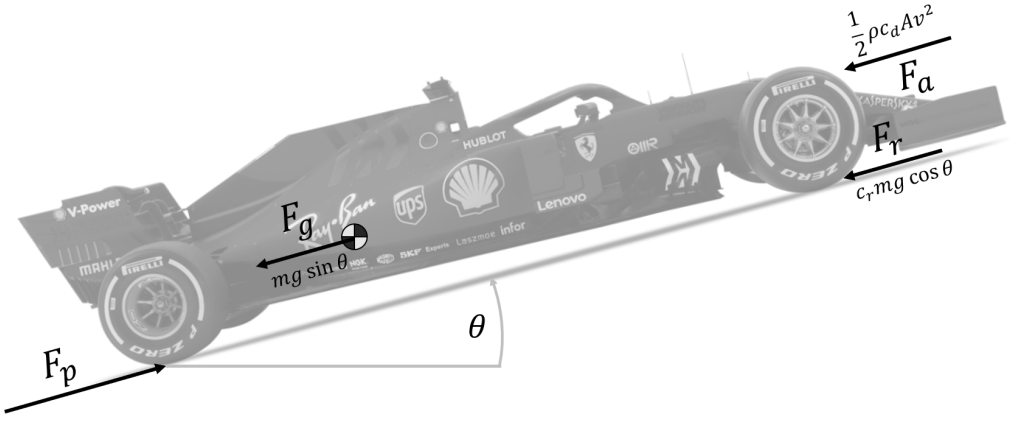

Figure 5.10: Free body diagram for a vehicle driving on a slanted surface. (adapted from [83])

data, provided in [82]. Dyno tractive effort in the mentioned data is as follows

$$F_t = m\,\frac{dv}{dt} + \frac{1}{2}\rho\, c_d\, A\, v^2 \tag{5.22}$$

Figure 5.11 shows the accuracy of the introduced dynamics model in estimating the tractive effort for the driving cycle shown in Figure 5.12.

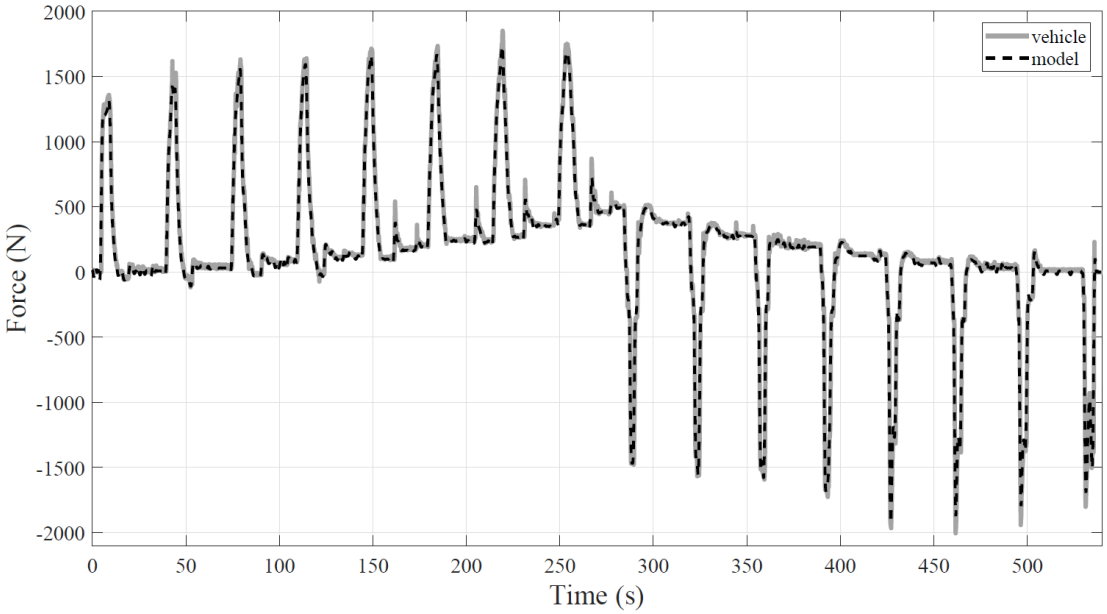

Figure 5.11: Measured dynamometer tractive effort (including inertia and aerodynamic forces) compared to modeled tractive force from vehicle longitudinal dynamics for a driving cycle shown in Figure 5.12. Overall rms error is 62.8 N.

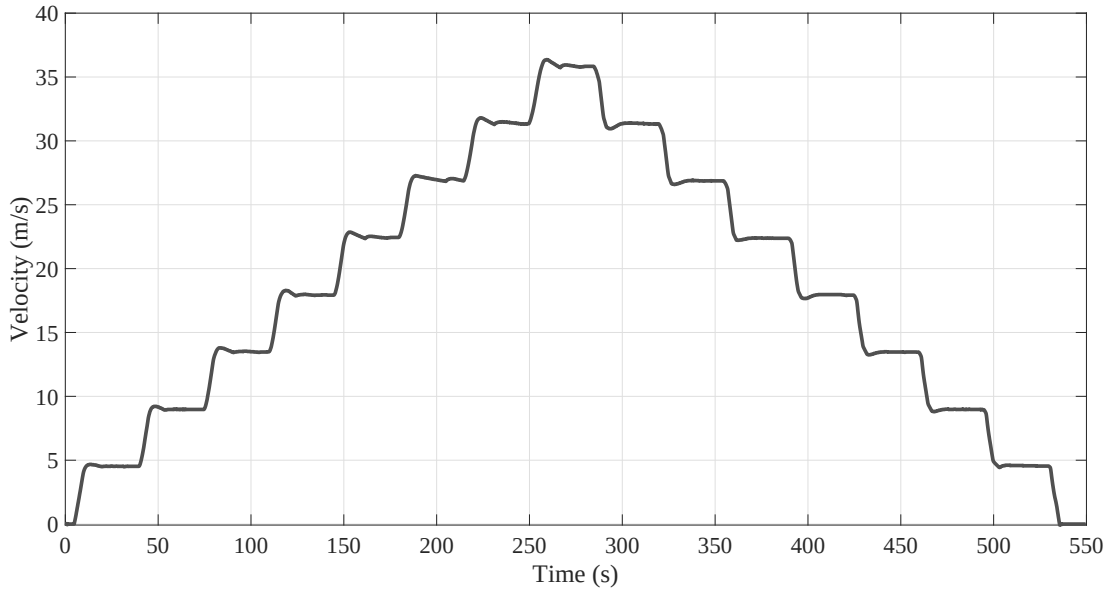

Figure 5.12: Drive cycle used for evaluation of longitudinal vehicle model. This drive cycle includes sets of time periods of constant velocity.

5.3 Control Unit

Control unit with an embedded EMS is responsible for getting a toque/power request from the driver and generate the required control inputs. The logic should consider component limits, vehicle limits, and other parameters to ensure the feasibility of the final decision. Implemented control strategy in the actual vehicle for our case study is a rule-based control strategy. We use the developed control logic tool by MathWorks, Stateflow, to implement the rule-based controller in the control unit. In this section, we will try to derive and tune the rules for the control unit, based on the actual vehicle data [82] combined with other performed studies on the powertrain of the Prius 2010 [84–86].

The first parameter that control unit should decide about is whether the ICE should be on or off. Also, it is important to note that whether powertrain is providing power (positive power demand or propulsion) or captures power (negative power demand or braking). Based on our observation, three important tuning factors of power demand threshold, P_{th}, vehicle speed threshold, v_{th}, and state of charge threshold, SOC_{th}, are deciding about different cases. Based on this, we summarize the rules as below

Propulsion:
if $P_{dmd} \geq P_{th}$ or $v \geq v_{th}$ or $SOC \leq SOC_{th}$ then **Case 1**
if $P_{dmd} < P_{th}$ and $v < v_{th}$ and $SOC > SOC_{th}$ then **Case 2**
Braking:
if $v \geq v_{th}$ then **Case 3**
if $v < v_{th}$ then **Case 4**

If we want to tag each of these cases, Case 1 is propulsion with engine on, Case 2 is propulsion with engine off, Case 3 is braking with engine on, and Case 4 is braking with engine on. For each of these cases, there is a special set of control inputs for components, summarized as bellow

Case 1:
Engine speed $\omega_e = f_1(P_{dmd})$
Battery power $P_b = f_2(SOC)$
Engine Torque $T_e = (P_{dmd} - P_b)/\omega_e$
MG1 speed, ω_{mg1}, obtained by (5.12)
MG1 torque, T_{mg1}, obtained by (5.13)
MG1 power, P_{mg1}, obtained by (5.3) MG2 speed, ω_{mg2}, obtained by (5.15)
MG2 torque, $T_{mg2} = (P_b - P_{mg1})/\omega_{mg2}$
Brake power, $P_{brk} = 0$

In case 1, f_1 and f_2 are both a 1-D lookup table, shown in Figure 5.13. These tables have been derived based on comparing the model output and the available data. Control strategy for case 2 is

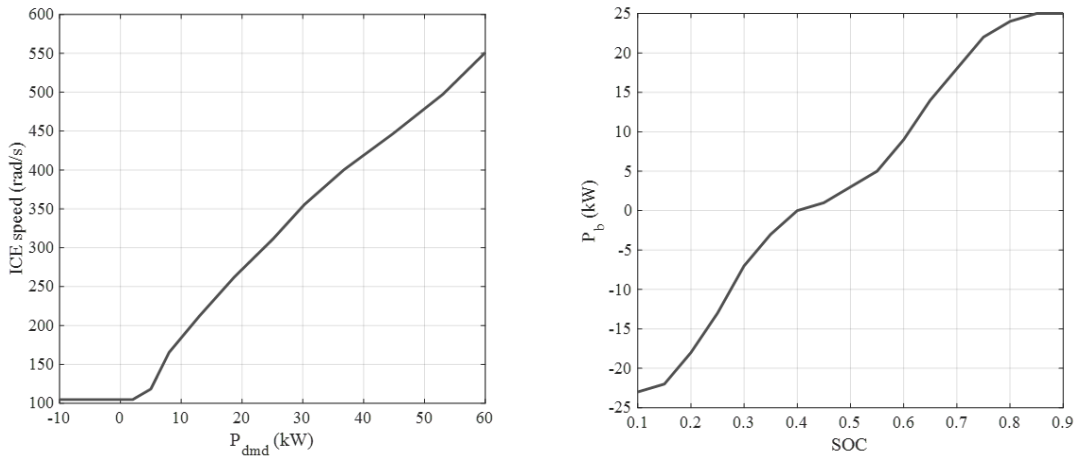

(a) ICE speed vs power demand.

(b) Battery power vs SOC.

Figure 5.13: 1-D lookup tables in Simulink model to obtain control inputs in case 1. We refer to these lookup tables using f_1 for the left and f_2 for the right figure.

Case 2:
Engine speed $\omega_e = 0$
Engine Torque $T_e = 0$
MG1 speed, $\omega_{mg1} = 0$
MG1 torque, $T_{mg1} = 0$
MG2 speed, ω_{mg2}, obtained by (5.15)
MG2 torque, $T_{mg2} = P_{dmd}/\omega_{mg2}$
Brake power, $P_{brk} = 0$

Case 3 and case 4 are conditions when regenerative braking should be used as much as possible. Feasible regenerative braking fraction can be considered as a 1-D lookup table, getting vehicle speed as an input. This lookup table have been shown in Figure 5.14. In case 3, unlike the case 4, engine is kept on while braking to avoid frequent changes in engine mode and energy loss while restarting the engine. Obtained rules in these two cases have been summarized below

Case 3:

Engine speed $\omega_e = 1000\,rpm$

Engine power $P_e = 1kW$, to keep idling

Engine torque $T_e = P_e/\omega_e$

MG1 speed, ω_{mg1}, obtained by (5.12)

MG1 torque, T_{mg1}, obtained by (5.13)

MG2 speed, ω_{mg2}, obtained by (5.15)

MG2 torque, $T_{mg2} = f_3(v) \cdot P_{dmd}/\omega_{mg2}$

MG2 power, $P_{mg2} = T_{mg2} \cdot \omega_{mg2}$

Brake power, $P_{brk} = P_{dmd} - P_{mg2}$

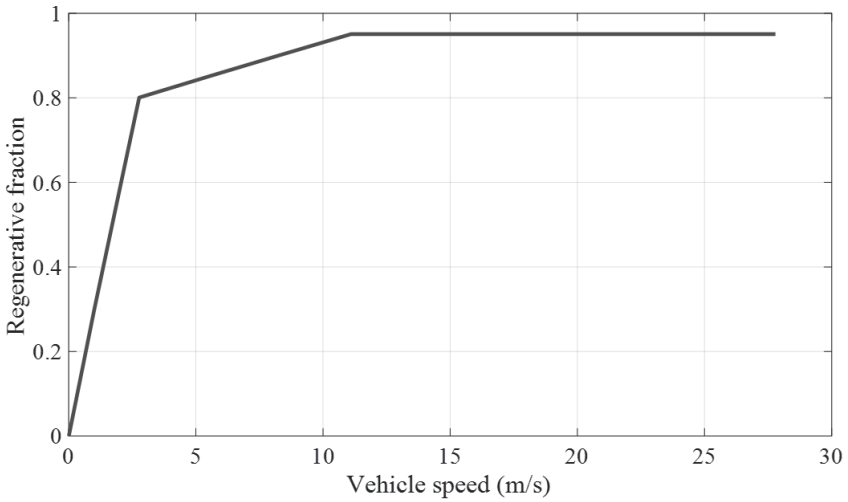

Figure 5.14: Regenerative braking fraction as a function of vehicle speed. We refer to this lookup table as f_3. Note that least amount of mechanical braking is always required to ensure vehicle stability during braking.

Finally, for the case 4 which is braking with ICE off, we have derived following rules

Case 4:
Engine speed $\omega_e = 0$
Engine torque $T_e = 0$
MG1 speed, ω_{mg1}, obtained by (5.12)
MG1 torque, $T_{mg1} = 0$, obtained by (5.13)
MG2 speed, ω_{mg2}, obtained by (5.15)
MG2 power, $P_{mg2} = f_3(v) \cdot P_{dmd}$
MG2 torque, $T_{mg2} = P_{mg2}/\omega_{mg2}$
Brake power, $P_{brk} = P_{dmd} - P_{mg2}$

5.4 Driver

The driver is responsible for following a given reference speed. This can be done by comparing the current vehicle speed with the reference vehicle speed and generating the torque and power demand from the powertrain. To model driver, we use a combination of closed-loop and open-loop approaches. For a given speed, vehicle dynamics can specify the expected force and power load on the vehicle, and hence generate the required torque/power request. However, due to model uncertainty and powertrain limits, just supplying the request from open-loop approach might not give an acceptable reference following. We use a PI controller to compensate for this using a vehicle speed feedback from the vehicle model. We use the trial and error approach to tune the PI controller parameters, considering the coordination of vehicle speed and the reference speed. We fix PI parameters for later evaluation of the model. It should be noted that significant portion of the power/torque request have been provided by the open-loop vehicle model and PI controller just compensates for the rest of this request. Hence, PI parameters trivially influence the overall model results. Schematic of the driver model is shown in Figure 5.15.

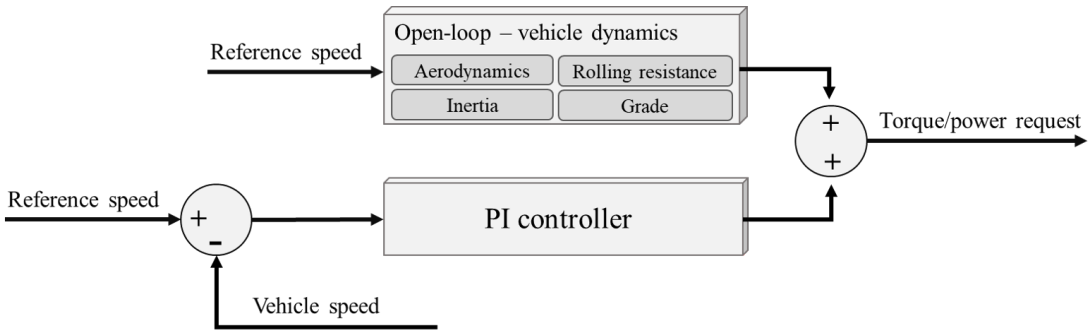

Figure 5.15: Schematic of the driver model.

5.5 Evaluation

To evaluate the fidelity of the developed model, we have compared the results of the model with available experimental data [82], obtained by experimenting the vehicle on the dynamometer and logging the operation signals. Data is in the form of different signals (SOC, fuel consumption, etc.) for a few driving cycles. Note that we have kept a few driving cycles intact while modeling and obtaining the model parameters. Therefore, those driving cycles can truly test the performance of the developed model.

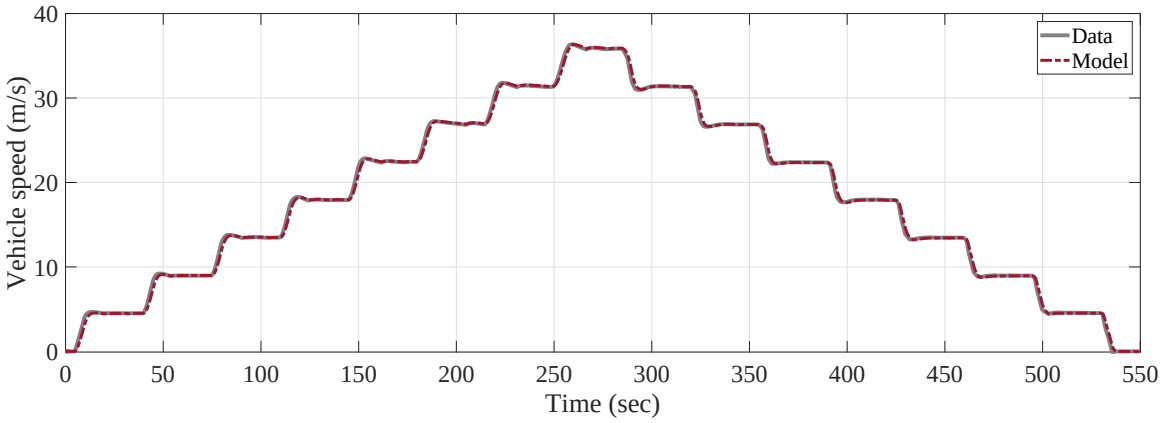

Figure 5.16: Reference vehicle speed compared with vehicle speed generated by model, trying to follow the reference speed. Overall rms error is 0.303 m/s.

As it can be noted, the first four figures are for a driving cycle with a set of steady-state velocities. This is the main driving cycle we have concentrated while extracting the model parameters. To further evaluate the developed model, we assess and compare some signals from data with model signals for the UDDS driving cycle. Results are provided in the following figures. Discrepancies are mainly due to unmodeled

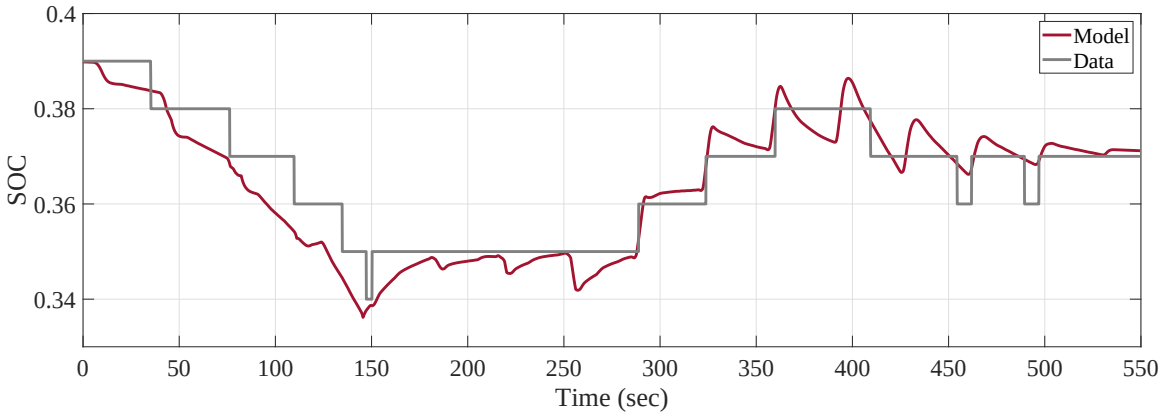

Figure 5.17: Provided SOC profile in data, compared to model SOC profile. Overall rms error is 0.0053 with maximum error of 0.0118 in absolute value.

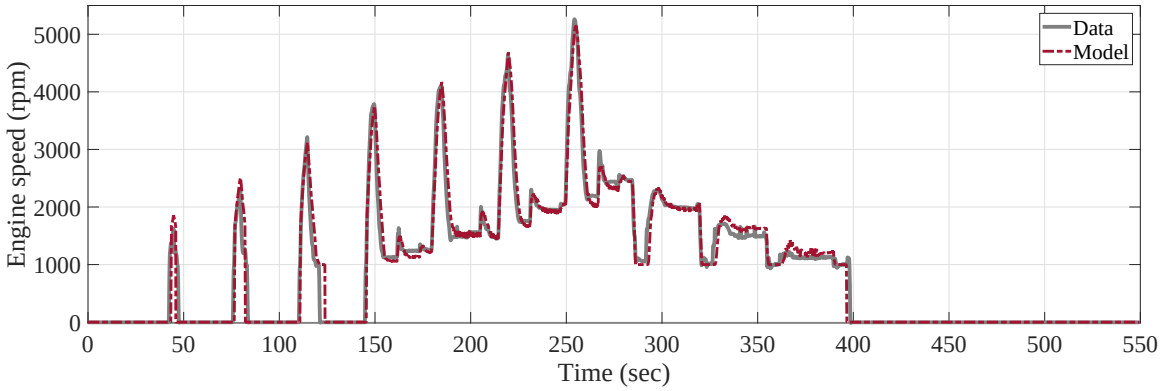

Figure 5.18: Engine speed profile in data, compared to model engine speed profile. Overall rms error is 106.69 rpm.

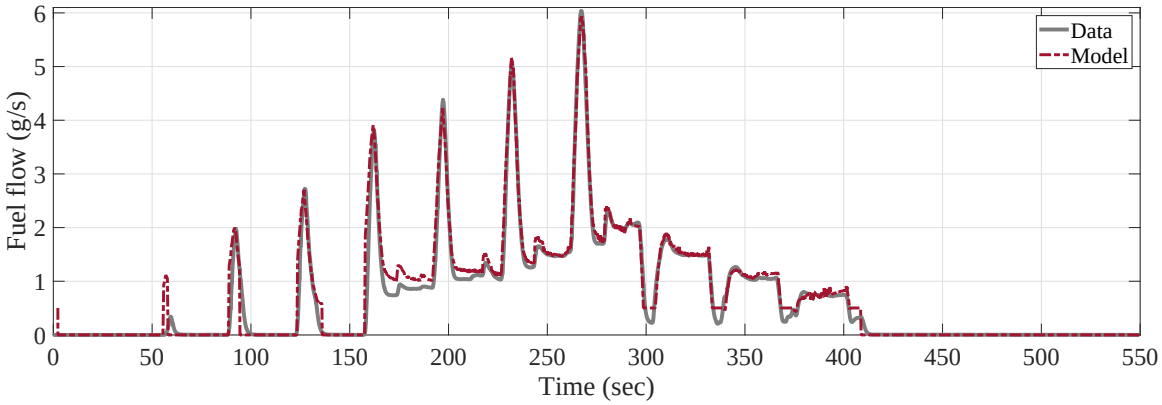

Figure 5.19: Fuel consumption in data compared to model fuel consumption. Overall rms error is 0.091 g/s.

system dynamics (e.g., power-split and engine dynamics, higher order dynamics of battery voltage). Particularly, the discrepancy of SOC profiles is more clear because of integrative nature of this signal over time. However, we observe that signal trends for each case are comparable which means model generated results have an acceptable agreement with actual experimental results. Also, overall rms error for each case is trivial. Therefore, this level of model abstraction have avoided significant loss of model fidelity. Table 5.3 summarizes the results of evaluating the model for different driving

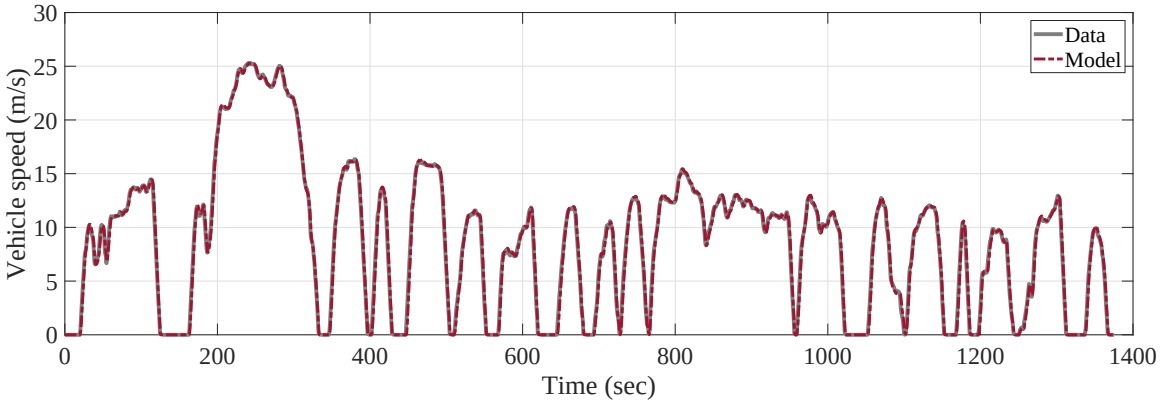

Figure 5.20: Reference vehicle speed compared with vehicle speed generated by model, trying to follow the reference speed. Overall rms error is 0.424 m/s.

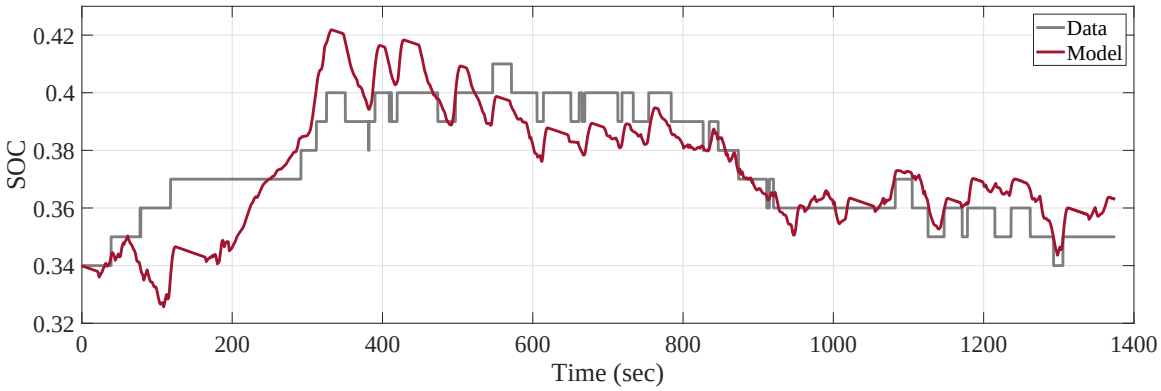

Figure 5.21: Provided SOC profile in data, compared to model SOC profile. Overall rms error is 0.0098 with maximum error of 0.0322 in absolute value.

cycles. This table includes the result for overall consumed fuel and the SOC at the final point of driving cycle. Since we want to evaluate the performance of various proposed energy management strategies from the fuel economy perspective, it is important to make sure that the model is producing comparable total fuel consumption to the actual

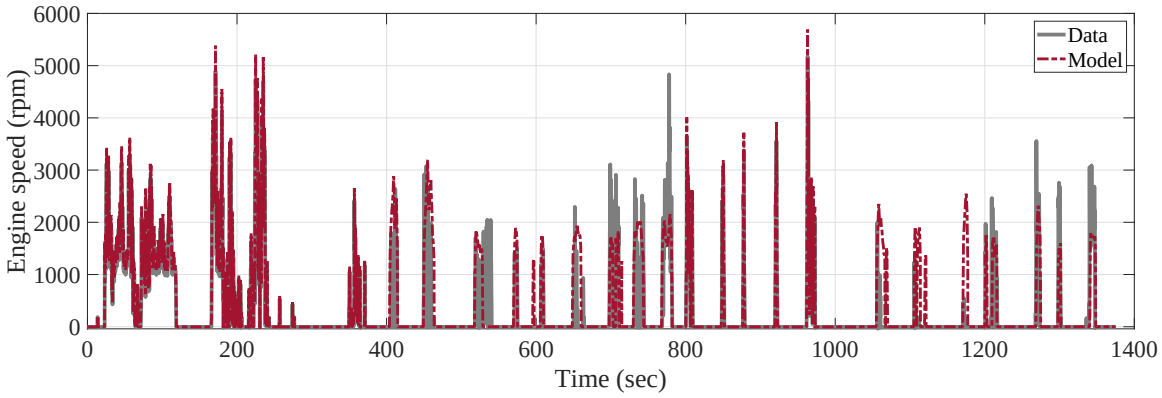

Figure 5.22: Engine speed profile in data, compared to model engine speed profile. Overall rms error is 122.53 rpm.

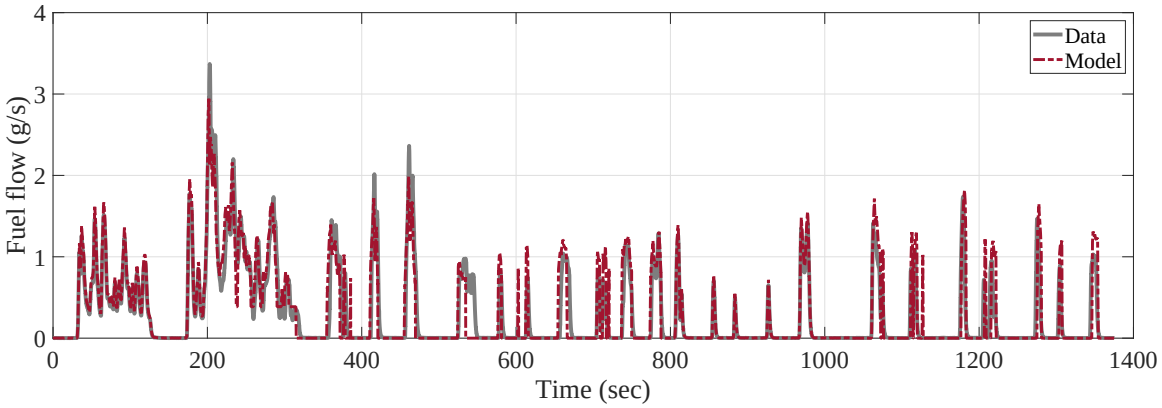

Figure 5.23: Fuel consumption in data compared to model fuel consumption. Overall rms error is 0.105 g/s.

fuel consumption for the vehicle, during testing. Table 5.3 implies that model is very close to an actual vehicle considering fuel economy. Also note that, in some cases that model and data fuel consumption difference is not trivial, this difference is partially compensated by the final SOC difference. Energy dissipation, energy consumption, and energy balance of the model matches acceptably to the actual vehicle. As a result, the developed high-fidelity model is an appropriate tool for evaluating the performance of proposed energy management strategies.

Table 5.3: Model vs Data

Driving cycle	Fuel consumption (g)			Final SOC		
	data	model	diff.	data	model	diff.
Steady state	294.88	299.36	1.52%	0.37	0.371	0.001
UDDS	306.61	315.99	3.06%	0.35	0.363	0.013
US06	572.13	556.62	-2.71%	0.44	0.419	-0.021
Highway	439.98	511.07	3.46%	0.40	0.408	0.008

Chapter 6

Fast Offline Energy Management Strategy

6.1 Introduction

In the offline analysis, it is assumed that the prior knowledge about the operating condition is available in advance. In automotive applications, particularly for the powertrain design and control, the offline analysis includes analyzing the model or vehicle performance for a given driving cycle. As discussed before, the driving cycle is a set of data for vehicle speed, road grade, and vehicle acceleration/deceleration, discretized in time. Driving cycles are the primary inputs for offline analysis. There are available standard driving cycles, and at the same time, a driving cycle can be customized for different application.

Offline EMS analysis is crucial from many perspectives. This analysis can be used to generate benchmarks for further applications as a part of pre-processing. Benchmark solutions mostly show the optimal or the reference strategy. Based on benchmarks or reference strategies, other control strategies can be designed or evaluated. For instance, if the objective is to develop a real-time EMS for a HEV, using artificial intelligence to classify the driving condition and decide about the power demand distribution among components, offline EMS can provide the reference solutions for the operation of powertrain for a large set of driving scenarios. Produced data can be used then to train a neural network [87] or any other machine learning algorithm.

Another substantial utilization of offline EMS is for design and dimensioning

purposes. In this case, the objective could be designing an electric motor, ICE, or transmission to have a desirable performance in some conditions. These conditions are most likely to happen in the actual driving scenarios and can be derived back from a driving cycle using an offline EMS. The objective can be also selecting a combination of ICE, electric motor, and other components, from a set of previously manufactured or available components. Offline EMS can help to realize which combination of components could potentially result in user's preferable performance. It can also be the case that some components such as battery pack or power electronics are modular, and the objective is to find an optimal number of modules to use based on an offline EMS, to get a trade-off between cost and performance.

Dynamic programming has been considered as the main approach for offline EMS [88]. As discussed before, this algorithm can generate globally optimal results for a nonlinear model which is constrained nonlinearly. However, despite recent trials to achieve a faster way of implementing DP [89–91], computational time still remains a major drawback.

In this chapter, we will try to approach the offline energy management problem using convex optimization. Convex optimization can also produce the globally optimal results but in significantly lower amount of time. Low computation time is a great advantage, especially for applications which require iteratively solving the optimization problem. To use the convex optimization, the model should be specified in convex format, a process which is known as convexification. In this chapter, we will show that considering an appropriate set of parameters, powertrain model can be convexified without losing meaningful accuracy. We will present a novel convex presentation of a power-split powertrain. Finally, we will solve the convex optimization problem using dedicated solvers for various driving cycles and compare the results with DP.

6.2 Convex Model

In this section, we will consider different vehicle components and will try to derive a convex mathematical model. We will also examine how the convex model fits into the actual nonlinear model. Figure 6.1 shows the schematic of the power flow between components in the selected powertrain. Our main focus in convex modeling of the powertrain is on power and torque as optimization parameters, which as we will see would result in accurate convex model.

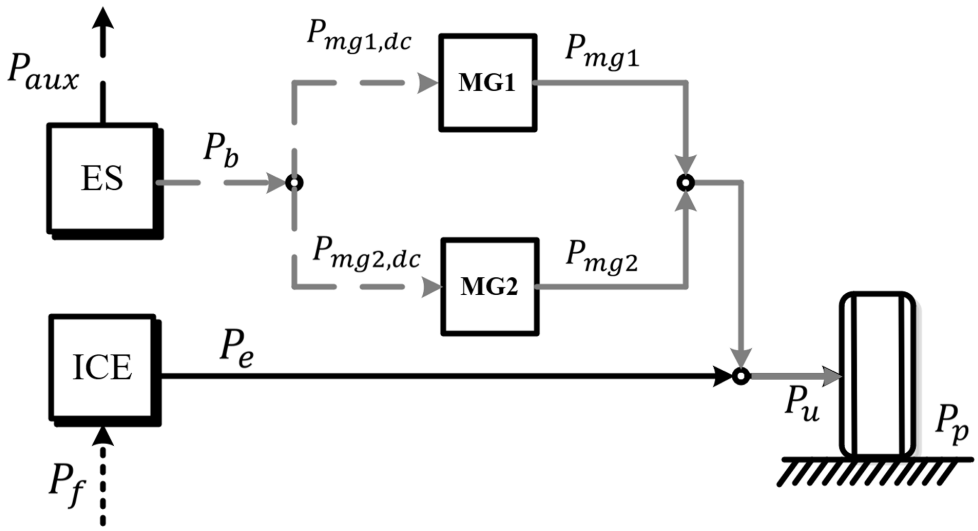

Figure 6.1: Power flow in the powertrain. Arrows show the positive direction for power flow. Dashed lines denote electrical connections, where solid lines stand for mechanical connections. Also, power can flow both ways in connections shown in gray, whereas black connections can transfer power just in a single direction.

6.2.1 Pre-processing

For a given driving cycle of $\{[v(t), \theta(t)] \,|\, 0 \leq t \leq T\}$, we discretize the driving cycle first, considering total discretization of N to get $\{[v(k), \theta(k)] \,|\, k = 1, 2, ..., N\}$. N is a hyper-parameter, which should be decided in advance. While larger N would give finer trajectories and signals as the solution, but in turn will increase the computation time by adding more optimization variables. In our analysis for different driving cycles, we consider N in such a way to get a discretization interval of $\Delta t = T/N = 1\, sec.$

In the next step, we find the acceleration/deceleration using a simple approximation of

$$a(k) = \frac{v(k+1) - v(k)}{\Delta t} \qquad k = 1, 2, ..., N-1 \tag{6.1}$$

We then use the driving cycle data with explained vehicle dynamics in chapter 5, to get the overall power load and force load on the vehicle for $k = 1, 2, ..., N$ as

$$F_a(k) = \frac{1}{2} \rho \, c_d \, A \, v(k)^2 \tag{6.2}$$

$$F_r(k) = c_r \, m \, g \, \cos(\theta(k)) \tag{6.3}$$

$$F_g(k) = m \, g \, \sin(\theta(k)) \tag{6.4}$$

$$F_i(k) = m\,a(k) \tag{6.5}$$

$$\mathcal{F}(k) = F_a(k) + F_r(k) + F_g(k) + F_i(k) \tag{6.6}$$

$$\mathcal{P}(k) = (F_a(k) + F_r(k) + F_g(k) + F_i(k)) \cdot v(k) \tag{6.7}$$

Where as discussed before, F_a, F_r, F_g, and F_i are loads due to aerodynamic drag, rolling resistance, road grade, and inertia, respectively. Moreover, $\mathcal{P}(k)$ and $\mathcal{F}(k)$ are overall demanded power and force load for a given driving cycle. Note that we use the convention of positive toque and power for accelerating and propulsion and negative for braking and regeneration. Also note that all other constant parameters are summarized in Table 6.1 and 5.2.

Considering the wheel slip losses approximated by the wheel efficiency, η_w, and total drivetrain gear ratio, r_d, and drivetrain efficiency, η_d, we can write:

$$\mathcal{T}_{ps}(k) = \frac{\mathcal{F}(k) \cdot r_w}{r_d \cdot (\eta_w \cdot \eta_d)^{sgn(\mathcal{P}(k))}} \tag{6.8}$$

$$\mathcal{P}_{ps}(k) = \frac{\mathcal{P}(k)}{(\eta_w \cdot \eta_d)^{sgn(\mathcal{P}(k))}} \tag{6.9}$$

Where $\mathcal{T}_{ps}(k)$ and $\mathcal{P}_{ps}(k)$ are requested torque and power from driving cycle at power-split powertrain.

According to powertrain schematic shown in Figure 5.3, ring gears for PGS1 and PGS2 and as a result, MG2 are mechanically coupled to the wheels with constant gear ratios. Using this, we can write

$$\omega_{R_1}(k) = \omega_{R_2}(k) = \frac{v(k) \cdot r_d}{r_w} \tag{6.10}$$

$$\omega_{mg2}(k) = r_2 \cdot \omega_{R_2}(k) \tag{6.11}$$

6.2.2 Power-split

Based on the quasi-static model for power-split, explained in Chapter 5, for the PGS1 we can write

$$T_{R_1}(k) = -\frac{r_1 \cdot T_e(k)}{1 + r_1} \tag{6.12}$$

$$T_{mg1}(k) = -\frac{T_e(k)}{1 + r_1} \tag{6.13}$$

$$\omega_{mg1} = (1 + r_1)\,\omega_e - r_1\,\omega_{R_1} \tag{6.14}$$

If we multiply both sides of two (6.13) and (6.14) equalities together and replace ω_{R_1} using (6.10), we will end up in following equation for MG1 power

$$P_{mg1}(k) = -P_e(k) + \left(\frac{r_1 \cdot r_d}{(1 + r_1) \cdot r_w} \cdot T_e(k) \cdot v(k)\right) \tag{6.15}$$

It is obvious that in this equation, MG1 power is an affine function of ICE power and torque. For the PGS2, we can write

$$T_{R_2}(k) = r_2 \cdot T_{mg2}(k) \tag{6.16}$$

$$P_{mg2}(k) = T_{mg2}(k) \cdot \omega_{mg2}(k) \tag{6.17}$$

Finally, power-split should satisfy the power and torque demand. So we can consider following equations

$$P_e(k) + P_{mg1}(k) + P_{mg2}(k) \geq \mathcal{P}_{ps}(k) \tag{6.18}$$

$$T_{R_1}(k) + T_{R_2}(k) \geq \mathcal{T}_{ps}(k) \tag{6.19}$$

Note that we have used inequalities in these equations. This means that powertrain should always equal or exceed the demand, and we let the mechanical brakes to dissipate the excess energy by compensating the excess torque. However, it is obvious that in the case of the globally optimal solution in terms of energy consumption, the utilization of the mechanical brakes should be minimized. Hence, we expect that these constraints to hold tight whenever it is feasible.

Overall convex model of the power-split are equations (6.12), (6.15), (6.16), (6.17), (6.18), and (6.19). All of these equations are affine and hence convex.

6.2.3 Internal Combustion Engine

In this section, we present a novel convex quadratic model for the internal combustion engine, rather than a simple affine Willans approximation [92]. The proposed ICE model considers the limitations on engine power and engine torque and is more accurate than affine approximation. For the engine fuel maps, engine efficiency or brake specific fuel consumption are expressed as a function of engine speed and engine torque. We presented an example of this in contour maps in Figure 5.5. To transform this figure to

a convex manifold, we replace the engine speed axis with engine power to approximate engine fuel power as a convex function of ICE torque and ICE power. This substitution is mainly because of the fact that even for the simplest case of $P_f = \alpha \cdot P_e$ with $P_e = T_e \cdot \omega_e$, P_f is obviously not a convex function of T_e and ω_e.

We use a 2-D convex quadratic function as following for the engine fuel power

$$P_f = f(P_e, T_e) = [P_e \quad T_e] \cdot A \cdot \begin{bmatrix} P_e \\ T_e \end{bmatrix} + b^T \cdot \begin{bmatrix} P_e \\ T_e \end{bmatrix} + c \tag{6.20}$$

in which $A \in S_+^2$, $b \in R^2$, and c is a scalar. Note that we assumed A belongs to the set of positive semidefinite matrices so that (6.20) be convex. A, b, and c can be obtained by fitting (6.20) to set of engine data. Since it is reasonable to have a zero fuel power output for zero input power and torque, we can assume that $c = 0$.

To approximate engine using (6.20), fit this convex quadratic model into engine operating data including M data points using least squares approach. The objective is to obtain the following parameters

$$A = \begin{bmatrix} a_1 & a_2 \\ a_2 & a_3 \end{bmatrix} \succeq 0 \ , \ b = \begin{bmatrix} b_1 \\ b_2 \end{bmatrix} \tag{6.21}$$

with $\succeq$ denoting matrix inequality. We want to obtain mentioned parameters by minimizing the

$$J = \sum_{m=1}^{M} \left(P_{f,data}^{(m)} - f(P_e^{(m)}, T_e^{(m)}) \right)^2 \tag{6.22}$$

We rewrite this equations as

$$J = R^\top R \tag{6.23}$$

in which R is residual M-vector, defined as

$$R = \begin{bmatrix} P_f^{(1)} - f(P_e^{(1)}, T_e^{(1)}) \\ P_f^{(2)} - f(P_e^{(2)}, T_e^{(2)}) \\ \vdots \\ P_f^{(M)} - f(P_e^{(M)}, T_e^{(M)}) \end{bmatrix} \tag{6.24}$$

As it can be seen from (6.24), R is an affine function of A and b. So we can write

$$R = W_{M\times 5}\begin{bmatrix} a_1 \\ a_2 \\ a_3 \\ b_1 \\ b_2 \end{bmatrix} + h \tag{6.25}$$

The problem of fitting a convex quadratic ICE model to a set of given data, can be written as semidefinite programming (SDP) optimization problem as we will explain. SDP is a set of convex optimization problems in form of [72]

$$\begin{aligned} \text{minimize} \quad & c^\top x \\ \text{subject to} \quad & x_1F_1 + x_2F_2 + ... + x_nF_n + G \preceq 0 \\ & Hx = d \end{aligned} \tag{6.26}$$

with $F_i, G \in \mathbf{S}^k$ ($\mathbf{S}^k$ is a set of all $k \times k$ symmetric matrices) and $\preceq$ denotes matrix inequality. The complex inequality in this for of optimization problems is known as linear matrix inequality (LMI).

In order to write SDP fitting problem, we relax the (6.23) to have

$$J \geq R^\top R \tag{6.27}$$

Relaxation is a common practice in convex optimization, during which tight equality constraints are replaced with relaxed inequality constraints to make the problem convex. However, it should be explained that relaxation does not influence the final optimal result. In our case, since J is the objective of the optimization to be minimized, it is obvious that in case of optimal solution, (6.27) should hold tight to avoid unnecessary increase in the objective function.

Using the fact that $I_M \succ 0$ (I_M is a $M \times M$ identical matrix) and I_M is invertible, we can write (6.27) as following using Shur complement

$$\begin{bmatrix} I_M & R \\ R^\top & J \end{bmatrix} \succeq 0 \tag{6.28}$$

Schur complement condition states that for a partitioned symmetric matrix of X as

$$X = \begin{bmatrix} D & B \\ B^\top & C \end{bmatrix} \tag{6.29}$$

with non-singular D, following criteria holds for positive semi-definiteness of X

$$\text{if } D \succ 0 \text{ then} \quad X \succeq 0 \Leftrightarrow C - B^\top D^{-1} B \succeq 0 \tag{6.30}$$

where $C - B^\top D^{-1} B$ is Schur complement of X.

Finally, the overall SDP can be written as

$$\begin{aligned} &\text{minimize} \;\; J \\ &\text{subject to} \;\; \begin{bmatrix} I_M & R \\ R^\top & J \end{bmatrix} \succeq 0 \\ &\qquad\qquad \begin{bmatrix} a_1 & a_2 \\ a_2 & a_3 \end{bmatrix} \succeq 0 \\ &\qquad\qquad R = W \begin{bmatrix} a_1 \\ a_2 \\ a_3 \\ b_1 \\ b_2 \end{bmatrix} + h \end{aligned} \tag{6.31}$$

Problem is first parsed with CVX [93] and then solved by MOSEK [94]. CVX is an optimization modeling language, developed for disciplined convex programming. CVX provides an environment to implement the convex mathematical optimization problem and provides the sufficient inputs for the dedicated solver. MOSEK is a solver for mathematical optimization problems, with a focus on large-scale convex optimization problems (LP, QP, and Conic).

The fitting result in following for the given ICE data points in [82], using standard units for torque and power.

$$A = \begin{bmatrix} 0 & -0.0074 \\ -0.0074 & 2.7129 \end{bmatrix} \;,\; b = \begin{bmatrix} 3.55364 \\ -178.1220 \end{bmatrix} \tag{6.32}$$

Figure 6.2 shows the ICE data points and corresponding convex quadratic function.

ICE convex model gets mechanical power and ICE torque as inputs and generates the consumed fuel power. It should be noted that using the actual data points to derive

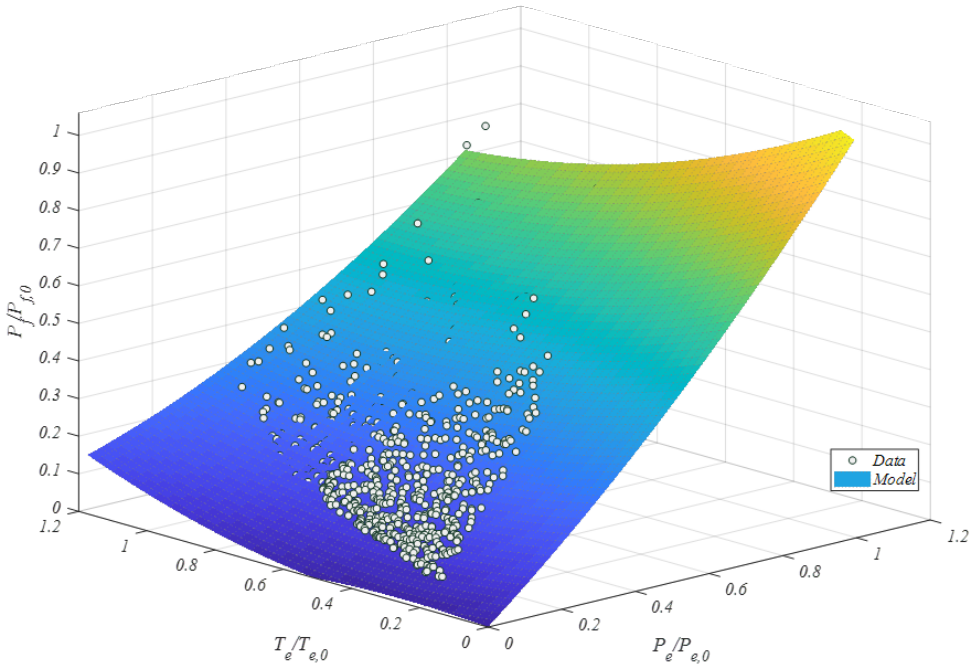

Figure 6.2: Convex quadratic model for the ICE is identified by fitting (6.20) to the engine operating points, using semidefinite programming. Normalized rms error is 0.9%.

the convex ICE model would result in a more accurate model rather than just fitting a convex model to ICE fuel map. In the ICE fuel map, most of the regions are rarely get used during an actual driving cycle. Using ICE data points for driving cycles to fit the convex model would emphasize more on the accuracy of the model on those regions that are likely to be used in the ICE fuel map.

We also consider power and torque constraints for the developed convex ICE model as

$$0 \leq P_e(k) \leq P_{e,max} \tag{6.33}$$

$$0 \leq T_e(k) \leq T_{e,max} \tag{6.34}$$

6.2.4 Motor Generator Units and Power Electronics

We use two different approaches in convex modeling of the MG1, MG2, and related power electronics. As we discussed in pre-processing, we can calculate the MG2 speed for a given driving cycle in advance using (6.11). We take advantage of this, similar to [95, 96] to obtain a convex quadratic model for each particular MG2 speed, with MG2 torque as an input and MG2 DC power as the output. This model can be written as

$$P_{mg2,dc}(k) = p_2(\omega_{mg2}(k)) \cdot T_{mg2}(k)^2 + p_1(\omega_{mg2}(k)) \cdot T_{mg2}(k) + p_0(\omega_{mg2}(k)) \quad (6.35)$$

where $p_2 \geq 0$, p_1, and p_0 are some coefficients, obtained for given MG2 speed. As a result, there is a different convex quadratic model for different MG2 speeds. We can consider that $p_0 = 0$ for any given speed, since it is reasonable to assume for a zero torque, dc power would be zero. Despite the ICE case, we use the MG2 efficiency map, show in Figure 5.7, to fit the quadratic curve by minimizing the sum of the square of the errors to obtain p_2 and p_1. We use the built-in fit function in MATLAB to perform the fitting. An example of MG2 operating points from efficiency map and derived convex model are shown in Figure 6.3 for four different MG2 speeds. Obtained parameters considering standard units for torque and power are as following

$$\begin{aligned}
&\omega_{mg2} = 2000\ rpm \quad \text{then} \quad p_2 = 0.2813 \quad p_1 = 213.5611 \\
&\omega_{mg2} = 4000\ rpm \quad \text{then} \quad p_2 = 0.3937 \quad p_1 = 421.4786 \\
&\omega_{mg2} = 6000\ rpm \quad \text{then} \quad p_2 = 0.6287 \quad p_1 = 630.4131 \\
&\omega_{mg2} = 8000\ rpm \quad \text{then} \quad p_2 = 1.9669 \quad p_1 = 842.5708 \qquad (6.36)
\end{aligned}$$

(6.37)

Moreover, for the MG2, the maximum and the minimum torque will be calculated at each moment with a specific ω_{mg2}. As a result, we consider the following constraints on MG2

$$T_{mg2,min}(\omega_{mg2}(k)) \leq T_{mg2}(k) \leq T_{mg2,max}(\omega_{mg2}(k)) \quad (6.38)$$

where $T_{mg2,min}(\omega_{mg2}(k))$ and $T_{mg2,max}(\omega_{mg2}(k))$ are calculated from motor maximum/minimum curve. Since MG2 torque is constrained to be within the maximum and minimum available torque, MG2 power will also be inside the maximum and minimum power, so checking power constraint would be redundant.

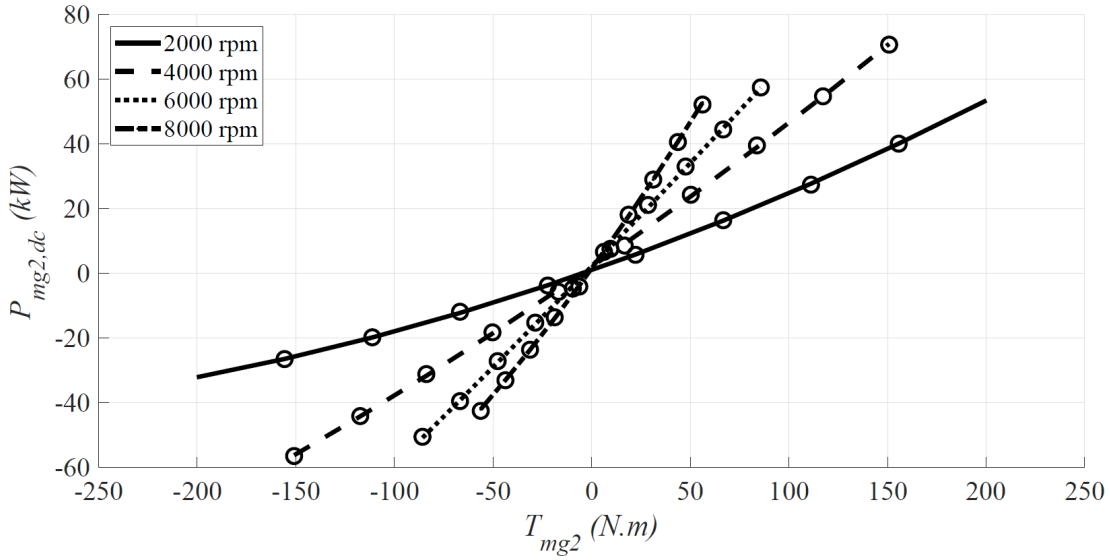

Figure 6.3: Convex quadratic model for MG2 input dc power for some given speeds. Average rms error for these four models is 0.161 kW.

For the MG1 however, neither speed nor torque is available for a given driving cycle, and they are problem parameters to be determined. Hence, we consider a simple convex quadratic model for the MG1 dc power and corresponding power electronics as

$$P_{mg1,dc}(k) = q_2 \cdot P_{mg1}(k)^2 + q_1 \cdot P_{mg1}(k) + q_0 \tag{6.39}$$

in which $q_2 \geq 0$, q_1, and q_0 are model parameters. Again we can consider $q_0 = 0$ to get zero dc power for given zero mechanical power. Unlike MG2, model parameters are not speed-dependent. We use the same approach as ICE to use the actual MG1 data points, obtained by the developed high-fidelity model to find the q_2 and q_1. Figure 6.4 shows the defined model as well as some operational power points for the MG1. Parameters are as following for power unit in Watts

$$q_2 = 2.069e-06 \quad q_1 = 1.003 \tag{6.40}$$

Following constraints also hold for the MG1

$$P_{mg1,min} \leq P_{mg1}(t) \leq P_{mg1,max} \tag{6.41}$$

$$T_{mg1,min} \leq T_{mg1}(t) \leq T_{mg1,max} \tag{6.42}$$

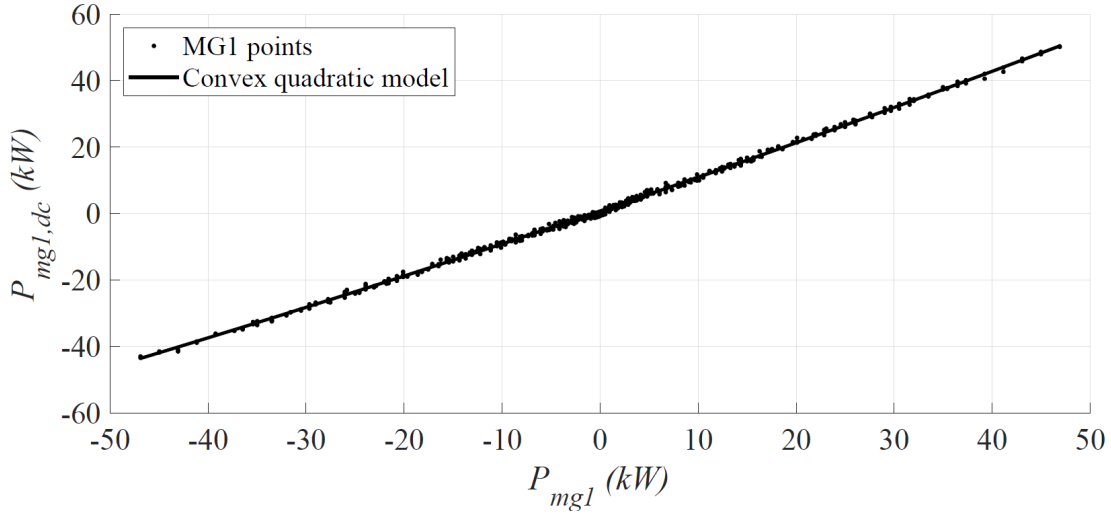

Figure 6.4: Convex quadratic model for MG1 dc power as a function of MG1 mechanical power. Overall rms error for this models is 0.341 kW.

where $P_{mg1,max}$ and $T_{mg1,max}$ are mentioned in Table 6.1 and are considered to be same with the absolute value of $P_{mg1,min}$ and $T_{mg1,min}$, respectively.

6.2.5 Battery

Power balance at battery terminal is obtained by following equation

$$P_b(k) = P_{aux} + P_{mg1,dc}(k) + P_{mg2,dc}(k) \tag{6.43}$$

where P_b is the battery electric power and P_{aux} is the auxiliary load on the battery, assumed to be a constant value for our analysis but can be replaced by any other feasible complex equation.

As we discussed before in the section regarding the battery model in Chapter 5, we can consider the following equation for battery current

$$I_b = \frac{V_{oc} - \sqrt{V_{oc}^2 - 4R_0P_b}}{2R_0} \tag{6.44}$$

We take the same approach as [97, 98] to approximate a convex battery model. First, we consider an affine function of battery charge for battery OCV as follows

$$V_{oc} = \frac{Q_b(t)}{\tilde{C}} + V_0 \tag{6.45}$$

where $\tilde{C}$ denotes battery equivalent capacitance. Constant values of V_0 and $\tilde{C}$ can be identified by affine approximation of SOC-OCV curve, similar to Figure 6.5, since there is a linear relationship between SOC and Q_b. Then, we approximate the stored energy in battery as

$$E_b = \frac{1}{2}\tilde{C}V_{oc}^2 - E_0 \tag{6.46}$$

where E_0 denotes reference battery energy, obtained by following equation

$$E_0 = \frac{1}{2}\tilde{C}V_0^2 \tag{6.47}$$

For a reasonably fine discretization in time, we can use Euler method to write

$$E_b(k+1) = E_b(k) - V_{oc}(k)\, I_b(k)\, \Delta t \tag{6.48}$$

We use (6.48) in combination with (6.44) and (6.45) to finally achieve

$$E_b(k+1) = E_b(k) - \frac{\Delta t}{R\tilde{C}}\left[E_b(k) + E_0 - \sqrt{\left(E_b(k)+E_0\right)\left(E_b(k)+E_0-2R\tilde{C}P_b(k)\right)}\right] \tag{6.49}$$

Note that right-hand side of (6.49) is concave since it is a summation of an affine term plus geometric mean of two terms that are non-negative and affine themselves. Moreover, power and energy limitations on battery are

$$P_{b,min} \leq P_b(t) \leq P_{b,max} \tag{6.50}$$

$$E_{b,min} \leq E_b(t) \leq E_{b,max} \tag{6.51}$$

with $E_{b,min}$ and $E_{b,max}$ as corresponding battery energy for the maximum and minimum battery SOC. Note that all required constant parameters, used in these equations are summarized in Table 6.1.

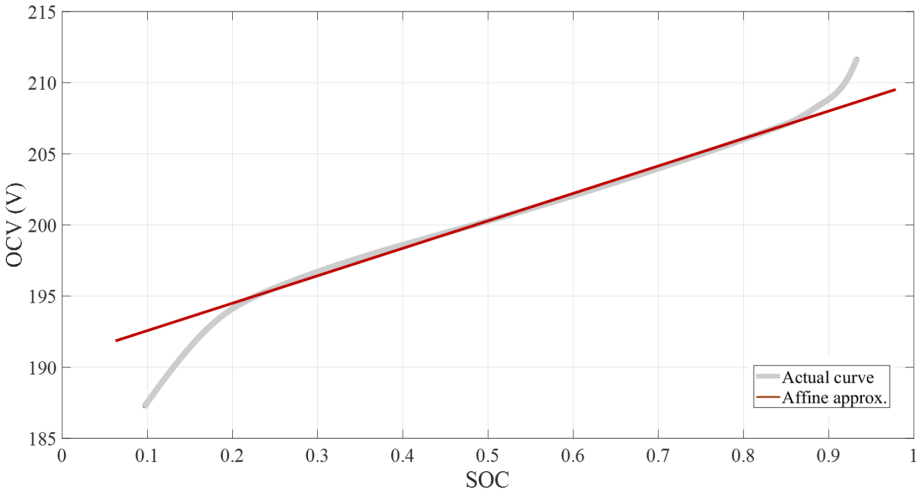

Figure 6.5: Affine approximation of open circuit voltage based on SOC.

6.3 Optimal Control Problem

Using the developed models for the components, we from the optimal control problem for a given driving cycle. We consider the total fuel consumption over the driving cycle as our optimization objective, however, any further objective can be added with a regularizer to form a multi-objective optimization problem. Final optimal control problem has an objective to minimize, subject to some equality/inequality equations. These equations are due to component models and constraints.

To efficiently solve the optimal control problem, we form the problem in the convex optimization problem format. As we discussed before, convex optimization problem is in the following format [72]

$$\begin{aligned} &\text{minimize } f_0(x) \\ &\text{subject to } f_i(x) \leq 0 \qquad i = 1, 2, ...n \\ &\qquad\qquad h_i(x) = 0 \qquad i = 1, 2, ...m \end{aligned} \tag{6.52}$$

where all $f_i(x) \leq 0 \quad i = 1, 2, ...n$ functions should be convex on $x \in \mathbb{R}^n$, and all $h_i(x) \leq 0 \quad i = 1, 2, ...m$ should be an affine function of x. General practice to form a convex optimization problem includes convexification and relaxation. We have done convexification by deriving convex models for vehicle components. Moreover, as we can see, we cannot have convex functions inside equality constraints. In these

cases, equalities are relaxed and replaced with inequalities, so that the overall problem becomes a convex optimization problem. In our case, we will do relaxation for a few constraints, and will make sure that it is not changing the final results, by checking the constraints for the optimal solution.

We express the final optimization problem for offline fuel-efficient EMS of the power-split powertrain for a given driving cycle as

minimize

$$\sum_{k=1}^{N} \mathbf{P_f}(k) \cdot \Delta t \tag{6.53}$$

subject to

$$\mathbf{P_e}(k) + \mathbf{P_{mg1}}(k) + \mathbf{P_{mg2}}(k) \geq \mathcal{P}_{ps}(k) \tag{6.54a}$$

$$\frac{r_1}{1+r_1} \cdot \mathbf{T_e}(k) + r_2 \cdot \mathbf{T_{mg2}}(k) \geq \mathcal{T}_{ps}(k) \tag{6.54b}$$

$$\mathbf{P_f}(k) \geq [\mathbf{P_e}(k) \quad \mathbf{T_e}(k)] \cdot A \cdot \begin{bmatrix} \mathbf{P_e}(k) \\ \mathbf{T_e}(k) \end{bmatrix} + b^T \cdot \begin{bmatrix} \mathbf{P_e}(k) \\ \mathbf{T_e}(k) \end{bmatrix} \tag{6.54c}$$

$$0 \leq \mathbf{P_e}(k) \leq P_{e,max} \tag{6.54d}$$

$$0 \leq \mathbf{T_e}(k) \leq T_{e,max} \tag{6.54e}$$

$$\mathbf{P_{mg2,dc}}(k) \geq p_2(k) \cdot \mathbf{T_{mg2}}(k)^2 + p_1(k) \cdot \mathbf{T_{mg2}}(k) \tag{6.54f}$$

$$\mathbf{P_{mg2}}(k) = \mathbf{T_{mg2}}(k) \cdot \omega_{mg2}(k) \tag{6.54g}$$

$$T_{mg2,min}(k) \leq \mathbf{T_{mg2}}(k) \leq T_{mg2,max}(k) \tag{6.54h}$$

$$\mathbf{P_{mg1}}(k) = -\mathbf{P_e}(k) + \left(\frac{r_1 \cdot r_d}{(1+r_1) \cdot r_w} \cdot \mathbf{T_e}(k) \cdot v(k) \right) \tag{6.54i}$$

$$\mathbf{T_{mg1}}(k) = -\mathbf{T_e}(k)/(1+r_1) \tag{6.54j}$$

$$\mathbf{P_{mg1,dc}}(k) \geq q_2 \cdot \mathbf{P_{mg1}}(k)^2 + q_1 \cdot \mathbf{P_{mg1}}(k) \tag{6.54k}$$

$$P_{mg1,min} \leq \mathbf{P_{mg1}}(k) \leq P_{mg1,max} \tag{6.54l}$$

$$T_{mg1,min} \leq \mathbf{T_{mg1}}(k) \leq T_{mg1,max} \tag{6.54m}$$

$$\mathbf{P_b}(k) = P_{aux} + \mathbf{P_{mg1,dc}}(k) + \mathbf{P_{mg2,dc}}(k) \tag{6.54n}$$

$$\mathbf{E_b}(k+1) \leq \mathbf{E_b}(k) - \frac{\Delta t}{R\tilde{C}}\left[\mathbf{E_b}(k) + E_0 - \sqrt{(\mathbf{E_b}(k) + E_0)\left(\mathbf{E_b}(k) + E_0 - 2R\tilde{C}\mathbf{P_b}(k)\right)}\right] \quad (6.54o)$$

$$P_{b,min} \leq \mathbf{P_b}(k) \leq P_{b,max} \quad (6.54p)$$

$$E_{b,min} \leq \mathbf{E_b}(k) \leq E_{b,max} \quad (6.54q)$$

$$\mathbf{E_b}(N+1) = \mathbf{E_b}(1) \quad (6.54r)$$

with $k = 1, 2, ..., N$. Note that we have shown the optimization parameters in non-italic bold font to differentiate these parameters with other constant parameters. Table 6.1 shows the summary of constant parameters, used in the optimization problem. In the optimal control formulation, it is important to note that (6.54c), (6.54f), (6.54k), and (6.54o) are the relaxed version of (6.20), (6.35), (6.39), and (6.49), respectively. Since all of these equations are related to the energy consumption, inequality gap will always yield in unnecessary energy dissipation. For instance, inequality gap in (6.35) would result in larger $P_{mg2,dc}$ which in turn would deplete battery more by increasing P_b. As a result, for the case of optimal solution, we expect that these inequalities should hold tight to achieve smaller optimization objective. We will check this assumption later in this chapter.Concludingly, developed optimization problem is in the form of canonical convex optimization problems.

Table 6.1: Optimization Parameters

Category	Parameter	Symbol	Value
Vehicle	Frontal area	A	2.5 m^2
	Air density	ρ	1.23 kg/m^3
	Drag coefficient	c_d	0.25
	Total vehicle mass	m	1480 kg
	Gravity constant	g	9.81 m/s^2
	Rolling res. coef.	c_r	0.02
	Wheel radius	r_w	0.31 m
	Wheel efficiency	η_w	0.97
Power-split	PGS1 ratio	r_1	78/30
	PGS2 ratio	r_2	58/22
Drivetrain	Gear ratio	r_d	3.268
	Efficiency	η_d	0.95
MG1	Max. Torque	$T_{mg1,max}$	45 $N.m$
	Max. Power	$P_{mg1,max}$	42 kW
MG2	Max. Torque	$T_{mg2,max}$	207 $N.m$
	Max. Power	$P_{mg2,max}$	60 kW
Battery	Internal res.	R_0	0.32 Ω
	Equivalent capacitance	$\tilde{C}$	169.56 F
	Reference energy	E_0	2.608 MJ
	Maximum power	$P_{b,max}$	27 kW
Engine	Max. Power	$P_{e,max}$	73 kW
	Max. Torque	$T_{e,max}$	142 $N.m$

6.4 Results

We have considered expressing the optimzition problem in optimization programming languages (OPL) of CVX and YALMIP. We have also evaluated the performance of a few solvers such as SDPT3 [99], MOSEK [94], and Gurobi [100]. Finally, we solve the optimization problem using a disciplined convex programming package (CVX) in MATLAB [93] for different driving cycles. For most of the cases, we use SDPT3 numerical solver [99] to solve the optimization problem. All of the following numerical processes have been done using a personal computer with 3.40 GHz Intel Core i7 processor.

6.4.1 Relaxations

We used relaxations on some of the optimization constraints to form a convex optimization problem. We also mentioned that in the case of the fuel-optimal solution, these constraints should hold with equality to prevent unnecessary energy dissipation. As promised, in this section, we will check the validity of our assumptions to assure that relaxations have not changed the optimal results. Figure 6.6 shows the left hand and right hand sides of (6.54c), (6.54f), (6.54k), and (6.54o). As this figure suggests, two sides of these inequalities perfectly match each other, which means that these inequalities hold tight for the optimal results, and relaxations are valid.

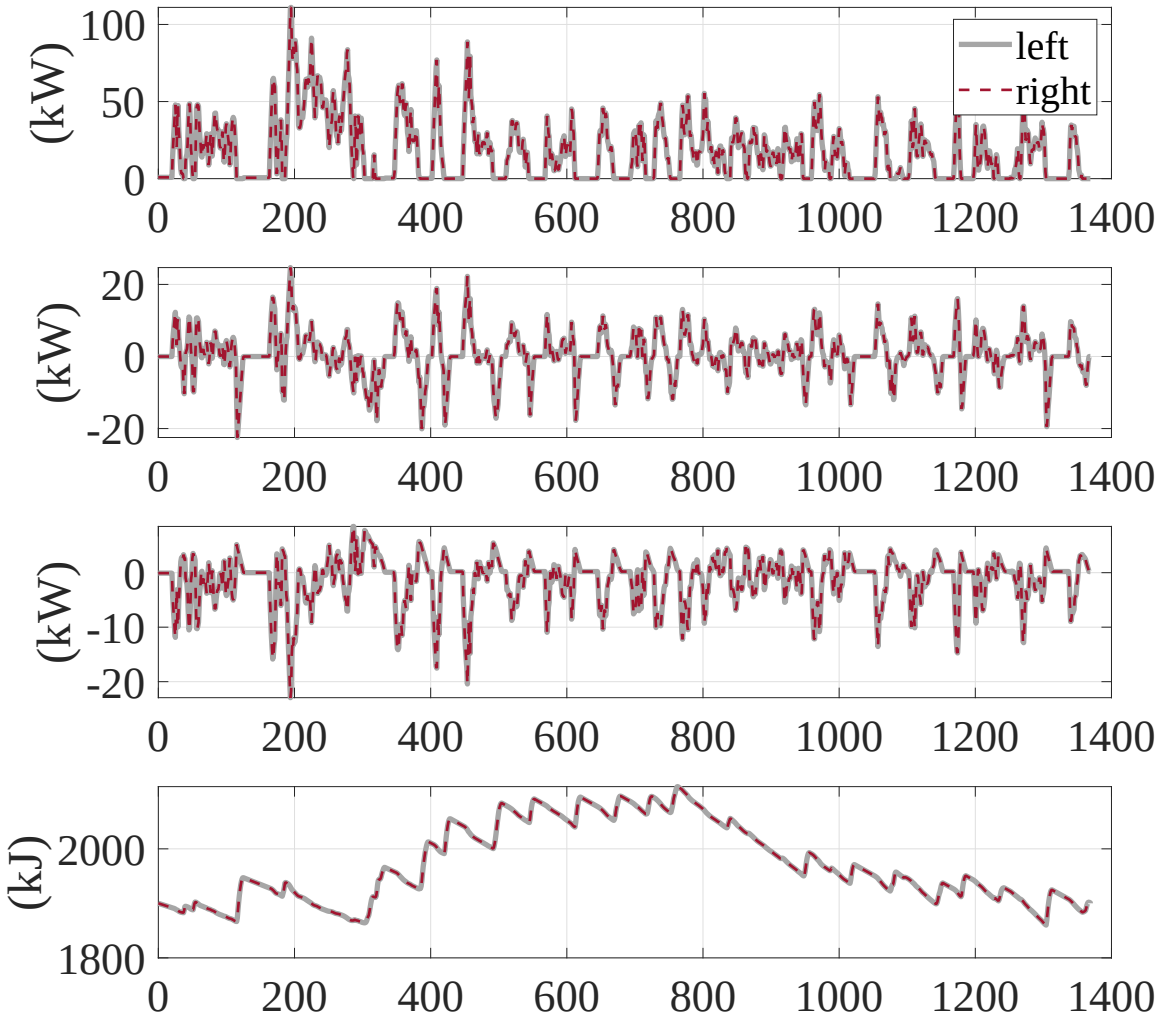

Figure 6.6: Both sides of (6.54c), (6.54f), (6.54k), and (6.54o) inequalities, sorted in order from top to bottom.

6.4.2 Results on Convex Model

In order to better evaluate the optimal results, we have also implemented DP on the convex model using the same approach as [91, 101], which is among the most efficient DP implementation packages in MATLAB. For the case of DP, in addition to N which is the total discretization intervals in time, there should be more hyper-parameters, set to decide about the discretization in states and control inputs for the dynamical system which is powertrain. We use SOC as the state with N_s number of discrete points and T_e, ω_e, and T_{mg2} as control inputs with N_{u_1}, N_{u_2}, and N_{u_3} points, respectively. N_s, N_{u_1}, N_{u_2}, and N_{u_3} are tuned to get a reasonable trade-off between computational time and the optimality of the results.

Figure 6.7, 6.8, and 6.9 show the optimal results, obtained by both solving the convex problem and DP, for the UDDS, JC08, and NEDC driving cycles. We consider the initial SOC of 37%, and upper and lower boundaries on SOC to be 80% and 20%, respectively.

Discrepancies in parameter trajectories are mostly due to the sub-optimality of DP. We should recall that optimality of DP substantially depends on initialization of the hyper-parameters. Sub-optimality gap can be improved using finer discretization for state variable and control inputs, which would increase processing time in return. Since SOC has a nature of integrating the errors over time, the discrepancy is more observable in the SOC trajectories. Apart from this, the output from both methods shows good agreement and trajectory trends are fairly comparable. We observed same behavior for all tested driving cycles.

Table 6.2 shows the comparison of DP and convex optimizer over convex model in terms of fuel consumption and the computation time for the tested driving cycles. Percentage of the differences are calculated based on the DP results. As it can be understood from this table, on the convex vehicle and powertrain model, the convex optimization problem solver is producing the absolute optimal results, within the numerical constraints that any numerical solver has. DP is also expected to generate optimal results theoretically. However, since DP implementation has discretization of the state and the control inputs, the results are slightly sun-optimal as the table suggests, around 2.40% on average for the tested driving cycles. Besides obtaining the optimal results, the substantial advantage of the convex approach is the computational time. The convex solver needs 97.43% less time on average, compared to DP, to

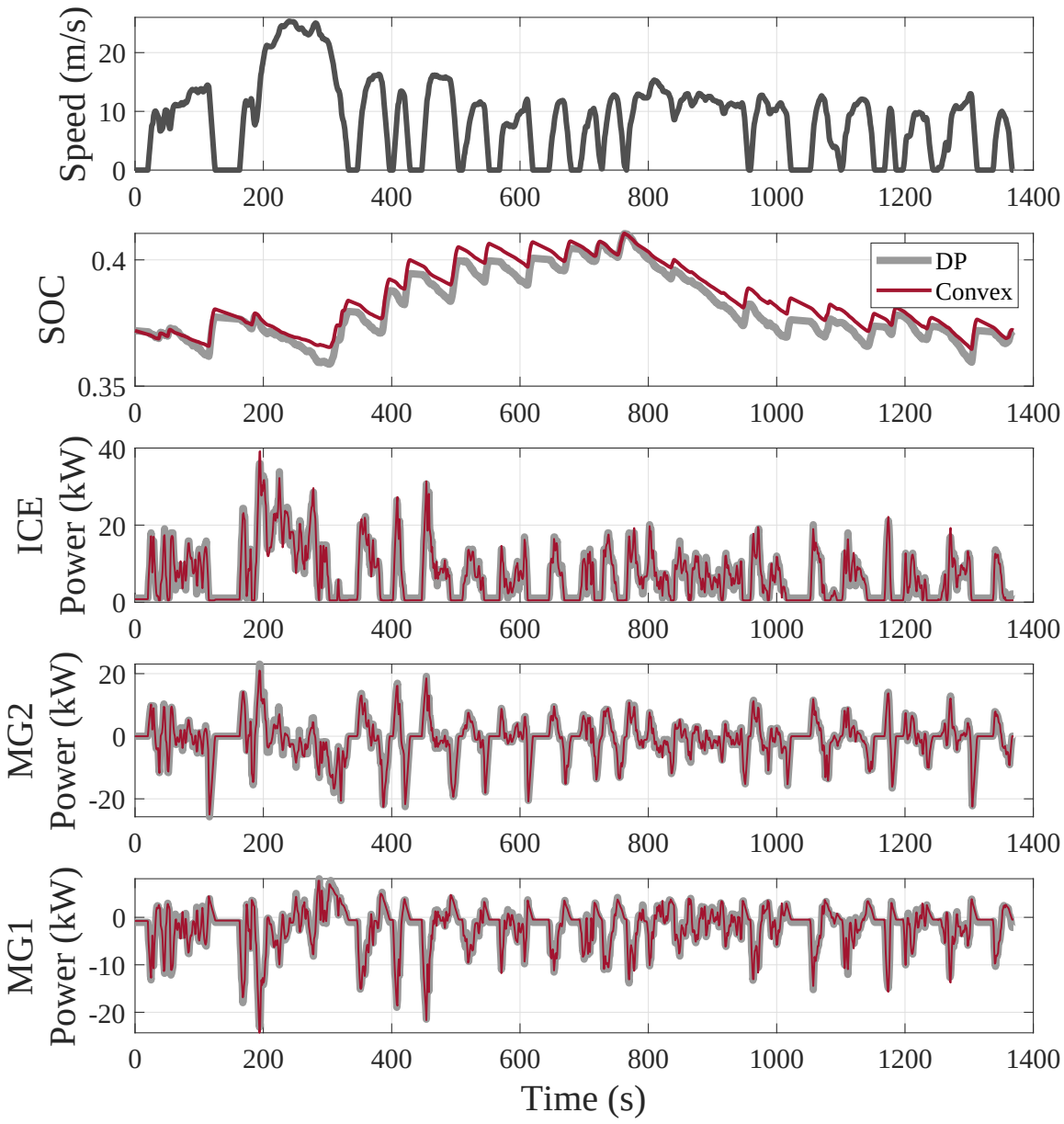

Figure 6.7: Result of battery SOC and mechanical power of Engine, MG2, and MG1, obtained from both DP and the convex solver for the UDDS driving cycle.

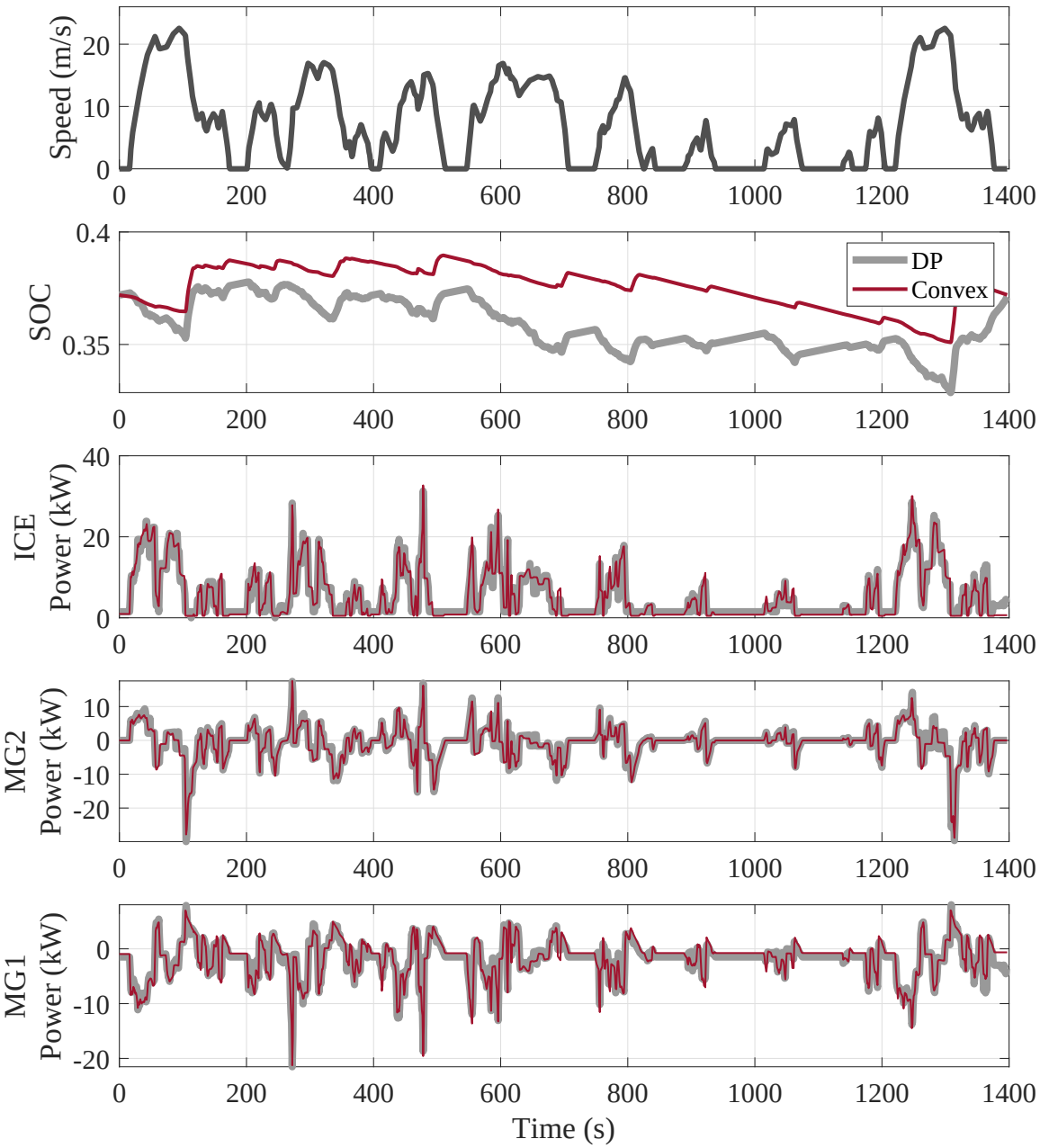

Figure 6.8: Result of battery SOC and mechanical power of Engine, MG2, and MG1, obtained from both DP and the convex solver for the JC08 driving cycle.

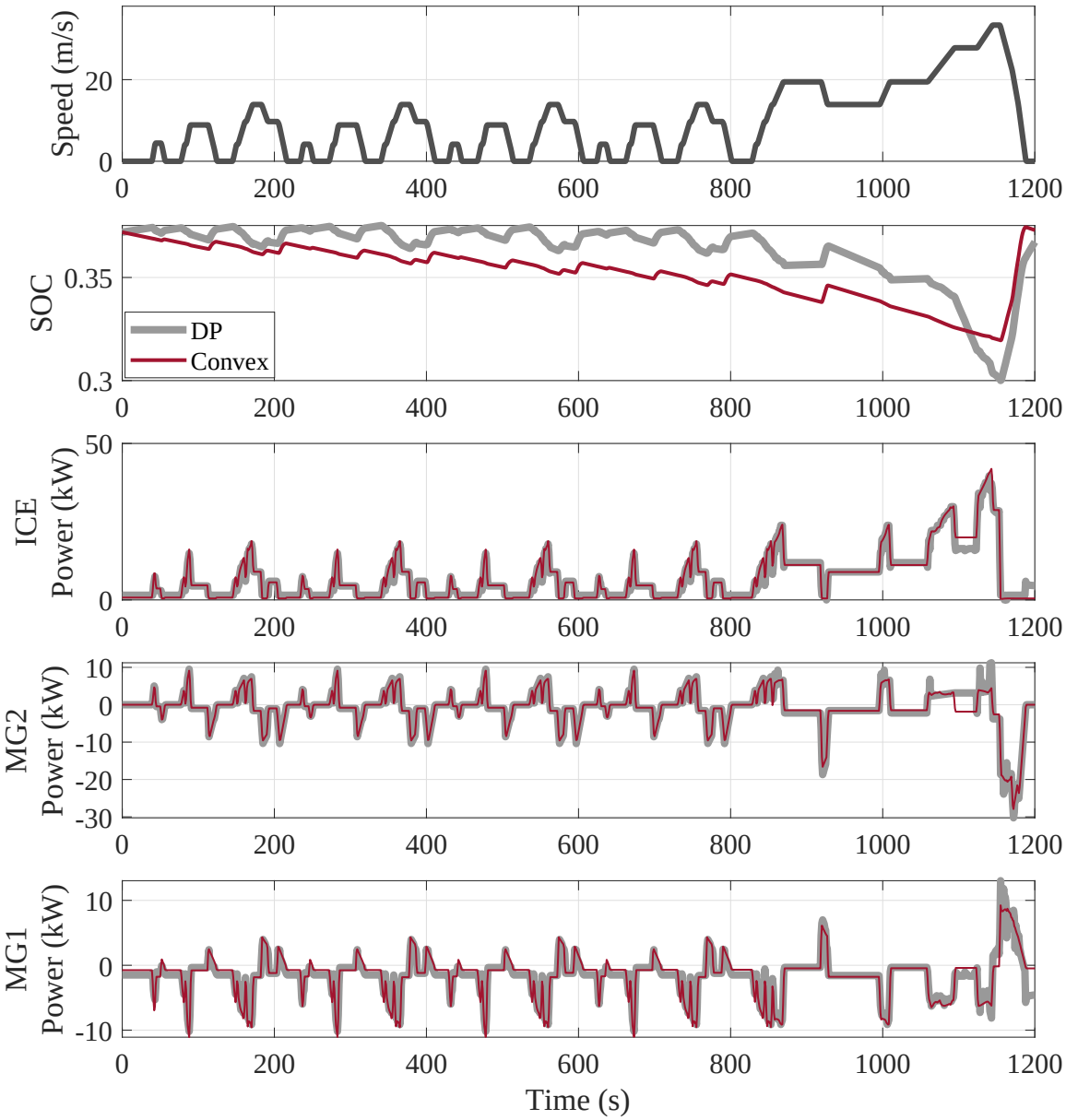

Figure 6.9: Result of battery SOC and mechanical power of Engine, MG2, and MG1, obtained from both DP and the convex solver for the NEDC driving cycle.

solve the optimization problem for the tested driving cycles. To realize how time-efficient convex solver is in dealing with vast problems, we note that for the case of UDDS driving cycle, for instance, the optimization problem has 16,180 constraints and 1,919,111 optimization variables in total.

Additionally, for the long driving cycles (time-wise) such as UDDS, the increase in the CPU time for the convex solver is less considerable than the increase in DP CPU time. Figure 6.10 and 6.11 show a better illustration of comparison of DP and convex approach in terms of the fuel consumption and the CPU time.

Table 6.2: Convex model results

Cycle	Quantity	Convex	DP	Difference
Steady State	Fuel consumption (g)	235.65	239.68	1.68%
	CPU time (s)	41.88	1308.10	96.80%
UDDS	Fuel consumption (g)	232.12	238.24	2.57%
	CPU time (s)	83.02	3729.63	97.77%
US06	Fuel consumption (g)	352.34	362.56	2.82%
	CPU time (s)	42.46	1446.69	97.07%
Highway	Fuel consumption (g)	383.81	391.29	1.91%
	CPU time (s)	54.19	1728.99	96.87%
NEDC	Fuel consumption (g)	290.31	297.51	2.42%
	CPU time (s)	57.54	3177.32	98.19%
JC08	Fuel consumption (g)	261.87	269.08	2.68%
	CPU time (s)	78.25	3702.47	97.89%

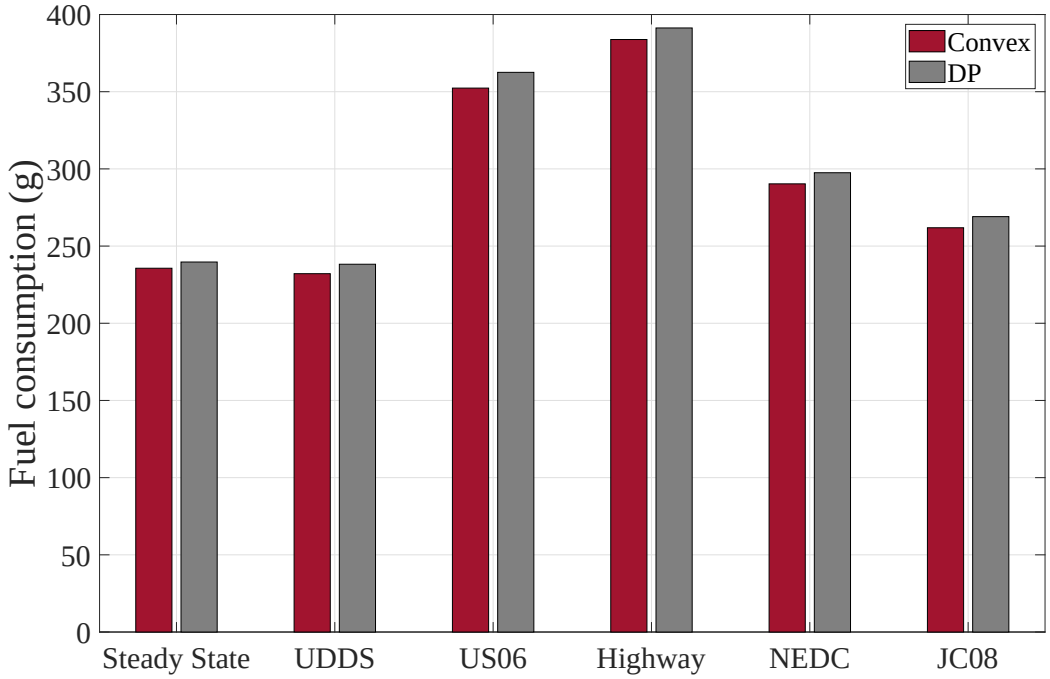

Figure 6.10: Result of fuel consumption, obtained by convex and DP approach, for tested driving cycles.

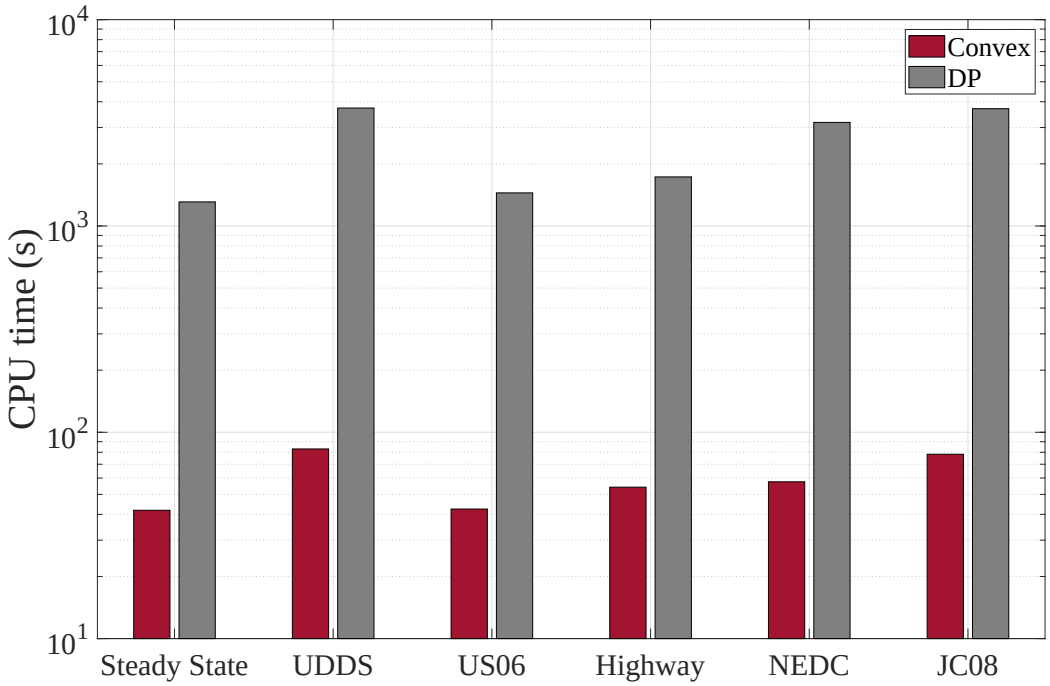

Figure 6.11: Result of computational time, obtained by convex and DP approach, for tested driving cycles. Note that y-axis is in logarithmic scale, so that results of convex approach are observable.

6.4.3 Trade-off Curve

As it is shown in the last discussion, convex optimization produces globally optimal results in an insignificant amount of time. This characteristic can be employed in applications which need solving optimal control problem iteratively for different initialization. Examples of these applications, as discussed in the first section of this chapter, is regarding design and real-time implementation.

To better show this capability, we examine a compelling case. In the optimization problem, we remove the strict constraint of (6.54r) and rewrite the objective function to be

$$\mu \cdot (E_b(1) - E_b(N+1)) + \sum_{k=1}^{N} P_f(k) \cdot \Delta t \tag{6.55}$$

The new assumption means that there is no strict constraint that initial and final battery state of energy or SOC should be the same. In this case, the optimization can be interpreted as a scalarized multi-objective optimization, trying to minimize fuel consumption and overall battery energy difference simultaneously with the trade-off constant of $\mu \geq 0$. Figure 6.12 shows the pareto-optimal curve for the new optimization problem, which is resulted by iterating the optimization problem for different values of $\mu : 0 \rightarrow \infty$. The shaded area also shows the feasible set, and any point in this area is correlated to a particular strategy to manage the power flow. Since the optimization problem is convex, shaded feasible set is also a convex set. In the feasible set, any point which is on the left and bottom of another point, is a result of a better strategy, since it uses less overall energy. However, points on the pareto-optimal front have no advantage to each other, and any of these points can be chosen as the optimal strategy based on the value of μ.

The derivative of the pareto-optimal curve indicates a trade-off between optimization objectives. From another perspective, λ can be seen as the equivalent factor in ECMS method, converting the electrical energy from the battery to the equivalent amount of fuel energy on the whole driving cycle. This figure clearly shows that for about right half side of ΔSOC axis, the trade-off between the total fuel consumption and gain or loss in the battery state of charge stays linear. However, the trade-off is getting harder in the left half of ΔSOC axis. This means much more fuel should be consumed to gain the same advantage in ΔSOC. To explain this, consider that Δm_1 grams of fuel should be consumed more to end up with $\Delta\text{SOC} = -31$ rather than $\Delta\text{SOC} = -30$. Now, to move from $\Delta\text{SOC} = -31$ to $\Delta\text{SOC} = -32$, Δm_2 more fuel is needed. We

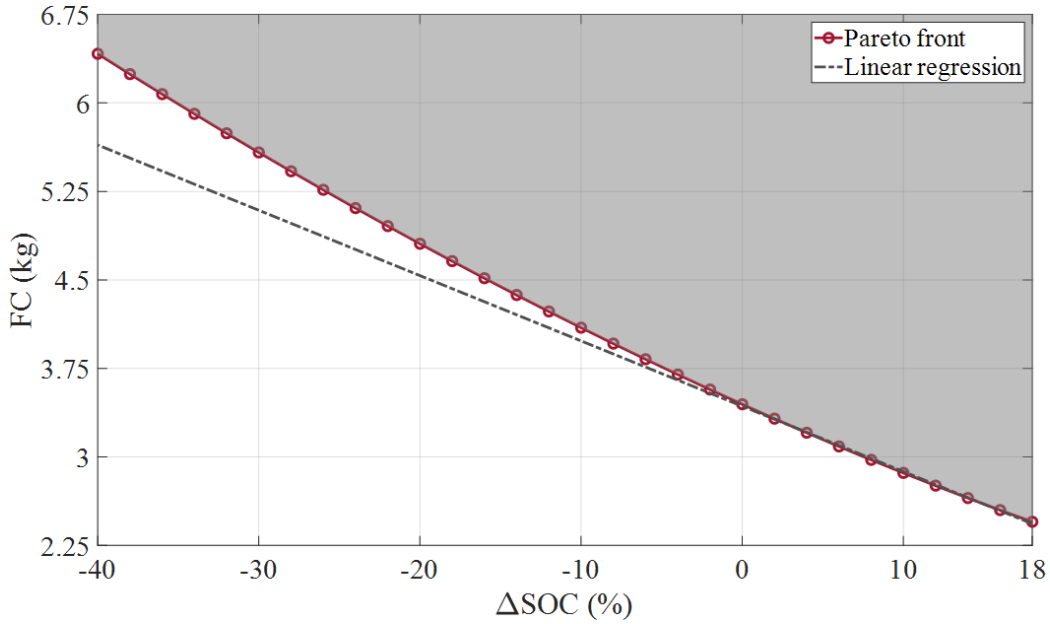

Figure 6.12: Pareto-optimal front for the multi-criterion convex optimization for US06 driving cycle. Vertical axis denotes fuel consumption. For horizontal axis, Difference of final and initial energy of battery is replaced by corresponding difference in state of charge which is $\Delta\text{SOC} = \text{SOC}(1) - \text{SOC}(N+1)$.

observe that $\Delta m_2 - \Delta m_1$ keeps growing as we move toward the left half of ΔSOC axis.

6.4.4 Results on High-fidelity Model

Although the convex approach to obtain the optimal EMS of the convex model outperforms DP by a large margin, it is important to check how the results of convex approach are applicable to the actual nonlinear vehicle model. For this purpose, developed high-fidelity model is highly useful. In this section, we will apply the obtained EMS of the convex approach on the high-fidelity model, and compare the results with DP results. Implemented DP in this section differs from the previous section since DP is now implemented on the nonlinear model.

We follow the following procedure. We get the optimal results of convex approach for different driving cycles. We are particularly interested in torque and power trajectories of the components. Then we make a control input signal out of these trajectories and apply the signals to the nonlinear vehicle model in the high-fidelity model. Finally, we check the overall fuel consumption and the final SOC.

Table 6.3 shows the comparison of the convex approach, DP, and built-in rule-based strategy performance on the high-fidelity model for the tested driving cycles. For the

Table 6.3: DP vs Model vs Convex

		Steady state	UDDS	US06	Highway	NEDC	JC08
FC (g)	DP	250.71	246.06	376.47	410.20	311.15	282.32
	Model	299.36	315.99	556.62	511.07	390.50	350.08
	Convex	257.11	251.21	384.73	425.16	321.70	289.76
	diff. 1 (%)	-16.25	-22.13	-32.37	-19.74	-20.32	-19.36
	diff. 2 (%)	-14.11	-20.50	-30.88	-16.81	-17.62	-17.23
	diff. 3 (%)	2.55	2.09	2.19	3.65	3.39	2.63
Final SOC (%)	DP	37.04	37.05	36.96	37.04	37.03	36.93
	Model	37.10	38.08	35.95	37.27	38.02	36.26
	Convex	38.57	35.72	39.15	37.75	38.52	38.25

results of this table, the staring SOC is 37%. Also the values of diff. 1, diff. 2, and diff. 3 are obtained using following equations

$$\text{diff.1} = \frac{FC_{DP} - FC_{Model}}{FC_{Model}} \times 100 \tag{6.56}$$

$$\text{diff.2} = \frac{FC_{Convex} - FC_{Model}}{FC_{Model}} \times 100 \tag{6.57}$$

$$\text{diff.3} = \frac{FC_{Convex} - FC_{DP}}{FC_{DP}} \times 100 \tag{6.58}$$

Table 6.3 shows that the performance of results from the convex approach are slightly deteriorated on the high-fidelity model. Convex approaches generate 2.75 % sub-optimal results on average on the nonlinear model compared to DP. This is mostly due to loss of accuracy in the constraints and the convexification process. However, since we took a novel approach to perform convex modeling which was more complex but accurate instead, the sub-optimality of the convex results on high-fidelity model is acceptable. Finally, we can observe that the result of convex approach produces

19.53 % more fuel-efficient results compared to the embedded rule-based strategy. This shows the existing considerable potential to improve the fuel efficiency just by using more advanced control strategy.

Figure 6.13 shows a better illustration of DP, convex, and rule-based approach comparison.

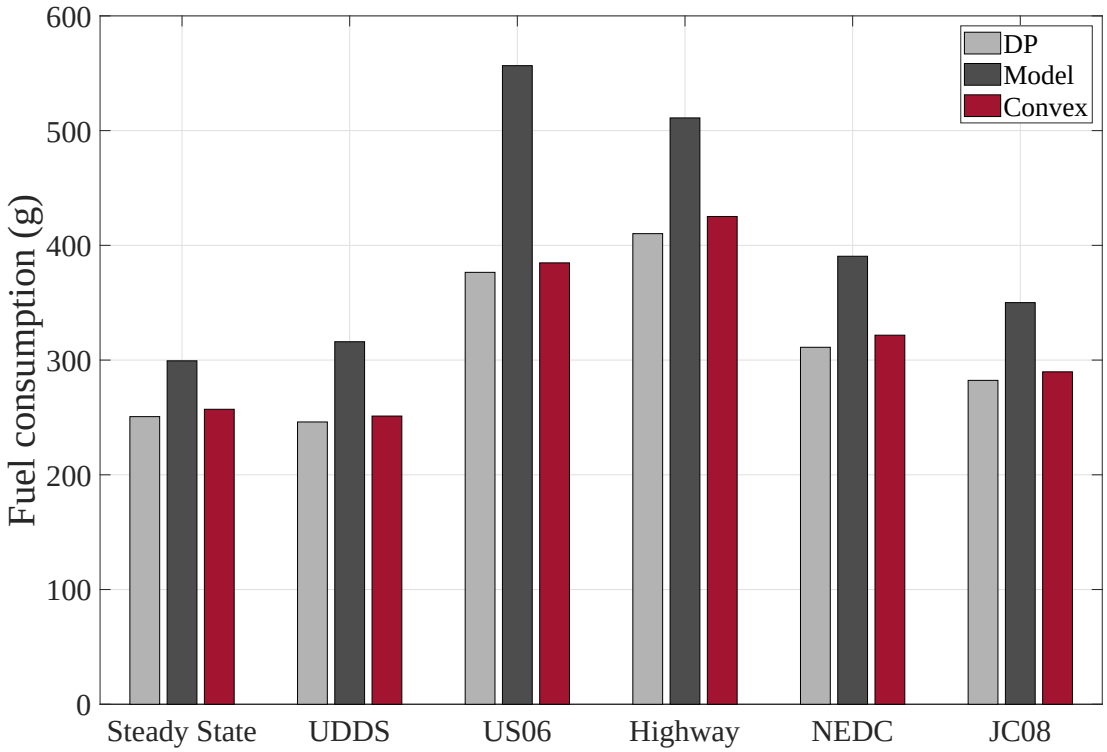

Figure 6.13: Results of fuel consumption, obtained by DP, rule-based, and convex approaches on high-fidelity model, for tested driving cycles.

Chapter 7

Real-time Energy Management Strategy for an Autonomous Vehicle

7.1 Introduction

In the previous chapter, we discussed the convex optimization approach for obtaining the control strategy to manage the power flow. The mentioned approach clearly signified the potential of improvement in fuel efficiency by employing a more advanced real-time strategy in energy management of the hybrid electric powertrain. Primary reasons for the superior performance of offline strategies is the access to the driving cycle in advance and loose constraints on computational time. However, this is not the case for real-time applications.

In this chapter, we are introducing a novel approach to address the EMS for an autonomous HEV (A-HEV). We believe the impact of autonomous mobility on vehicular transporation is such impressive that most of the vehicle elements, particularly regarding the control, should be re-designed accordingly. As a result, we discuss an autonomous-specific energy management strategy (ASEMS) for the mentioned powertrain. Examples of existing A-HEVs are Fiat-Chrysler Pacifica for Waymo fleet, Ford Fusion for Argo AI fleet, and Uber-Volvo XC90. These fleets are mainly focused on robotaxis, but it is interesting to note that Fiat Chrysler has announced a partnership with Aurora to create a fleet of commercial vans [102]. It can be clearly understood that

the total number of A-HEVs is growing rapidly. Almost for all of the existing A-HEVs, autonomous technology and the hybrid supervisory systems are separately developed and installed. Vehicles with installed and finalized powertrains are provided to the company, responsible for autonomous systems. These vehicles might have just minor changes in design, so that vehicle can accommodate extra devices for autonomous driving, or minor improvements in ADAS. Despite the ever-increasing prevalence of autonomous vehicles and substantial improvement potential in fuel-economy as a result of availability of the future driving data, this problem has not been thoroughly analyzed yet. Thus, to our knowledge, potentials of autonomous driving have not been investigated extensively to improve the EMS of the hybrid electric powertrain.

In this work, we take a unique approach to investigate the real-time EMS problem for A-HEVs. There is a common trend in real-time EMS analysis in the literature that either the real-time control performance is improved using the history of the driving data, or employing predicted driving condition. While showing desirable performance for regular HEVs, further enhancements on EMS is feasible by focusing on the autonomous driving aspect.

In this chapter, we use a more realistic approach, and integrate the EMS with motion planning problem of an A-HEV. Hierarchically, motion planning occurs after scene perception and situation awareness and should guarantee safe, comfortable, and feasible operation. While the generic motion planning problem is highly complex, in this section, we assume a simpler case. To perform the proof-of-concept without getting involved in scene perception, scene understanding, and situation awareness modules of AV, we consider following assumptions regarding the route

1. A-HEV operates in a clear route, with no obstacle interference.

2. Route data, including driveable space with identified boundaries is provided up to a distance horizon of H_d in front of the vehicle. As the vehicle moves forward, horizon also recedes in the spatial domain.

3. Route is part of the selected racing tracks. These tracks are Suzuka and Gilles Villeneuve racing tracks, shown in Figure 7.1 and 7.2.

Suzuka and Gilles Villeneuve circuit has been used for many racing events, particularly in the Formula One competition. In our case, using these race tracks is mostly to fix the framework and the route in which vehicle would operate and has less racing-related

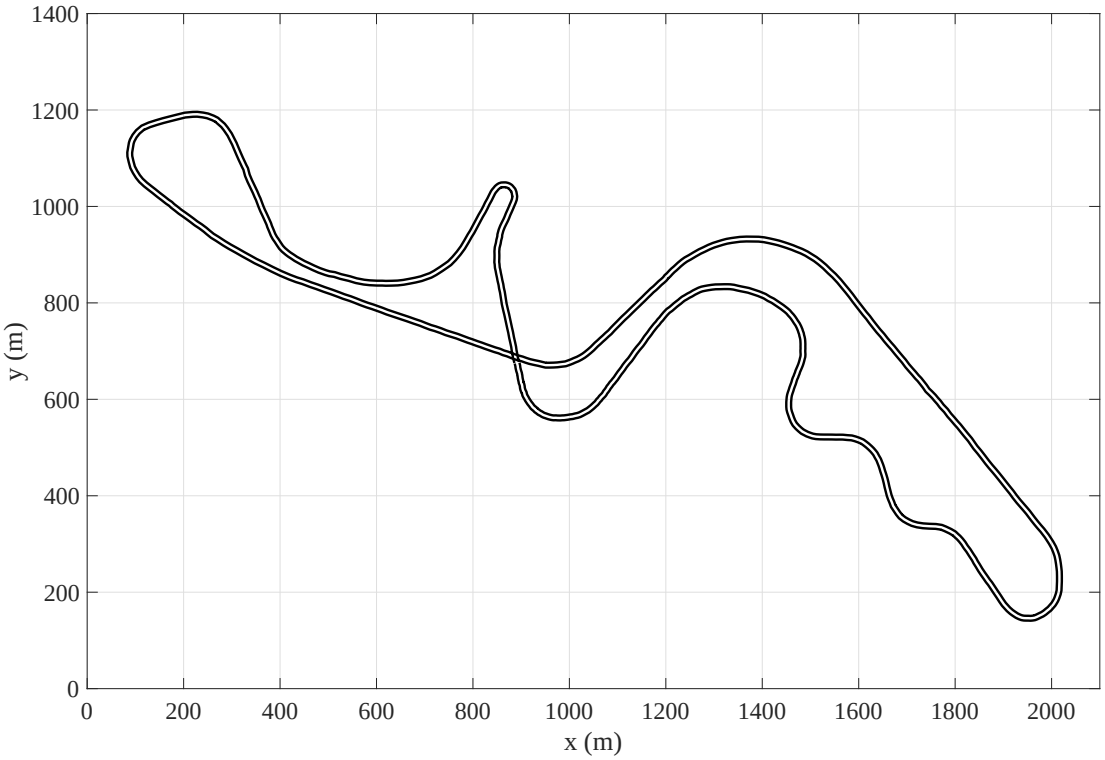

Figure 7.1: Layout of Suzuka circuit in Japan. Track length is 5807 m.

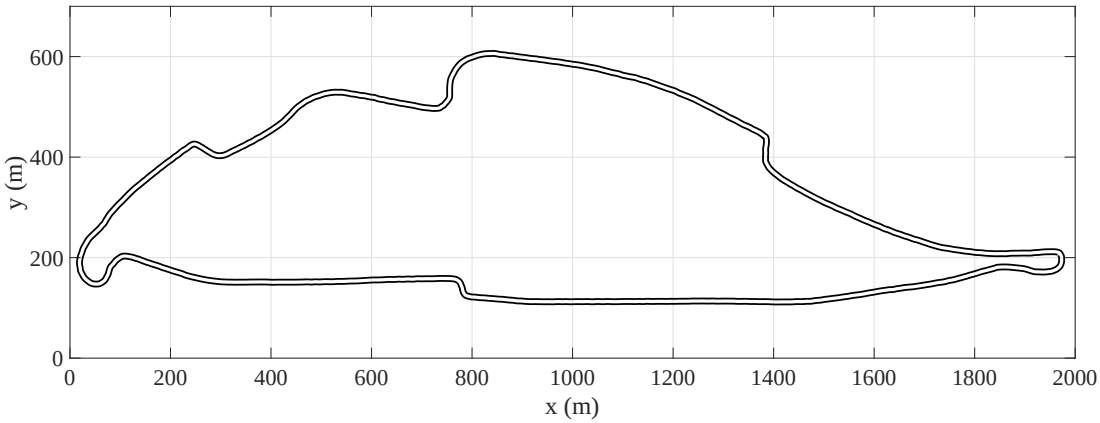

Figure 7.2: Layout of Gilles Villeneuve circuit in Montreal, Canada. Track length is 4361 m.

implication on our work. We should also note that we consider a flat version of these circuits, where we discard any road grade, banking or superelevation in the road geometry. In the rest of this chapter, we will present optimization-based algorithms to deal with path planning and trajectory planning of the vehicle in the race track. Then,

we will use the obtained motion data to address the EMS using model predictive control (MPC) approach, discussed in Chapter 4. This framework provides the required degree of abstraction for real-time EMS analysis for an A-HEV without getting obsessed with unnecessary complex aspects of autonomous mobility.

7.2 Path Planning

Deciding about the desired path between two points depends on the required objectives. Parameters such as path length, travel time, comfort, and physical obstacles affect the planned path. The output of the path planner creates a reference path for system controllers to follow. In our case, the objective is to find a path within the current location of the vehicle up to the observable horizon, considering the discussed three assumptions. Moreover, path planning will be performed in a receding horizon manner, which means as the vehicle travels further in the track, new segment of the road will be included and path planning will be performed again.

In this section, we take a similar approach as [37, 103, 104] to address the path planning problem for an autonomous vehicle by solving an optimization problem. First, we will form the discrete spatial domain optimization problem using vehicle dynamics and the given route, and then specify the path by solving the optimization problem, and finally discuss the results.

7.2.1 Discrete Path Planning

Spatial domain continuous equations of (7.1), (7.2), and (7.3) explain the motion of a the vehicle along the path, shown in Figure 7.3, ignoring the vehicle lateral dynamics

$$\frac{dx(s)}{ds} = \cos(\theta(s)) \tag{7.1}$$

$$\frac{dy(s)}{ds} = \sin(\theta(s)) \tag{7.2}$$

$$\frac{d\theta(s)}{ds} = \kappa(s) \tag{7.3}$$

These equations can be written in the definite integral form of following equations

$$x(s) = x_0 + \int_0^s cos(\theta(\zeta))\, d\zeta \tag{7.4}$$

$$y(s) = y_0 + \int_0^s sin(\theta(\zeta))\, d\zeta \tag{7.5}$$

$$\theta(s) = \theta_0 + \int_0^s \kappa(\zeta)\, d\zeta \tag{7.6}$$

As inferred from these equations, vehicle path, $z(s) = (x(s), y(s))$, is only a function of the path arc-length, s, path curvature, $\kappa(s)$, and the vehicle initial state, $(x(s_0), y(s_0), \theta(s_0))$. As a result, problem of path planning from the initial state up to a horizon can be just seen as obtaining the $\kappa(s)$. This simple model of a vehicle on a path is shown in Figure 7.3.

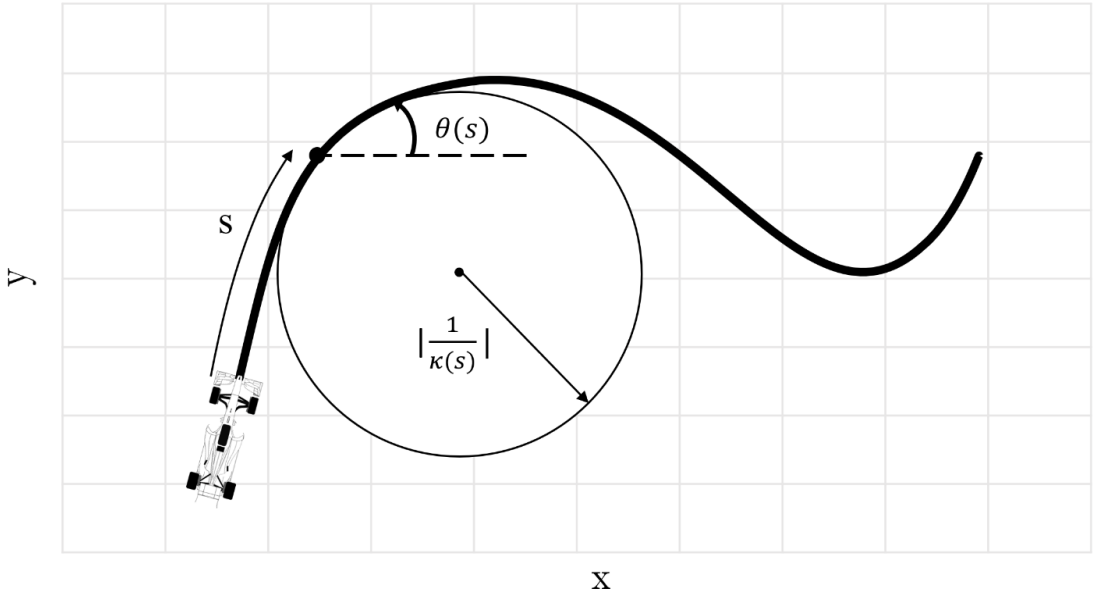

Figure 7.3: Schematic of a vehicle following a path. Vehicle coordinates, x and y, as well as orientation, θ, and path curvature, κ, are assumed to be dependent on spatial variable of s.

The route is given as the derivable road ahead of the vehicle with road boundaries. For the given route, we consider that the desired path to follow is the middle line between the boundaries of the road. We consider that this line is given with the road boundaries with a fine resolution in spatial parameter, s. In case the middle line is not given, and route data just includes the road boundaries, this line can be calculated easily as a part of pre-processing. Thus, we assume desired path to follow is available and given in the discrete format as $z_d(i) = \{(x_d(i), y_d(i)) \,|\, i = 0, 1, ..., N\}$. (see Figure 7.4). Assuming that the discretization in spatial parameter s is fairly fine, we can

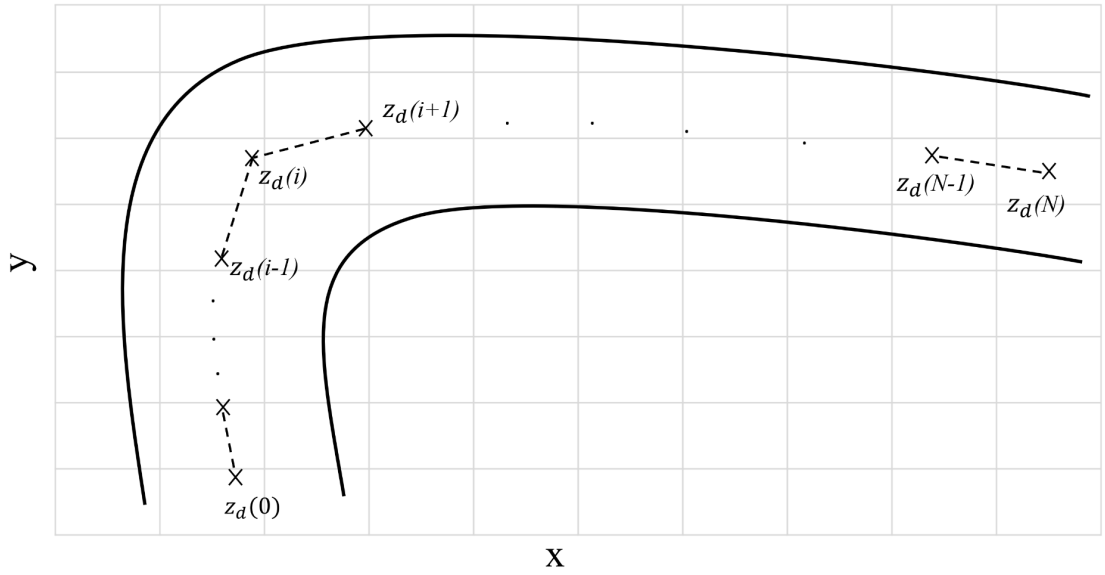

Figure 7.4: Layout of a given route up to a horizon, with road boundaries and the center line to follow.

write

$$\Delta s(i) = s(i+1) - s(i) = Dist(z_d(i), z_d(i+1)) \tag{7.7}$$

where $Dist()$ gives the Euclidean distance of the given 2D points. From control point of view, we can treat (x, y, θ) as vehicle states. Then for a given initial state of $(x(0), y(0), \theta(0))$ and control policy of $K = [\kappa(0)\ \kappa(1)\ ...\ \kappa(N-1)]^T$, vehicle will achieve the actual path of $Z = [z(0)\ z(1)\ ...\ z(N)]^T$, obtained by the following equations for $i = 0, 1, ..., N-1$

$$x(i+1) = x(i) + \Delta s(i) \cdot \cos(\theta(i)) \tag{7.8}$$

$$y(i+1) = y(i) + \Delta s(i) \cdot \sin(\theta(i)) \tag{7.9}$$

$$\theta(i+1) = \theta(i) + \Delta s(i) \cdot \kappa(i) \tag{7.10}$$

Example of route with center path to follow and the actual vehicle path is shown in Figure 7.5. In these equations, (7.8) and (7.9) are nonlinear in K. To achieve linearity, we can use the first and second terms in the Taylor expansion of trigonometric functions around an arbitrary chosen point of $\hat{K} = [\hat{\kappa}(0)\ \hat{\kappa}(1)\ ...\ \hat{\kappa}(N-1)]^T$. As a

result, we can rewrite the equations as

$$x(i+1) = x(i) + \Delta s(i) \cdot \left[\cos(\hat{\theta}(i)) - \mathrm{D}\theta(i) \cdot (K - \hat{K}) \cdot \sin(\hat{\theta}(i))\right] \tag{7.11}$$

$$y(i+1) = y(i) + \Delta s(i) \cdot \left[\sin(\hat{\theta}(i)) + \mathrm{D}\theta(i) \cdot (K - \hat{K}) \cdot \cos(\hat{\theta}(i))\right] \tag{7.12}$$

Also note that in these equations

$$\hat{\theta}(i) = \theta(0) + [\Delta s(0) \quad \Delta s(1) \quad \dots \quad \Delta s(i-1) \quad \overbrace{0 \cdots 0}^{N-i}] \cdot \hat{K} \tag{7.13}$$

$$\mathrm{D}\theta(i) = \left.\frac{\partial \theta(i)}{\partial K}\right|_{K=\hat{K}} = [\Delta s(0) \quad \Delta s(1) \quad \dots \quad \Delta s(i-1) \quad \overbrace{0 \cdots 0}^{N-i}] \tag{7.14}$$

Note that using linear approximation, we could also exclude θ as the state variable.

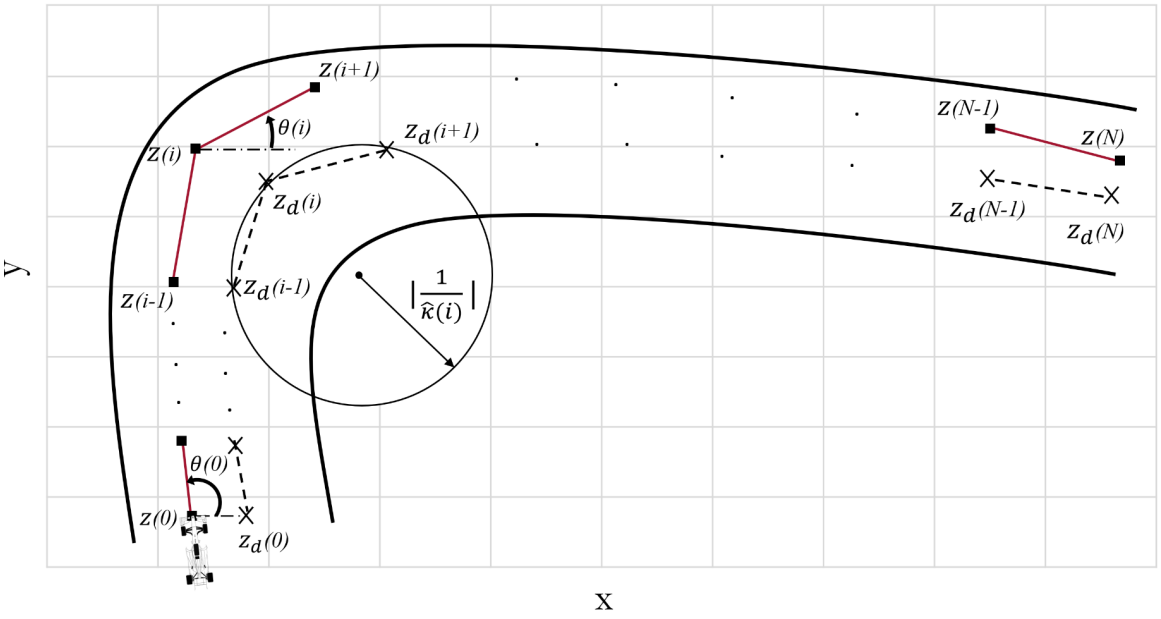

Figure 7.5: Illustration of desired path to follow and the actual vehicle path. Initial guess of $\hat{\kappa}(i)$ is shown as the curvature of local circumscribed circle.

The guess of $\hat{K}$ directly influences the accuracy of the linear model, compared to the nonlinear equations. One practice is to use the curvature of the local circumscribed circle as $\hat{\kappa}(i)$, shown in Figure 7.5. We note that for a given triangle with edges (a, b, c), the radius of the circumscribed circle is

$$r_c = |\frac{1}{\hat{\kappa}}| = \frac{4\sqrt{p(p-a)(p-b)(p-c)}}{abc} \tag{7.15}$$

$$p = \frac{a+b+c}{2} \tag{7.16}$$

Using these equations, we obtain the initial guess for $\hat{\kappa}(i)$, considering

$$\begin{aligned} a &= Dist(z(i-1), z(i)) \\ b &= Dist(z(i), z(i+1)) \\ c &= Dist(z(i-1), z(i+1)) \end{aligned} \tag{7.17}$$

Repeating this for $i = 1, 2, ..., N-1$ would result in initial guess of $\hat{K}$. Note that we consider a positive curvature sign for anti-clockwise turns and vice versa. Later on in this chapter, we will investigate this guess further to find a better candidate for $\hat{K}$.

7.2.2 Optimization Problem

For the path planning of the vehicle along the mentioned circuit, we will assume an iterative online process, where at each iteration, the route with the desired path to follow is given for some distance ahead which includes points $z_d(i) = \{(x_d(i), y_d(i)) \,|\, i = 0, 1, ..., N\}$. The desired route is the output of the preceding processes in autonomous driving, processed by other units such as perception, localization, and situation awareness. To form the optimization problem, pre-processing includes calculating the Δs, $\hat{K}$, $\hat{\theta}$, and Dθ using the (7.7), (7.13), (7.14), and (7.15), respectively.

Optimization objective we consider is the drive comfort and the travel time. To quantify these objectives, for a policy of K, we consider comfort to be expressed by

$$J_1(K) = \sum_{i=1}^{N-2} |\kappa(i-1) - 2\kappa(i) + \kappa(i+1)| \tag{7.18}$$

which is a measure of the second derivative of κ in discrete form and is convex in

K. The reason behind this choice of comfort criteria is based on the practice, where the smoothness of the driving can be highly deteriorated by sudden changes in the derivative of the vehicle path curvature. To better understand this, we can consider the common driving sense. Considering no-slip condition, path curvature is related to the tire yaw angle which is connected to the steering wheel. We have the experience that the most comfortable way to approach a corner in the road while driving is to steadily turn the steering wheel which keeps the derivative of the changes in the tire angle and hence the path curvature constant. Therefore, best practice to achieve better comfort is to avoid any sudden changes in the derivative of the path curvature by minimizing the second derivative of the path curvature.

In the context of path comfort, in fact, we are looking for a curve with its curvature linearly varying with the curve length. These curves are known as Euler spirals or clothoids, shown in Figure 7.6. In the transportation, these curves have been used in railway smooth transitioning and connection of two points since the late 1800s [105].

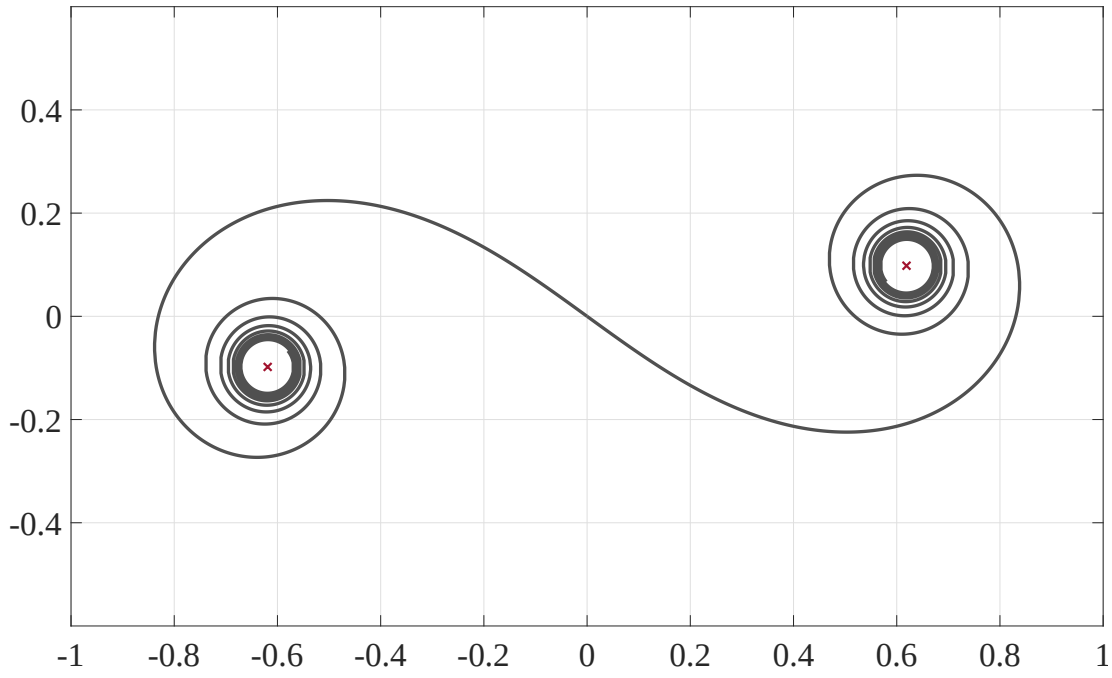

Figure 7.6: Example of an Euler spiral. Curvature varies linearly with arclength. Euler curve converges to the points shown with $\times$, from both sides.

For the second objective function, we focus on the potential travel time of the path. Assuming that the vehicle is capable of doing harsh acceleration/deceleration, the magnitude of the local curvature mainly determines the highest allowable vehicle

speed without slip. Simply, for a given path curvature

$$v_{max} = \sqrt{\frac{\mu\, N}{m\, \kappa}} \tag{7.19}$$

where μ is the lateral coefficient of friction for the tires and N is the normal force, exerted on the tires from the road. This force depends on the vehicle mass and the aerodynamic downforce. Therefore, to quantify the objective of the travel time, we consider the second objective function to be

$$J_2(K) = \sqrt{K^T \cdot K} \tag{7.20}$$

Finally, for the overall objective function, we use a scalarized sum of J_1 and J_2 with the regularizer of λ as following

$$J(K) = J_1(K) + \lambda J_2(K) \tag{7.21}$$

which is a convex function of K.

Also note that along the given points for the desired path, maximum allowable deviation from the points is also given as $\{\epsilon(i) |\, i = 0, 1, .., N\}$. Maximum deviation is responsible for assuring that vehicle remains safely on the track without violating the road boundaries. This imposes following convex quadratic constraint on the path coordinates

$$(x(i) - x_d(i))^2 + (y(i) - y_d(i))^2 \leq \epsilon(i)^2 \quad i = 0, 1, ..., N \tag{7.22}$$

As a result, final optimization problem can be written as a convex optimization problem as follows. Optimization parameters are presented in bold non-italic characters.

minimize

$$\sum_{i=1}^{N-2} |\boldsymbol{\kappa}(i-1) - 2\boldsymbol{\kappa}(i) + \boldsymbol{\kappa}(i+1)| + \lambda \sqrt{\mathbf{K}^T \cdot \mathbf{K}} \tag{7.23}$$

subject to

$$\begin{aligned} \mathbf{x}(i+1) =& \mathbf{x}(i) + \Delta s(i) \cdot \Big[\cos(\hat{\theta}(i)) - \mathrm{D}\theta(i) \cdot (\mathbf{K} - \hat{K}) \cdot \sin(\hat{\theta}(i))\Big] \\ & i = 0, 1, ..., N-1 \end{aligned} \tag{7.24a}$$

$$\begin{aligned}\mathbf{y}(i+1) =& \mathbf{y}(i) + \Delta s(i) \cdot \Big[\sin(\hat{\theta}(i)) + \mathrm{D}\theta(i) \cdot (\mathbf{K} - \hat{K}) \cdot \cos(\hat{\theta}(i))\Big] \\ & i = 0, 1, ..., N-1\end{aligned} \tag{7.24b}$$

$$(\mathbf{x}(i) - x_d(i))^2 + (\mathbf{y}(i) - y_d(i))^2 \leq \epsilon(i)^2 \quad i = 0, 1, ..., N \tag{7.24c}$$

7.2.3 Results

Starting from different points on the circuit with given initial coordinates and the orientation, we can solve the optimization problem to get the optimal optimization parameters of, K^*. As we discussed before, the discrete path is just a function of the initial state and the curvature, so given the K^*, we can find the optimal path. While H_d remains a hyper-parameter which changes depending on the condition, for the following cases, we consider that desired path which is the central line of the track is available as a set of $\{(x_d(i), y_d(i)) \mid i = 0, 1, .., N\}$ where $s(N) \leq 200$. This means vehicle plans for the route ahead up to the horizon of $H_d = 200$ meters. We also consider that $\{\epsilon[i] = 5 \,|\, i = 0, 1, ..., N\}$ where 5 meters is the approximation of the distance between the central line and the peripheral boundaries of the circuit. We use CVX [93] with SDPT3 solver [99] to solve the optimal control problem on a personal computer with 3.40 GHz Intel Core i7 processor. The CPU time for each iteration of solving the optimization problem is about 0.02 second.

We have shown result of two cases in Fig. 7.7 and Fig. 7.8 for two extreme values of λ. The initial state is chosen arbitrarily in the circuit and path is planned up to the observable horizon. Planned path related to $\lambda = 0$ considers J_1 as the optimization objective and corresponds to the most comfortable path, discarding the path travel time. On the other hand, $\lambda = \inf$ emphasizes just on the J_2 and corresponds to the potential fastest path.

We observe that the scheduled path for $\lambda = \inf$ resembles to what is called as the racing line in motorsport. Racing drivers prefer to follow the racing line since this path provides near-optimal cornering time. This is due to taking advantage of entire track length to increase the turn radius and hence the maximum cornering and exiting speed.

Moreover, Fig. 7.9 and Fig. 7.10 show how changing λ can influence the optimal policy of K^* in more details. For smaller values of the λ, the trade-off is mostly toward the comfort, which is acquired by minimizing the (7.18). In discrete form, this implies

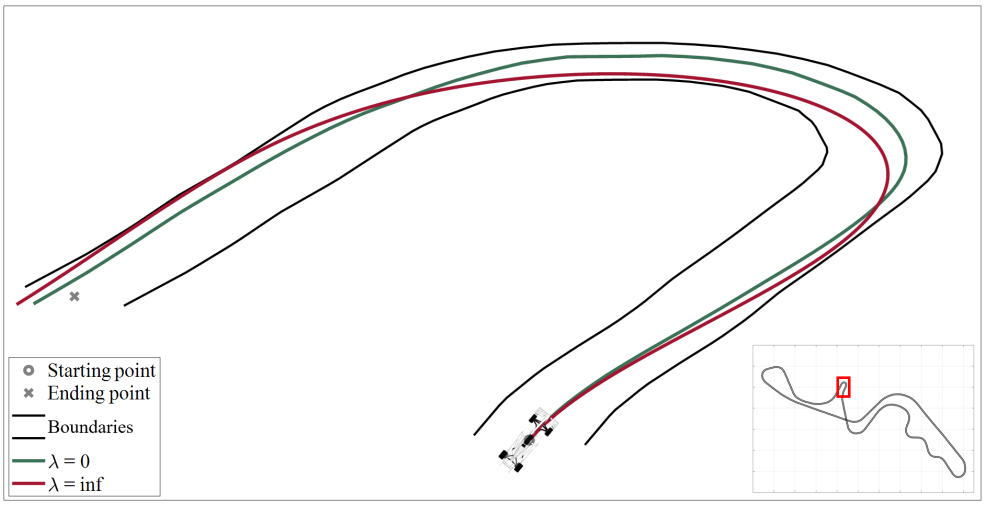

Figure 7.7: Layout of trun 11, the hairpin, in the Suzuka circuit, in a slanted view, with chosen path for two extreme values of λ. Path in each case is calculated using accurate nonlinear equations with the optimal optimization values of K^* which is the output of the optimizer.

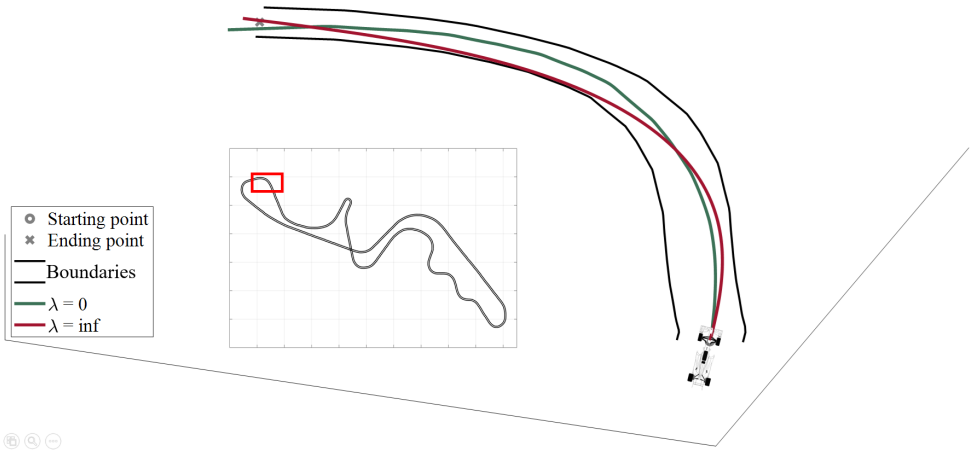

Figure 7.8: Layout of turn 13, the spoon curve, in the Suzuka circuit, in a slanted view, with chosen path for two extreme values of λ. Path in each case is calculated using accurate nonlinear equations with the optimal optimization values of K^* which is the output of the optimizer.

the least possible breakpoints in the K^* profile. On the other hand, moving toward bigger λ would emphasize more on minimizing the (7.20). This results in penalizing the large values of κ and trying to keep K^* profile around the $\kappa = 0$ axis.

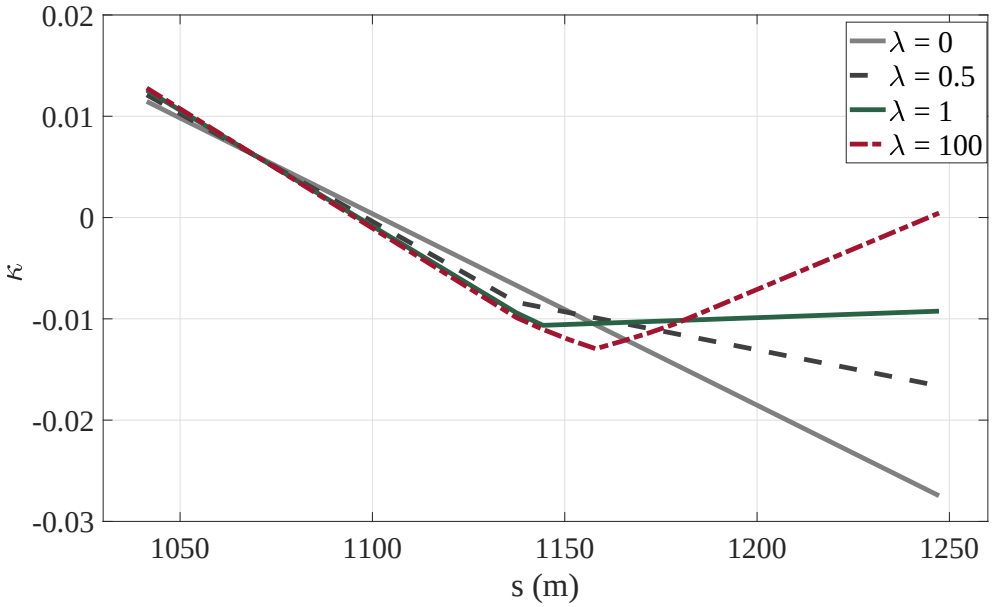

Figure 7.9: Optimal control policy of K for different regularizer values of λ for the case of Fig. 7.7.

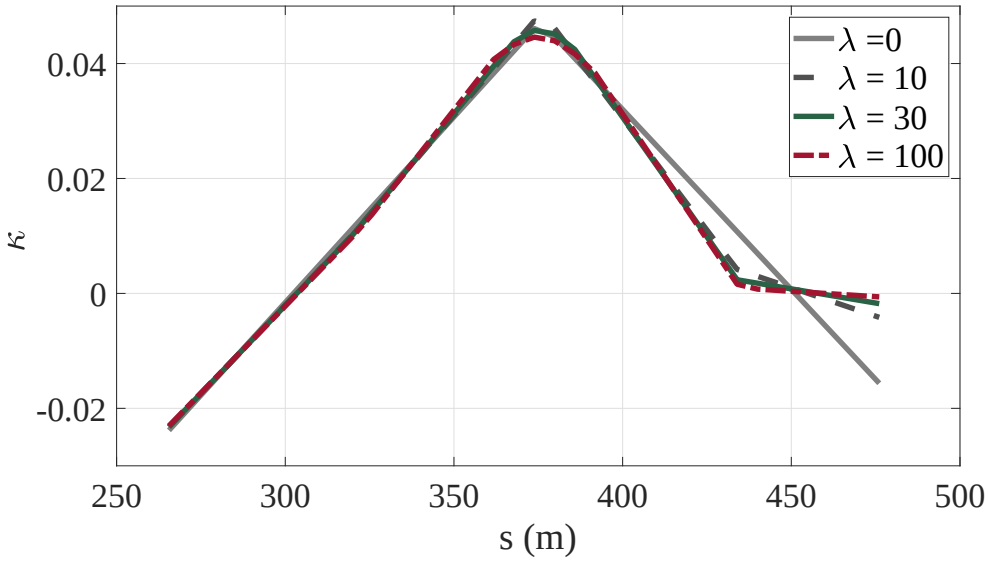

Figure 7.10: Optimal control policy of K for different regularizer values of λ for the case of Fig. 7.8.

7.2.4 Improving Accuracy of the Linear Model

In the previous section, we proposed using linear equations for obtaining the path for a given curvature, K. We obtained linear equations using the Taylor expansion

of the actual nonlinear model around an initial guess, $\hat{K}$. For the $\hat{K}$, we used the local curvature of the circumscribed circle. Since we will use this path planner iteratively in a real-time application, another practice for choosing $\hat{K}$ is to use the optimal curvature parameters, K^*, from the previous iteration. Let's assume path planning occurs iteratively for the vehicle. Moving from the current iteration to the next, vehicle state (position and orientation) and the route in the observable horizon is updated. Imagine we have obtained the current optimal curvature values, $K_M^* = [\kappa_M^*(0) \quad \kappa_M^*(1) \ ... \ \kappa_M^*(N-1)]^T$. Moving to the next iteration, we should obtain $K_{M+1}^* = [\kappa_{M+1}^*(0) \quad \kappa_{M+1}^*(1) \ ... \ \kappa_{M+1}^*(N-1)]^T$. This time, rather than the method used previously, we can use the K_M^* and consider the guess of

$$\hat{\mathcal{K}}_{M+1} = [\kappa_M^*(1) \quad \kappa_M^*(2) \ ... \ \kappa_M^*(N-1) \quad 0]^T \tag{7.25}$$

Using this, we can also eliminate the need for calculating the local curvature with (7.15) and (7.16) and hence, reducing the total processing time. Using the previously calculated optimal solution to initialize the current optimization problem is well-known technique of warm start. To illustrate the advantage of this approach, we have solved the optimization problem for both cases of using $\hat{K}$ and $\hat{\mathcal{K}}$ to find the optimal value of $J(\hat{K})$ and $J(\hat{\mathcal{K}})$ for 582 different points on the Suzuka circuit with value of $\lambda = 0.5$. Results are summarized in Table 7.1. This table clearly shows that using $\hat{\mathcal{K}}$ yields in

Table 7.1: Optimal value comparison

Condition	Number of cases	% in total	Mean of % improvement in J
$J(\hat{\mathcal{K}}) \leq J(\hat{K})$	333	57.22%	38.89%
$J(\hat{\mathcal{K}}) > J(\hat{K})$	249	42.78%	29.15%

smaller J in most of the cases. We find percentage of improvement in J as following

$$\begin{aligned} &\frac{J(\hat{K}) - J(\hat{\mathcal{K}})}{J(\hat{K})} \times 100 \quad if\ J(\hat{\mathcal{K}}) \leq J(\hat{K}) \\ &\frac{J(\mathcal{K}) - J(\hat{K})}{J(\hat{\mathcal{K}})} \times 100 \quad if\ J(\hat{\mathcal{K}}) > J(\hat{K}) \end{aligned} \tag{7.26}$$

Mean value of (7.26) over all the points is reported in the fourth column of the table. As it can be inferred, in those cases that using $\hat{\mathcal{K}}$ is better, the gap between $J(\hat{\mathcal{K}})$ and $J(\hat{K})$ is more considerable. This means not only using $\hat{\mathcal{K}}$ is preferable in most of the cases, but also improvement is more considerable in each case compared with using $\hat{K}$. We will use the initial guess of $\hat{\mathcal{K}}$ for the rest of this work, for linearizing the model.

7.3 Trajectory Planning

In the previous section, we considered a path planning problem with overall travel time and comfort as the main objectives. The obtained path consists of the information of vehicle coordinates x, y, vehicle orientation θ, and path curvature κ, as the function of the spatial parameter of the arc length s. Given the path, the crucial step is defining the trajectory. The trajectory can be simply seen as obtaining the arc length as a function of the time. As a result, velocity, acceleration, and the jerk will be accurately known for the given path. In this section, we consider the governing equations of trajectory planning and the constraints to formulate an optimization problem. Later, we will show the results of formulated optimization-based trajectory planning for a few cases.

7.3.1 Discrete Trajectory Planning

In the first step, we re-sample the obtained path using M linearly spaced points in arc length, s. So the given path is

$$\{(x(i), y(i), \theta(i), \kappa(i)) \mid i = 1, 2, ..., M\} \tag{7.27}$$

and

$$\Delta s(i) = s(i+1) - s(i) = \frac{H_d}{M-1} \qquad i = 1, 2, ..., M-1 \tag{7.28}$$

Constraints on tangential (longitudinal) acceleration, a_t, are due to propulsion/braking limits, no-slip tire condition, and comfort. The governing limit would be the minimum of these values in the absolute value. Similarly, for the lateral acceleration, a_l, constraints should guarantee a comfortable cornering while having no lateral tire slip. Taking into account all the mentioned criteria, we consider the following constraints on the longitudinal and lateral acceleration

$$a_{t,min} \leq a_t(i) \leq a_{t,max} \tag{7.29}$$

$$a_{l,min} \leq a_l(i) \leq a_{l,max} \tag{7.30}$$

While $a_{t,min}$, $a_{t,max}$, $a_{l,min}$, and $a_{l,max}$ can be arc-length (s) dependent and can be calculated as part of the pre-processing, we consider constant values in this work. Since there is no difference in our case for left and right hand turns, we consider that

$$a_{l,min} = -a_{l,max} \tag{7.31}$$

As we discussed before, lateral speed along the path is zero which means

$$v_l(i) = 0 \tag{7.32}$$

The main equation governing the spatial domain trajectory planning is

$$v(s)\, dv(s) = a(s) ds \tag{7.33}$$

Considering a constant $a_t(i)$ for $s(i)$ up to $s(i+1)$, integration of mentioned equation would yield in

$$v_t(i+1)^2 - v_t(i)^2 = 2a_t(i)\Delta s(i) \tag{7.34}$$

For the lateral acceleration, it is well known to use the following equation

$$a_l(i) = v_t(i)^2 \cdot \kappa(i) \tag{7.35}$$

We should note that the velocity is always tangential to the path and there is no lateral slip along the path for the vehicle. Also for this tangential speed, we consider

$$0 \; \frac{m}{s} \leq v_t(i) \leq v_{t,max} \tag{7.36}$$

We decide on this constraint considering both powertrain capabilities in total produced power and existing regulations regarding the allowed top speed.

Final equation in this context is simply the travel time for each Δs as

$$\Delta t(i) = t(i+1) - t(i) = \frac{\Delta s(i)}{v_t(i)} \tag{7.37}$$

7.3.2 Optimization Problem

Similar to path planning, we try to address the trajectory planning problem using an optimization-based approach. We consider similar objectives as path planning for trajectory planning as well. For the overall travel time, we simply consider

$$J_1 = \frac{\sum_{i=1}^{M-1} \Delta t(i)}{H_d} \tag{7.38}$$

Note that we have used H_d which is the observable horizon distance, in the denominator. Since we will use regularizer to form the final objective function, this will help mitigate the effect of chosen H_d on the calibration of the regularizer.

Drive comfort has a substantial effect on overall driving experience from an AV. Social acceptance of AVs is directly linked to the driving impression of passengers and how comfort is comparable to human-operated driving. There exist numerous criteria for quantifying comfort. In this article, we use constraints on longitudinal and lateral acceleration/deceleration as well as following objective function

$$J_2 = \sqrt{\frac{\sum_{i=1}^{M} a_t(i)^2}{M}} \tag{7.39}$$

J_2 penalizes the rms error of the acceleration/deceleration compared to constant speed. Again, using M in the denominator of J_2 formulation will help us to separate the effect of chosen M on the regularizer.

For the final objective function, we use a regularization of these two objective functions as

$$J = J_1 + \alpha J_2 \tag{7.40}$$

α is the hyper-parameters, which should be determined before optimization. This

tuning parameter depends on the desired trade-off between the explained objectives.

In order to formulate a convex optimization problem, we choose a new variable of

$$u = v_t^2 \tag{7.41}$$

We also note that for the path planning, the initial value of the tangential speed, $v_t(1)$, is known.

As a result, the overall optimization problem for trajectory planning for a given path is

minimize

$$\frac{\sum_{i=1}^{M-1} \mathbf{\Delta t}(i)}{H_d} + \alpha \cdot \sqrt{\frac{\sum_{i=1}^{M} \mathbf{a_t}(i)^2}{M}} \tag{7.42}$$

subject to

$$\mathbf{u}(i+1) - \mathbf{u}(i) = 2\mathbf{a_t}(i)\Delta s(i) \qquad i = 1, 2, ..., M-1 \tag{7.43a}$$

$$\mathbf{u}(1) = v_t(1)^2 \tag{7.43b}$$

$$0 \leq \mathbf{u}(i) \leq v_{t,max}^2 \qquad i = 1, 2, ..., M \tag{7.43c}$$

$$a_{t,min} \leq \mathbf{a_t}(i) \leq a_{t,max} \qquad i = 1, 2, ..., M \tag{7.43d}$$

$$\mathbf{a_l}(i) = \mathbf{u}(i) \cdot \kappa(i) \qquad i = 1, 2, ..., M \tag{7.43e}$$

$$-a_{l,max} \leq \mathbf{a_l}(i) \leq a_{l,max} \qquad i = 1, 2, ..., M \tag{7.43f}$$

$$\mathbf{\Delta t}(i) \geq \frac{\Delta s(i)}{\sqrt{\mathbf{u}(i)}} \qquad i = 1, 2, ..., M-1 \tag{7.43g}$$

Note that in these equations, we have differentiated all the optimization parameters using a bold non-italic math style. The objective function of (7.42) is a convex function of optimization parameters since it is the sum of an affine term with a normalized Euclidean norm of a vector. (7.43a), (7.43b), and (7.43e) are affine linear constraints. Furthermore, (7.43g), the relaxed version of (7.37), is convex since the right hand side is a inverse of a positive parameter. Obviously, for the case of the optimal solution, this constraint holds tight to avoid an unnecessary increase in J_1. As the final result, the optimization problem is convex.

7.3.3 Results

We use CVX [93] with SDPT3 [99] or MOSEK [94] solvers to solve the optimization problem on a personal computer with 3.40 GHz Intel Core i7 processor. We choose the hyper-parameter of M in a way to achieve accurate results within a reasonable time. The CPU time for each iteration of solving the optimization problem is about 0.01 second.

Following figures show the results of the presented optimization-based path and trajectory planning for few cases. For each case, used parameters are summarized in Table 7.2.

Table 7.2: Parameters

	Path planning				Trajectory planning					
	H_d	ϵ	N	λ	M	α	$v_{t,max}$	$a_{t,max}$	$a_{t,min}$	$a_{l,max}$
Case 1.1	$200\,m$	$5\,m$	100	inf	150	0	$30\,m/s$	$3\,m/s^2$	$-10\,m/s^2$	$2\,m/s^2$
Case 1.2	$200\,m$	$5\,m$	100	inf	150	0	$30\,m/s$	$5\,m/s^2$	$-10\,m/s^2$	$4\,m/s^2$
Case 1.3	$200\,m$	$5\,m$	100	0.1	150	0.01	$30\,m/s$	$3\,m/s^2$	$-10\,m/s^2$	$2\,m/s^2$
Case 1.4	$200\,m$	$5\,m$	100	0	150	0.1	$30\,m/s$	$3\,m/s^2$	$-10\,m/s^2$	$2\,m/s^2$
Case 2.1	$300\,m$	$8\,m$	200	inf	300	0	$30\,m/s$	$5\,m/s^2$	$-10\,m/s^2$	$4\,m/s^2$
Case 2.2	$300\,m$	$8\,m$	200	$1e-3$	300	0	$30\,m/s$	$5\,m/s^2$	$-10\,m/s^2$	$4\,m/s^2$
Case 2.3	$300\,m$	$8\,m$	200	0.1	300	0.01	$30\,m/s$	$3\,m/s^2$	$-10\,m/s^2$	$2\,m/s^2$
Case 2.4	$300\,m$	$8\,m$	200	0	300	0.1	$30\,m/s$	$3\,m/s^2$	$-10\,m/s^2$	$2\,m/s^2$
Case 3.1	$100\,m$	$5\,m$	50	0.1	100	0	$30\,m/s$	$3\,m/s^2$	$-10\,m/s^2$	$2\,m/s^2$
Case 3.2	$100\,m$	$5\,m$	50	0.1	100	0.003	$30\,m/s$	$3\,m/s^2$	$-10\,m/s^2$	$2\,m/s^2$
Case 3.3	$100\,m$	$5\,m$	50	0.1	100	0.01	$30\,m/s$	$3\,m/s^2$	$-10\,m/s^2$	$2\,m/s^2$
Case 3.4	$100\,m$	$5\,m$	50	0.1	100	0.1	$30\,m/s$	$3\,m/s^2$	$-10\,m/s^2$	$2\,m/s^2$
Case 4.1	$500\,m$	$6\,m$	300	inf	500	0	$50\,m/s$	$10\,m/s^2$	$-20\,m/s^2$	$10\,m/s^2$
Case 4.2	$500\,m$	$6\,m$	300	0	500	0	$50\,m/s$	$10\,m/s^2$	$-20\,m/s^2$	$10\,m/s^2$
Case 4.3	$500\,m$	$6\,m$	300	inf	500	inf	$50\,m/s$	$10\,m/s^2$	$-20\,m/s^2$	$10\,m/s^2$
Case 4.4	$500\,m$	$6\,m$	300	0	500	inf	$50\,m/s$	$10\,m/s^2$	$-20\,m/s^2$	$10\,m/s^2$

Starting from Figure 7.11, Case 1.2 is capable of performing harsher lateral and tangential acceleration compared to Case 1.1. Parameters of λ and α are tuned for both of these cases to achieve the fastest possible path and trajectory. Consequently, this leads to a higher speed profile for Case 1.2 and less travel time as a result. Tuning

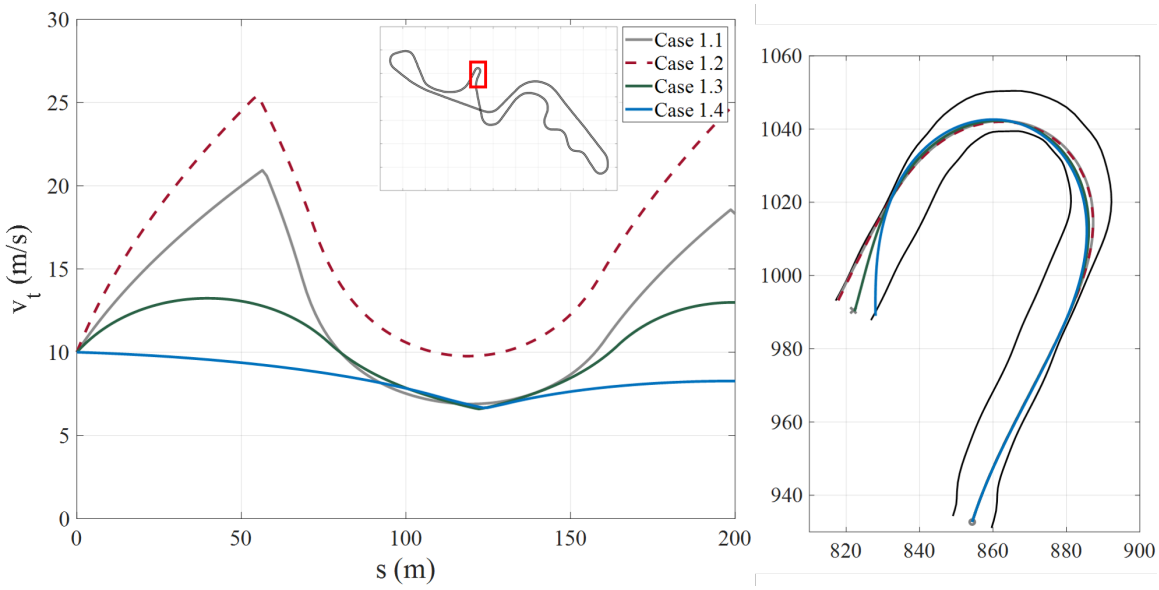

Figure 7.11: Optimal path and trajectory planning for Case 1, the hairpin of Suzuka circuit, for different parameters.

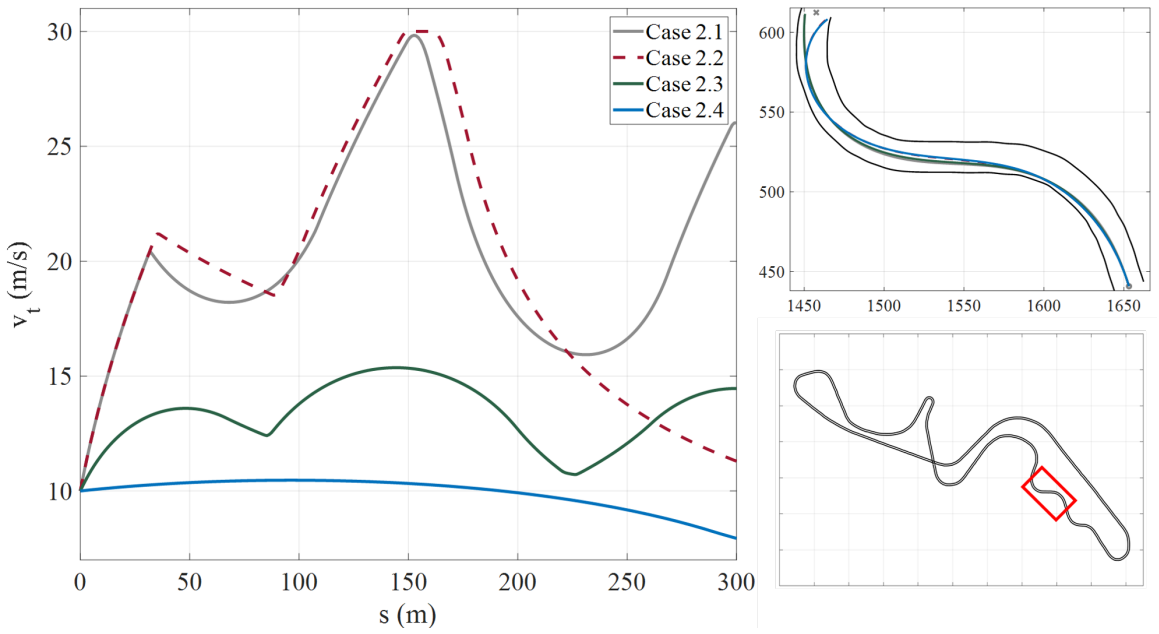

Figure 7.12: Optimal path and trajectory planning for Case 2, the S curves of Suzuka circuit, for different parameters.

of λ and α parameters differ from Case 1.3 to Case 1.4, in a way that Case 1.4 is tuned to have a more comfortable path and trajectory. As it can be seen in this figure, Case 1.4 path resembles more to a clothoid, and the speed profile is smoother. These come

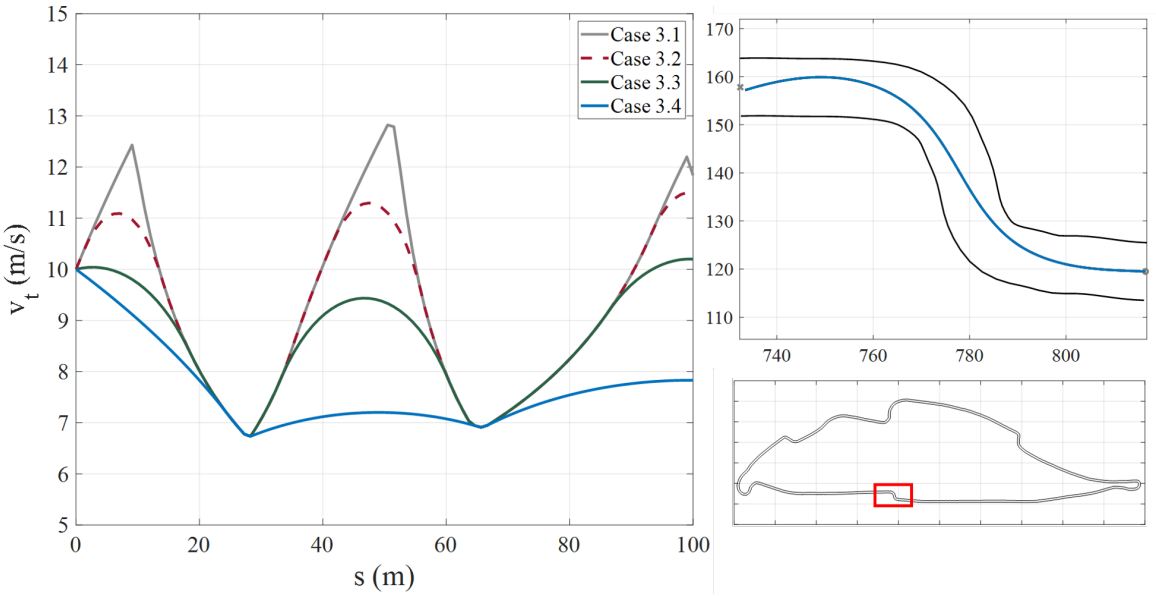

Figure 7.13: Optimal path and trajectory planning for Case 3, the turns 13 and 14 (Wall of Champions) of Gilles Villeneuve circuit, for different parameters.

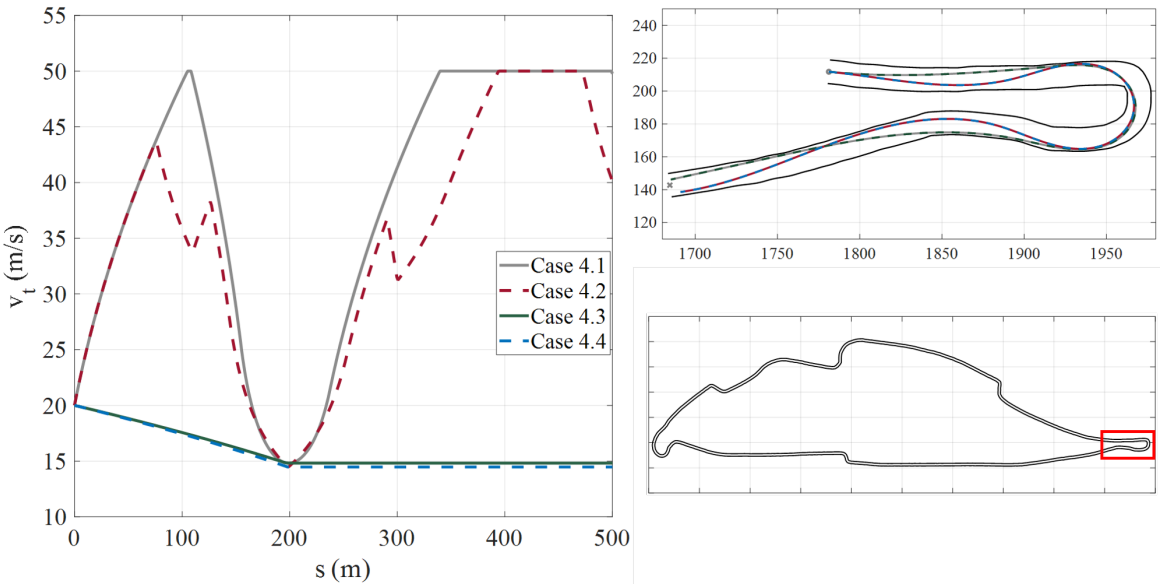

Figure 7.14: Optimal path and trajectory planning for Case 4, the turns 10 and 11 (L'Epingle) of Gilles Villeneuve circuit, for different parameters.

with a significant increase in travel time.

Figure 7.12 show a wider segment of the track for a longer observable horizon. Moving from the first to the last case, parameter tuning changes in benefit of comfort. From Case 2.1 to Case 2.2, comfort is gained from the path planning side, while moving

from Case 2.3 to Case 2.4 , comfort is the result of both comfortable path planning and trajectory planning.

Figure 7.13 analyzes the effect of tuning α individually on the trajectory by keeping λ constant which means the path is the same for all cases of Case 3.1 to Case 3.4. It is interesting to see how increasing the α results in avoiding harsh acceleration/deceleration for a long period of times in the speed profile, to provide smoother drive experience. This in turn significantly increases the overall travel time.

Finally, Figure 7.14 considers a special case. We have assumed a greater allowable top speed, tangential acceleration, and tolerable lateral acceleration to make a similar case to a racing scenario. For Case 4.1 and Case 4.2, α is tuned in the same way to achieve the fastest trajectory. However, λ is chosen to obtain the fastest potential path for Case 4.1 and the most comfortable path for Case 4.2. The results of comparing the trajectory for these two cases is truly fascinating. For the speed profile, the main constraint is the lateral acceleration. We also discussed that the path curvature determines the fastest allowable speed, given the maximum lateral acceleration. Since Case 4.1 have tuned to obtain the fastest potential path, by avoiding large curvature values, the maximum allowable speed is higher for the Case 4.1 compared to Case 4.2. Travel time of Case 4.1 is clearly less than Case 4.2. This confirms the fact that for the case of achieving the fastest travel time between two given points, this objective should be considered both in path planning and trajectory planning. For Case 4.3 and Case 4.4, the speed profiles are almost similar, since the merely constant speed profile has the best comfort. However, there is a bottleneck for the speed in $s \approx 200\,m$. This is the apex of the corner and the maximum speed should not exceed $\approx 15\,m/s$ to be in the safe margin of lateral acceleration. This pushes the speed profiles for Case 4.3 and Case 4.4 to uniformly decrease up to this point and stay constant since after. Although the speed profiles are the same, planned path for these two cases are different. Since Case 4.4 tries to connect initial and the end point mostly using segments of Euler spirals, which is the results of setting $\lambda = 0$, the overall driving experience for this case is more comfortable, compared to Case 4.3.

7.4 Iterative Motion Planning

In previous sections, we have shown the result of the developed optimization-based path and trajectory planning for few cases. Motion planning can be seen as performing

both path and trajectory planning. In this section, we will discuss the iterative motion planning for an AV in a racing track. This process gets the racing track geometrical information as well as the vehicle initial states (e.g., spatial coordinates, orientation, and speed) plus all required parameters (e.g., speed/acceleration constraints, tuning parameters, observable horizon) as the input. In the next step, the path planner would obtain the optimal path up to the observable horizon. Next, we provide the planned path as an input to the trajectory planner to obtain the optimal trajectory accordingly. Then, we will apply the planned trajectory up to the time of Δt_{step} and obtain the next vehicle states. We update the initial vehicle state and move to the next iteration to repeat the procedure again. The frequency of this procedure is $1/\Delta t_{step}$. As discussed before, the average CPU time for path and trajectory planning combined is about $0.03\,s$, which means that the highest feasible frequency is $\leq 33\,Hz$. We have shown the schematic of the explained procedure in Figure 7.15. As discussed in 7.2.4, the iterative approach has a significant effect on increasing the accuracy of the linearized path planning equations. In this context, we use the optimal curvature planning of the previous step, K^*, as the $\hat{K}$ for the current step. Note that nonlinear path equations have been linearized around $\hat{K}$ using the Taylor expansion.

We have also presented the results of applying the iterative approach to obtain the overall path and trajectory around the circuit for a few cases of parameter initialization in Figure 7.16 to 7.23. We have shown the parameters in each case in Table 7.3.

Table 7.3: Parameters

	Path planning				Trajectory planning						Iteration
	H_d	ϵ	N	λ	M	α	$v_{t,max}$	$a_{t,max}$	$a_{t,min}$	$a_{l,max}$	Δt_{step}
Case 1	$100\,m$	$5\,m$	100	0.1	150	0.005	$30\,m/s$	$3\,m/s^2$	$-10\,m/s^2$	$2\,m/s^2$	0.05
Case 2	$200\,m$	$5\,m$	300	inf	500	0	$80\,m/s$	$10\,m/s^2$	$-30\,m/s^2$	$20\,m/s^2$	0.1

We have tuned the parameters for Case 1 of iterative motion planning to emphasize more on the drive comfort. This case can be attributed to a passenger vehicle in the track. Both λ and α hyper-parameters, as well as the constraints on the acceleration and velocity, are initialized reasonably to provide comfort both in path and trajectory planning. This case tries to express the path mostly using Euler spirals and avoids harsh accelerations while driving. On the other hand, Case 2 resembles a motion

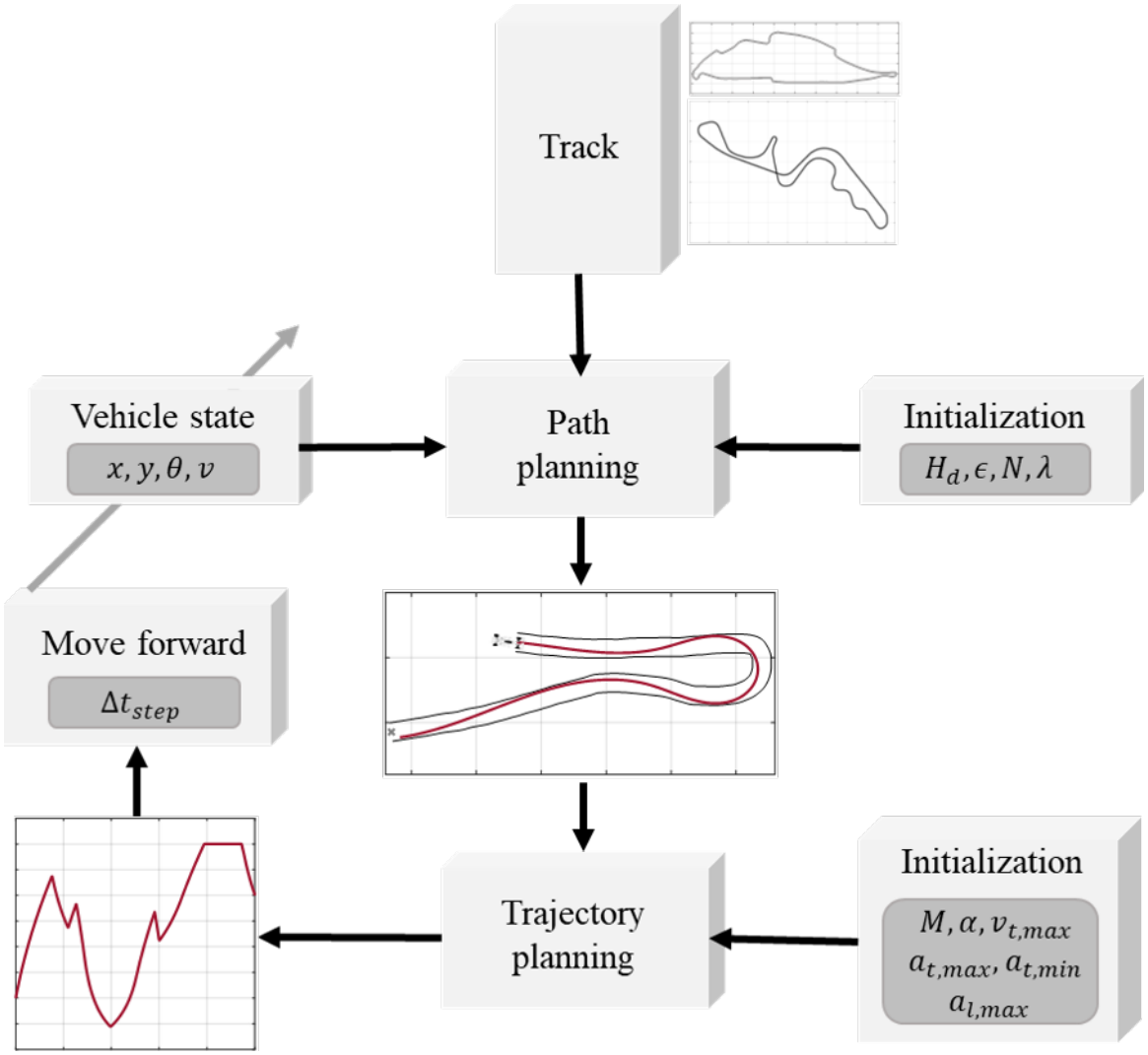

Figure 7.15: Schematic of the iterative motion planning approach for a AV in a racing track.

planning for a racing car in the track. $\lambda \to$ inf and $\alpha = 0$ to emphasize only on the travel time discarding the comfort. Constraints on the maximum tangential speed, lateral acceleration, and tangential acceleration/deceleration are reasonably affordable by a racing car. This significantly changes the path and the trajectory, to achieve the fastest motion in the track. The vehicle initial speed for both of these cases, as seen in the velocity profile, is set to $10\,m/s$. Lap time for the Case 1 is $t_{lap} = 361.6\,s$ and $t_{lap} = 284.95\,s$ for Suzuka and Gilles Villeneuve race tracks respectively, compared to the $t_{lap} = 112.6\,s$ and $t_{lap} = 96.7\,s$ for the Case 2. Note that even the Case 2 setting is inferior to the Formula 1 car in terms of the performance. Formula 1 cars can achieve

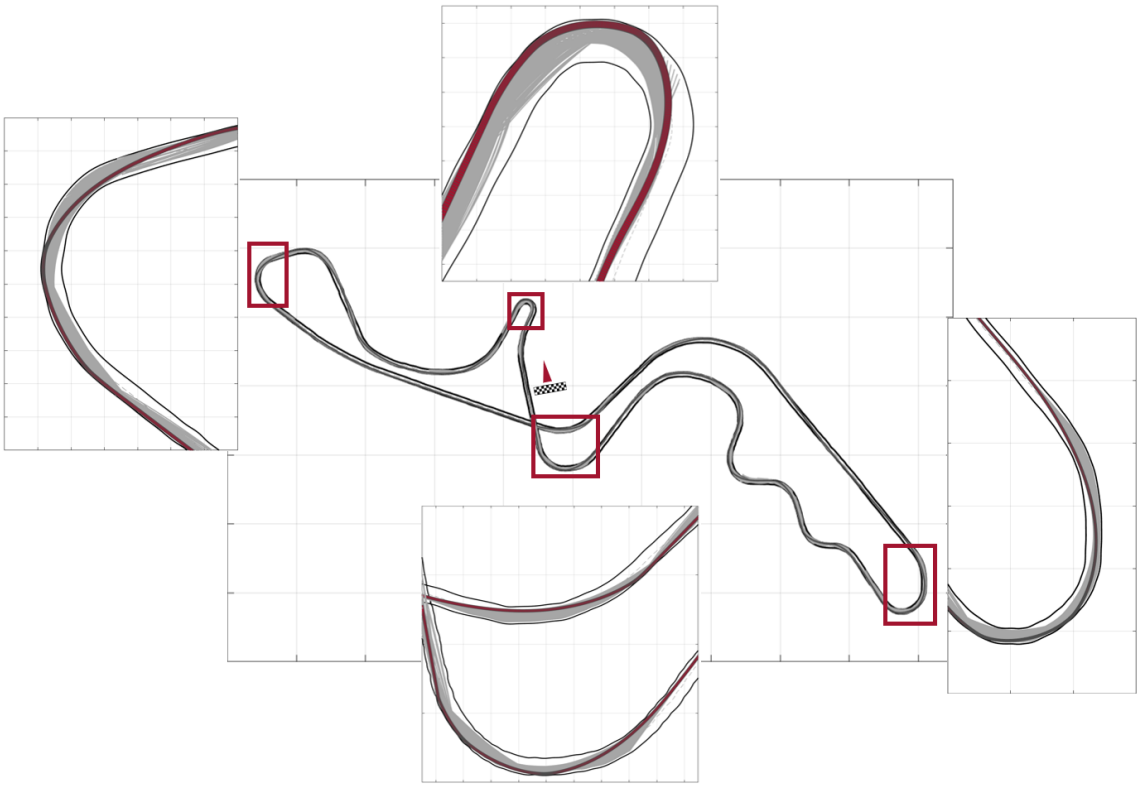

Figure 7.16: Iterative path planning for the Suzuka racing track, using the parameters of Case 1.

even higher braking deceleration and lateral acceleration. To have a comparison, note that in the time of writing this article, lap records during racing for these two circuits are $t_{lap} = 91.540\,s$ and $t_{lap} = 73.078\,s$, respectively.

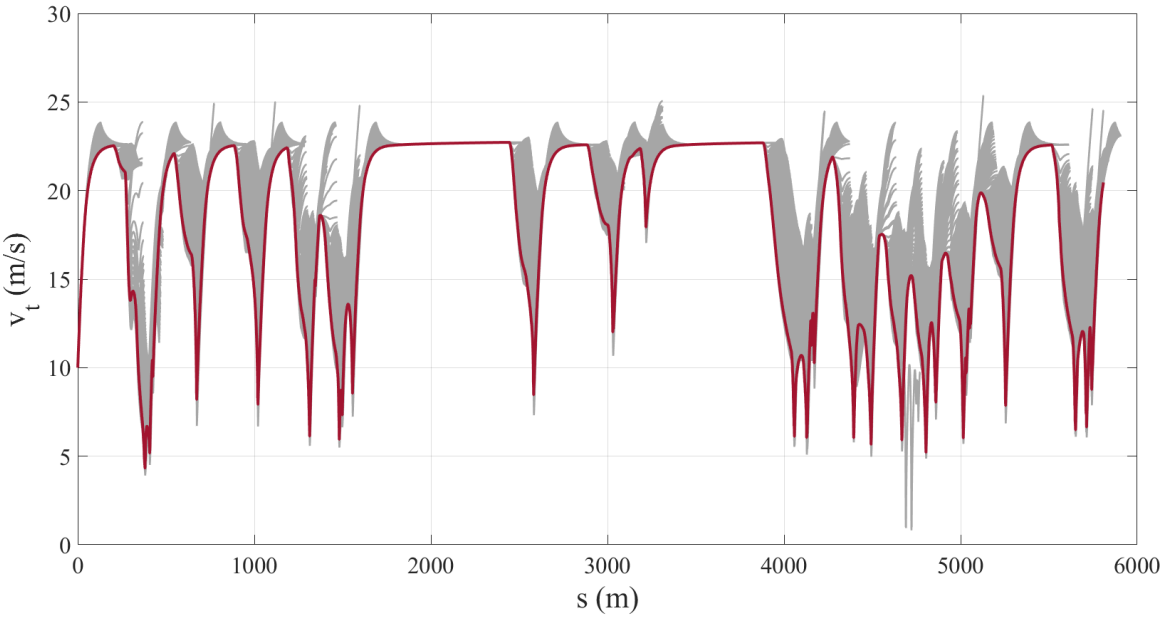

Figure 7.17: Iterative trajectory planning for the Suzuka racing track, using the parameters of Case 1.

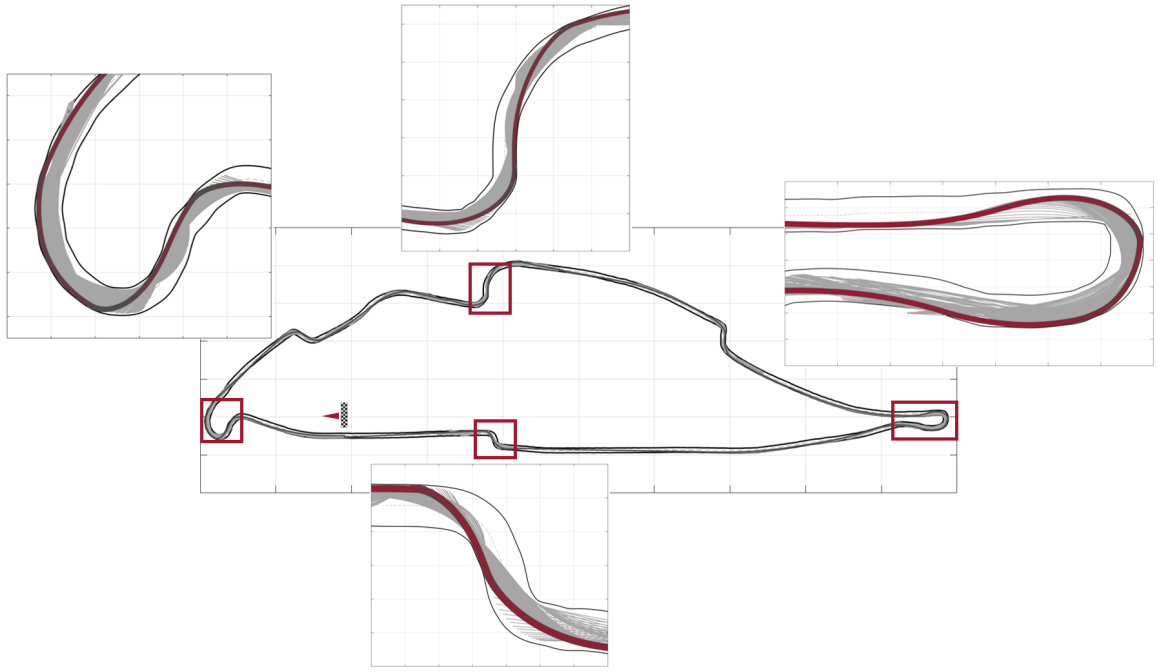

Figure 7.18: Iterative path planning for the Gilles Villeneuve racing track, using the parameters of Case 1.

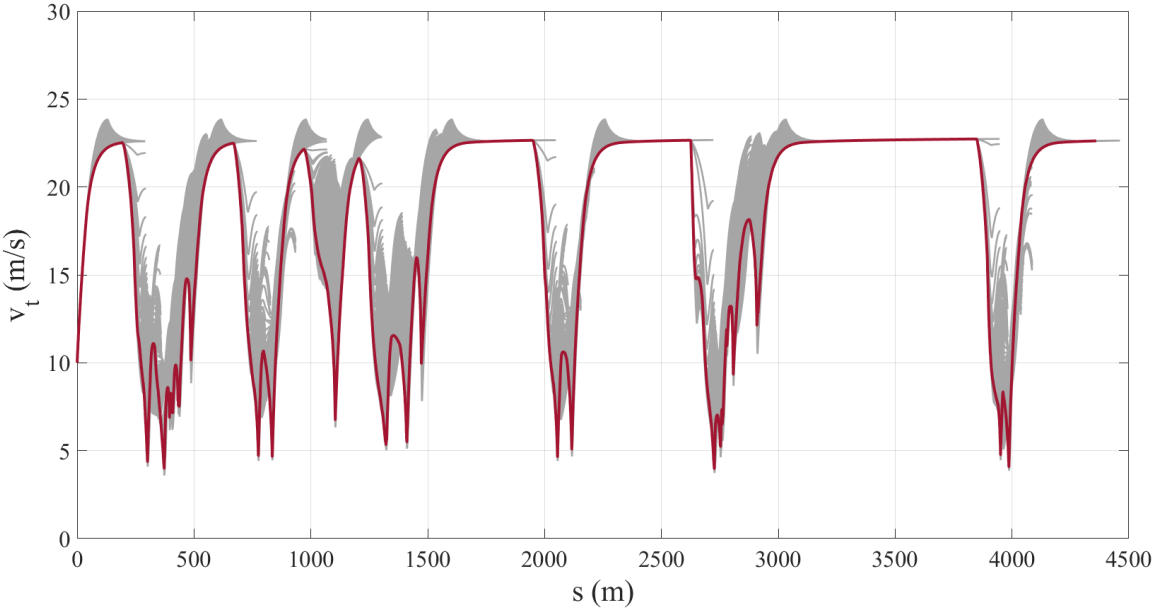

Figure 7.19: Iterative trajectory planning for the Gilles Villeneuve racing track, using the parameters of Case 1.

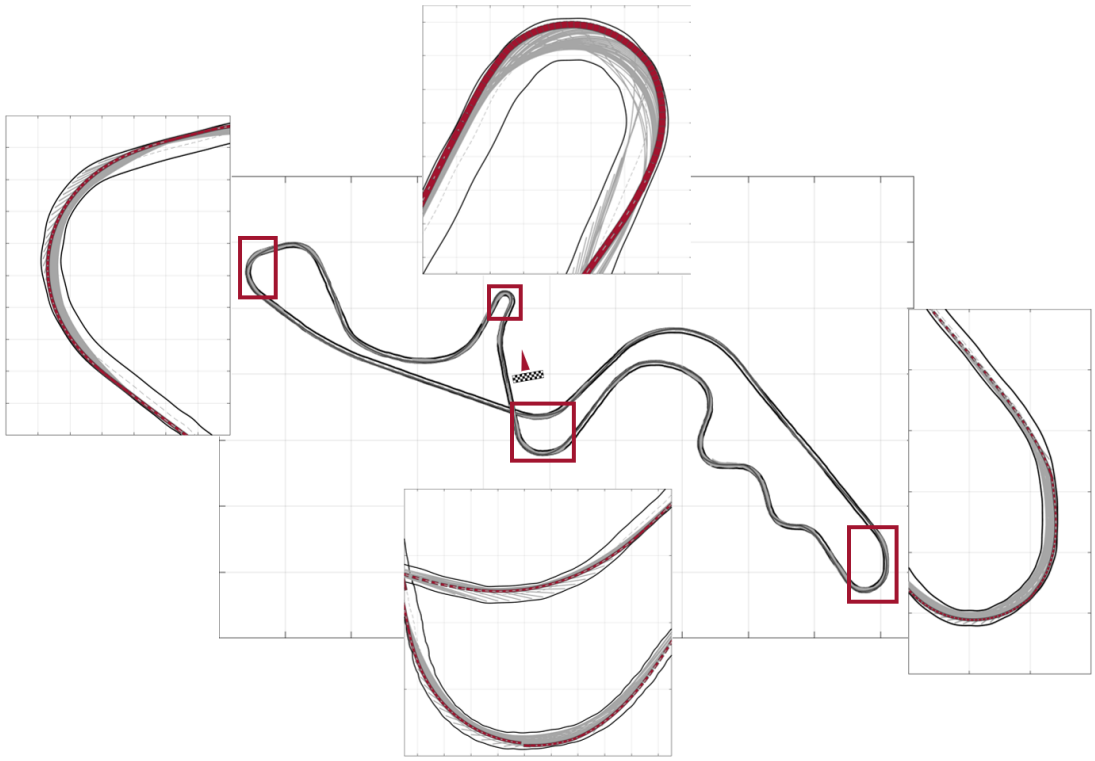

Figure 7.20: Iterative path planning for the Suzuka racing track, using the parameters of Case 2.

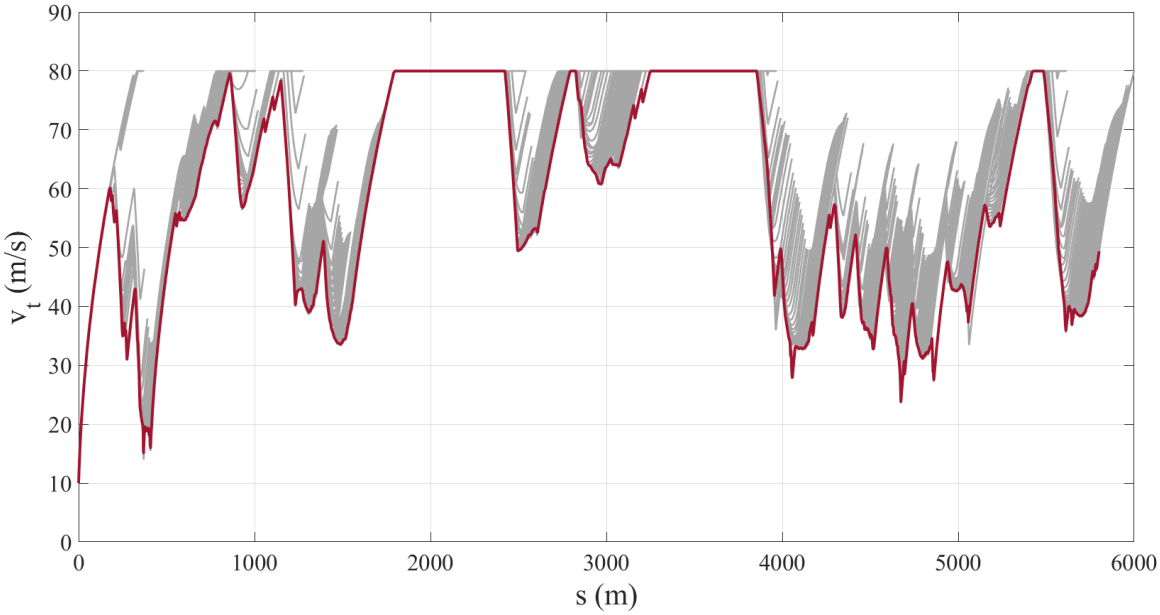

Figure 7.21: Iterative trajectory planning for the Suzuka racing track, using the parameters of Case 2.

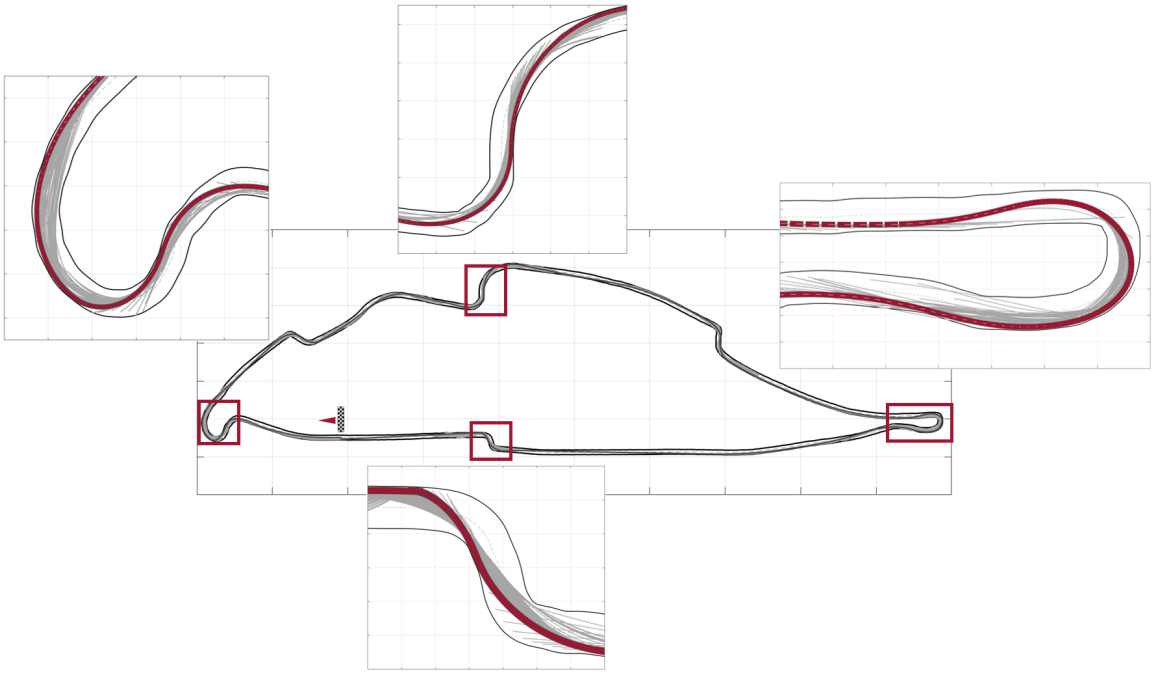

Figure 7.22: Iterative path planning for the Gilles Villeneuve racing track, using the parameters of Case 2.

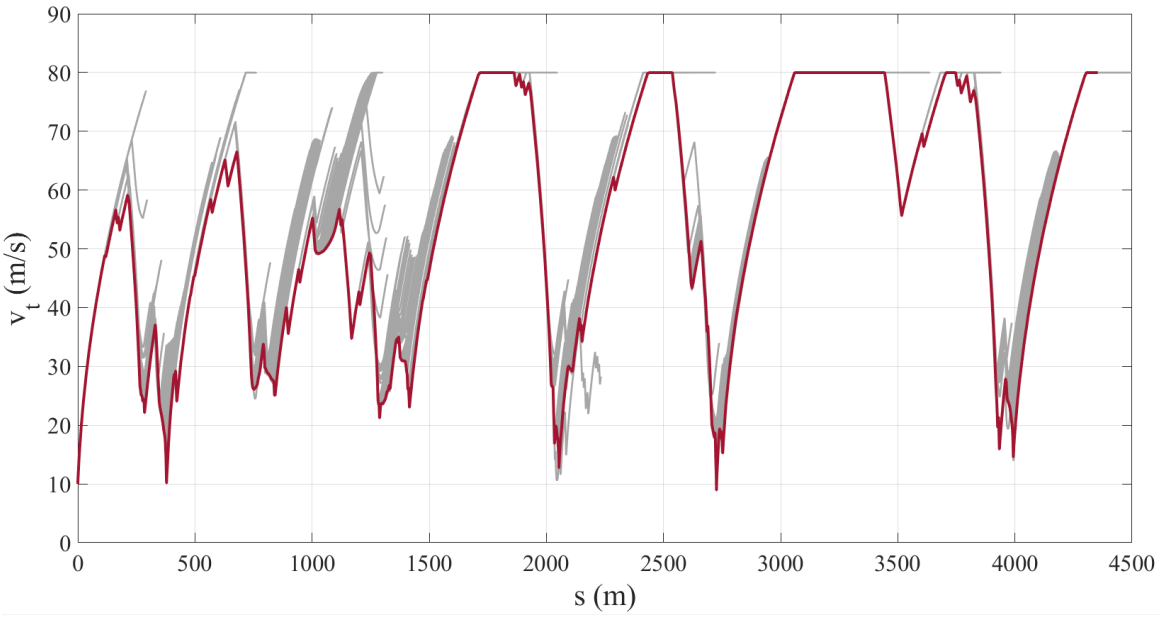

Figure 7.23: Iterative trajectory planning for the Gilles Villeneuve racing track, using the parameters of Case 2.

7.5 Real-time Energy Management

In the previous section, we discussed an optimization-based approach to perform the iterative motion planning for an A-HEV in a racing track. In the final part of this chapter, we slightly modify the introduced energy management strategy in chapter 6, to be able to integrate a real-time EMS with motion planning.

As mentioned, we will use the convex representation in chapter 6 for the real-time EMS combined with a receding horizon approach. We should note that derived convex representation is global and does not depend on the instantaneous operating condition. While we could use linearization or other approaches such as dynamic matrix control (DMC) to obtain a local abstract vehicle model to feed into the model predictive control, this leads to increased processing time and does not guarantee a better performance.

Our final goal of this integration is to develop an ASEMS (autonomous-specific energy management strategy) for the hybrid electric powertrain explained in Chapter 5 using the optimization-based approach introduced in chapter 6.

7.5.1 Optimization Problem

As a result of performing the motion planning algorithm for the initialized parameters, we obtain the vehicle trajectory up to the observable horizon. This time, we resample the provided motion planning data using N_e number of points in time, t, rather than the spatial variable, s. Again, the choice of N_e influences the accuracy and the computational burden. Given the initial and the target battery state of the charge, we calculate the initial and the target battery state of energy as $E_b^{initial}$ and E_b^{target}. Furthermore, for the given trajectory at each step, we do the pre-processing to obtain the power and torque load on the powertrain as $\mathcal{P}_{ps}(k)$ and $\mathcal{T}_{ps}(k)$, respectively. For $k = 1, 2, ..., N_e$, we solve the following convex optimization problem, introduced in Chapter 6, to obtain the fuel-optimal strategy for a given trajectory.

minimize

$$\sum_{k=1}^{N_e} \mathbf{P_f}(k) \cdot \Delta t \tag{7.44}$$

subject to

$$\mathbf{P_e}(k) + \mathbf{P_{mg1}}(k) + \mathbf{P_{mg2}}(k) \geq \mathcal{P}_{ps}(k) \tag{7.45a}$$

$$\frac{r_1}{1+r_1}\cdot \mathbf{T_e}(k) + r_2 \cdot \mathbf{T_{mg2}}(k) \geq \mathcal{T}_{ps}(k) \tag{7.45b}$$

$$\mathbf{P_f}(k) \geq [\mathbf{P_e}(k) \quad \mathbf{T_e}(k)] \cdot A \cdot \begin{bmatrix}\mathbf{P_e}(k)\\ \mathbf{T_e}(k)\end{bmatrix} + b^T \cdot \begin{bmatrix}\mathbf{P_e}(k)\\ \mathbf{T_e}(k)\end{bmatrix} \tag{7.45c}$$

$$0 \leq \mathbf{P_e}(k) \leq P_{e,max} \tag{7.45d}$$

$$0 \leq \mathbf{T_e}(k) \leq T_{e,max} \tag{7.45e}$$

$$\mathbf{P_{mg2,dc}}(k) \geq p_2(k)\cdot \mathbf{T_{mg2}}(k)^2 + p_1(k)\cdot \mathbf{T_{mg2}}(k) \tag{7.45f}$$

$$\mathbf{P_{mg2}}(k) = \mathbf{T_{mg2}}(k)\cdot \omega_{mg2}(k) \tag{7.45g}$$

$$T_{mg2,min}(k) \leq \mathbf{T_{mg2}}(k) \leq T_{mg2,max}(k) \tag{7.45h}$$

$$\mathbf{P_{mg1}}(k) = -\mathbf{P_e}(k) + \left(\frac{r_1 \cdot r_d}{(1+r_1)\cdot r_w}\cdot \mathbf{T_e}(k)\cdot v(k)\right) \tag{7.45i}$$

$$\mathbf{T_{mg1}}(k) = -\mathbf{T_e}(k)/(1+r_1) \tag{7.45j}$$

$$\mathbf{P_{mg1,dc}}(k) \geq q_2 \cdot \mathbf{P_{mg1}}(k)^2 + q_1 \cdot \mathbf{P_{mg1}}(k) \tag{7.45k}$$

$$P_{mg1,min} \leq \mathbf{P_{mg1}}(k) \leq P_{mg1,max} \tag{7.45l}$$

$$T_{mg1,min} \leq \mathbf{T_{mg1}}(k) \leq T_{mg1,max} \tag{7.45m}$$

$$\mathbf{P_b}(k) = P_{aux} + \mathbf{P_{mg1,dc}}(k) + \mathbf{P_{mg2,dc}}(k) \tag{7.45n}$$

$$\begin{aligned}\mathbf{E_b}(k+1) &\leq \mathbf{E_b}(k)\\ &- \frac{\Delta t}{R\tilde{C}}\left[\mathbf{E_b}(k) + E_0 - \sqrt{(\mathbf{E_b}(k)+E_0)\left(\mathbf{E_b}(k)+E_0-2R\tilde{C}\mathbf{P_b}(k)\right)}\right]\end{aligned} \tag{7.45o}$$

$$P_{b,min} \leq \mathbf{P_b}(k) \leq P_{b,max} \tag{7.45p}$$

$$E_{b,min} \leq \mathbf{E_b}(k) \leq E_{b,max} \tag{7.45q}$$

$$\mathbf{E_b}(1) = E_b^{initial} \tag{7.45r}$$

$$\mathbf{E_b}(N_e+1) = E_b^{target} \tag{7.45s}$$

These equations with the required parameters are discussed in Chapter 6 in a great detail.

7.5.2 Iterative Motion Planning and EMS

In this part, we discuss a procedure to integrate the EMS with the motion planning to form the ASEMS. For the given route up to the observable horizon, path and trajectory planning are performed initially to obtain the input velocity profile for the EMS. For the EMS, we use both the introduced optimization-based approach here and the obtained rule-based controller in Chapter 5. To have a better comparison, we use these two approaches simultaneously to find the power and torque split for any given trajectory at each step to obtain the control inputs for the components. These inputs are torque/speed for the ICE, MG1, and MG2. It is crucial to note the hierarchy of the procedure which starts with path planning and moves to trajectory planning and finally ends in EMS. This results in solving three consecutive convex optimization problems at each time step. While combining these problems to obtain a comprehensive optimization problem which generates path, trajectory, and powertrain control inputs at a same time might be feasible, but this leads to an unnecessarily complex and difficult to handle optimization problem with increased number of tuning parameters. Hence, we have considered the hierarchy shown in Figure 7.24.

We then proceed forward and apply these inputs for the time duration of Δt_{step} on the developed high-fidelity model in chapter 5. As we move to the next time step, we update the vehicle states, velocity and SOC, and we re-calculate the procedure again. The optimization-based controller finds the control input for the plant at each step by solving an optimization problem which has the predictions of convex model inside. Hence, this approach is a model predictive control approach and we will call this controller the MPC-based controller. Figure 7.24 shows an illustration of the explained procedure in a graphical format.

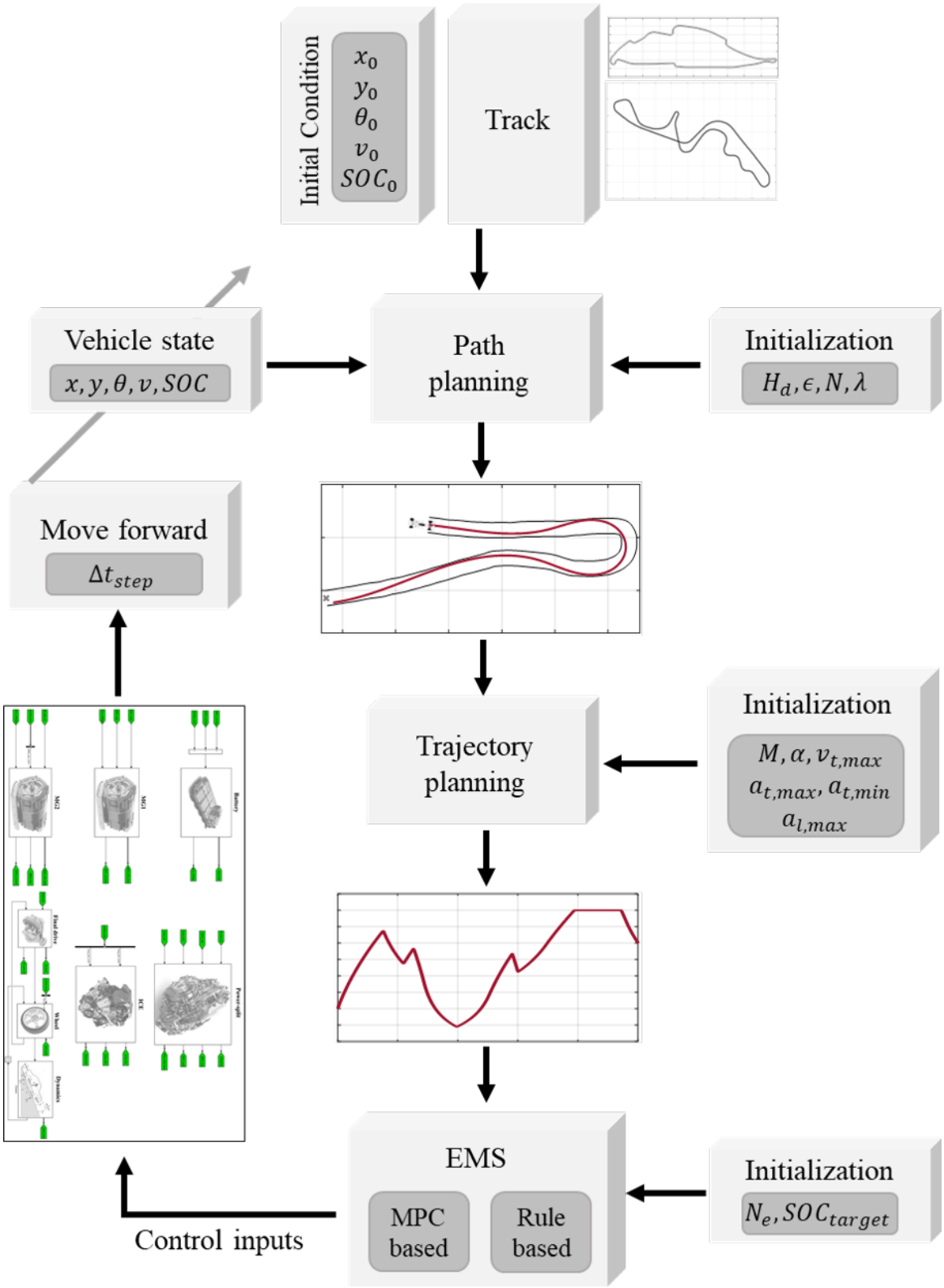

Figure 7.24: Schematic of the iterative motion planning integrated with EMS for an AV in a racing track.

7.5.3 Results

In the results of this section, our main focus is on performance evaluation of the real-time MPC-based EMS. Hence, except the observable horizon, we tune and fix the other motion planning parameters to replicate a case of a passenger vehicle in the track, with more concentration on the drive comfort. These parameters are shown in Table 7.4. We use $\lceil H_d \rceil$ for N and M to ensure that path and trajectory planning

Table 7.4: Fixed Motion Planning Parameters

Path planning			Trajectory planning					
ϵ	N	λ	M	α	$v_{t,max}$	$a_{t,max}$	$a_{t,min}$	$a_{l,max}$
$5\,m$	$\lceil H_d \rceil$	0.05	$\lceil H_d \rceil$	0.005	$25\,m/s$	$3\,m/s^2$	$-8\,m/s^2$	$1.5\,m/s^2$

happens with intervals of at most one meter. λ and α are tuned to shift the trade-off toward comfort. The maximum speed of $25\,m/s$ is equivalent to $90\,kph$ which is a typical high speed for roads. Moreover, maximum threshold of $1.5\,m/s^2$ for the lateral acceleration provides a comfortable drive in the turns [106].

For the N_e, we use $N_e = \lceil t_f - t_i \rceil$, where t_f and t_i are the final and the initial time of the given trajectory, respectively. This ensures that the optimization problem for EMS is solved with time intervals of at most one second. Solving three described optimization problems takes about $0.05\,s$ CPU time, so we choose $\Delta t_{step} = 0.1\,s$ to perform the iterative procedure with a frequency of $10\,Hz$.

Moreover, we set the initial and the target SOC to 40% and initial vehicle speed to $v_0 \approx 0$. With these parameters being set, we run the integrated model for different observable horizons of H_d, with both embedded MPC-based and rule-based controllers. Figure 7.25 and 7.26 show the velocity, fuel power, and SOC results for the one with rule-based controller. Furthermore, we show the speed profile results, as well as a few powertrain component signals, for $H_d = 100\,m$ in Figure 7.27 to Figure 7.28. Again we emphasize on the fact that we apply the control inputs from both MPC-based and rule-based approaches on the same high-fidelity vehicle model. This point is crucial for our performance comparison and conclusions, later in this work. We should also ensure that both approaches result in the comparable velocity profiles. This would guarantee that powertrain is satisfying the same power and torque demand.

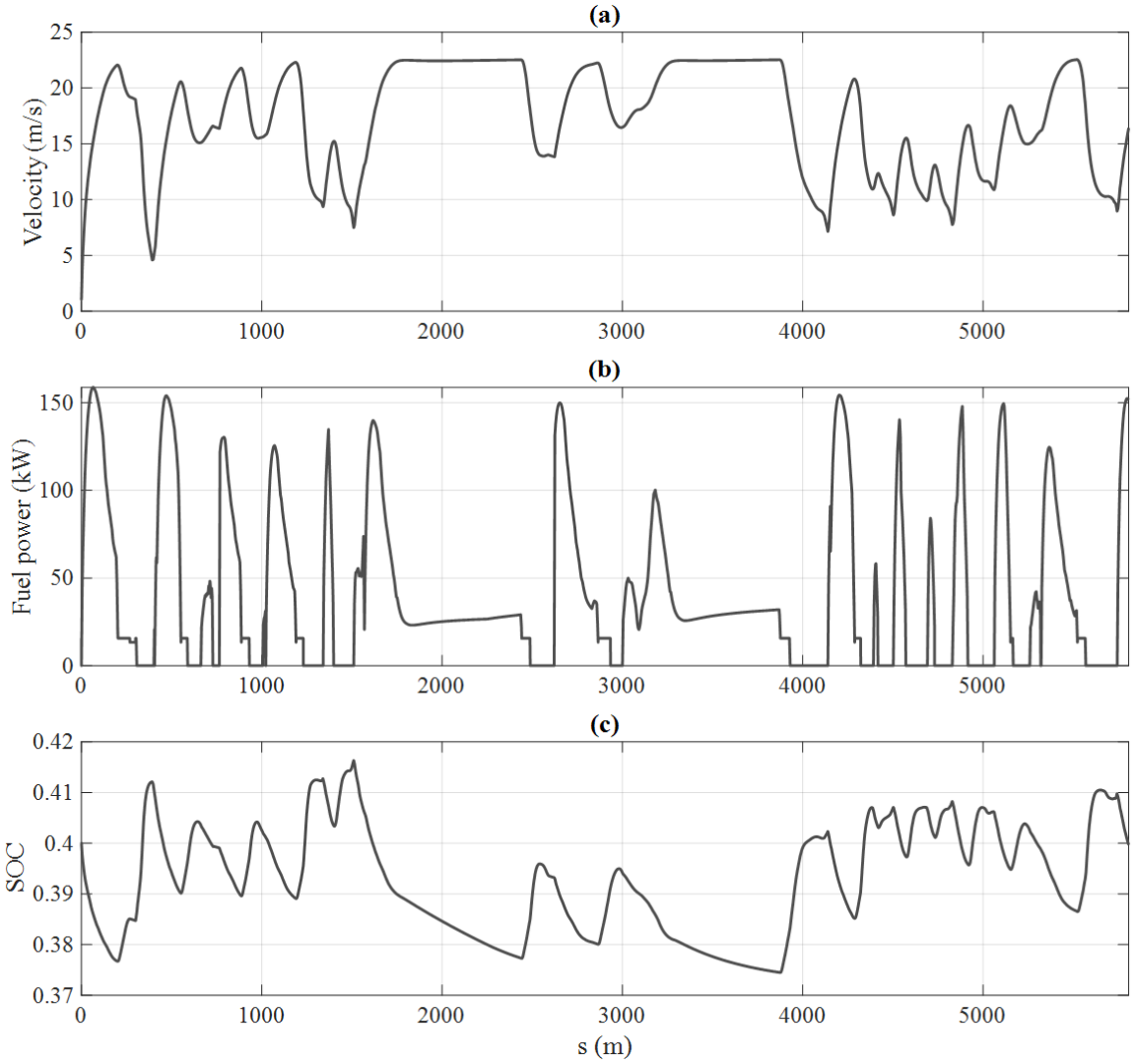

Figure 7.25: Results of trajectory and powertrain component signals for the rule-based approach, for a lap around Suzuka circuit.

We evaluate the integrated model for different values of the observable horizon of H_d. Observable horizon does not affect the performance of the rule-based controller. Hence, there is only a single velocity profile for all the cases. Figure 7.29 and 7.30 shows the results for the velocity profile of the integrated model, using both the MPC-based and rule-based controllers, for different values of H_d. These figures clearly illustrate that velocity profiles and hence the power/torque demands are totally comparable. Interestingly in these figures, it can be inferred that the integrated model with a higher H_d achieves a slightly higher vehicle tangential speed. Longer horizon helps

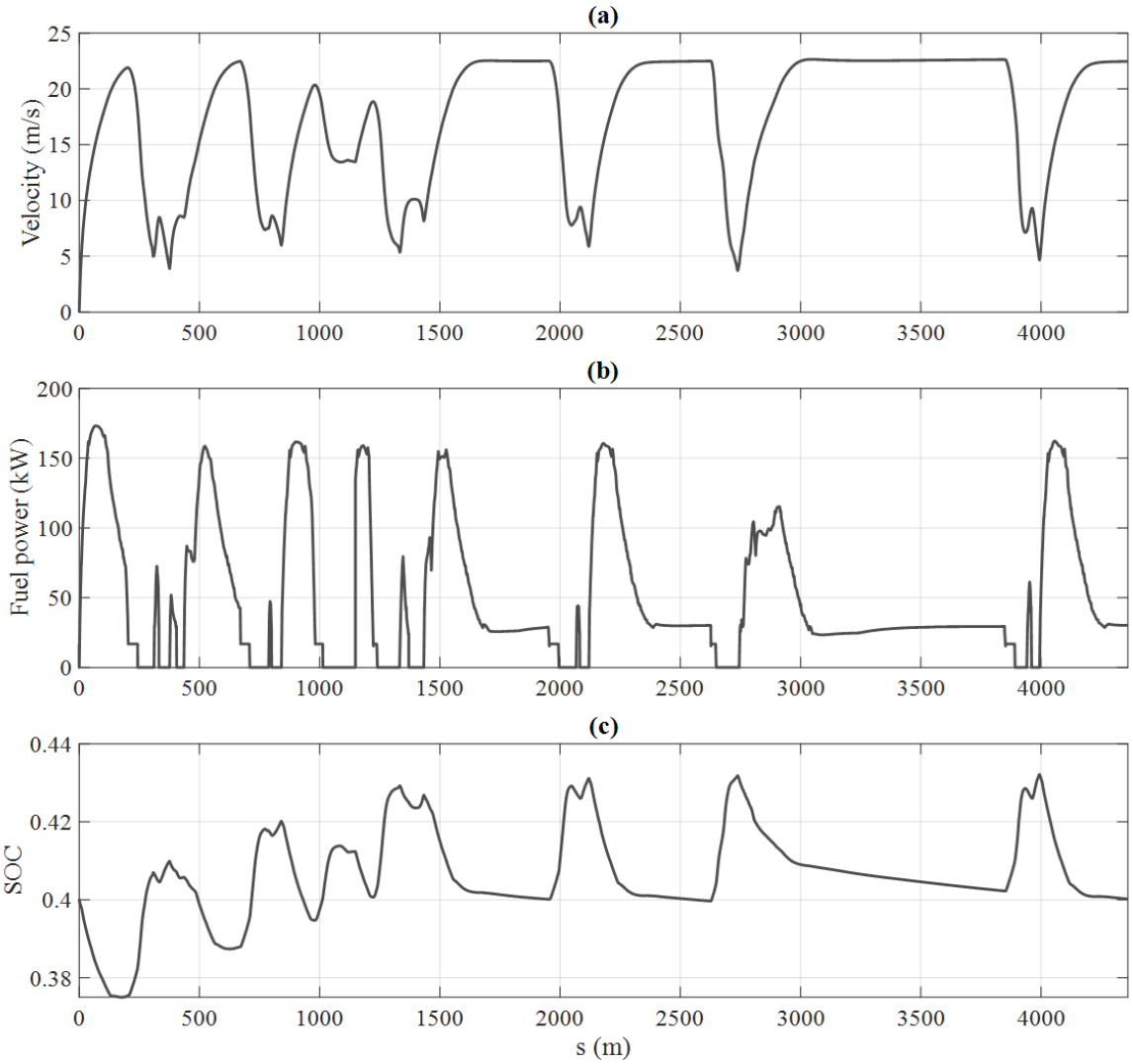

Figure 7.26: Results of trajectory and powertrain component signals for the rule-based approach, for a lap around Gilles Villeneuve circuit.

the controller to plan more accurately to meet the motion planning objectives within the powertrain limits such as the maximum battery power or ICE power. Besides, using the high-fidelity model as a plant for both rule-based and MPC-based controller, we have ensured that powertrain is providing similar power/torque for both the cases. Therefore, our comparison for the fuel consumption results would be sensible. We should also consider the final SOC while comparing fuel consumption results. The final SOC for the MPC-based method is the same as the initial SOC, since this is one of the constraints of the optimization problem, solved in each iteration. As a result of

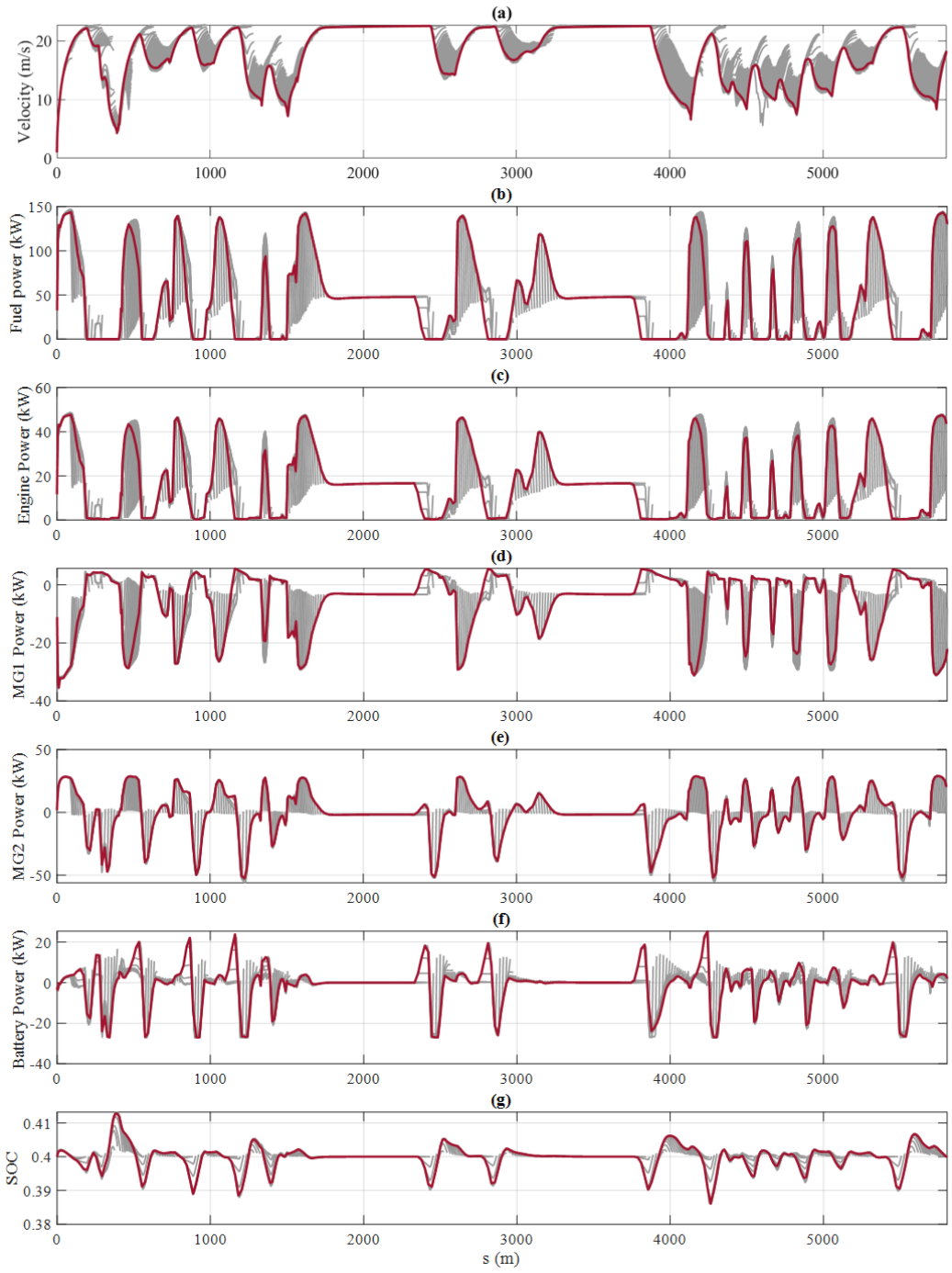

Figure 7.27: Results of trajectory and powertrain component signals for the MPC-based approach, for a lap around Suzuka circuit with $H_d = 100\,m$.

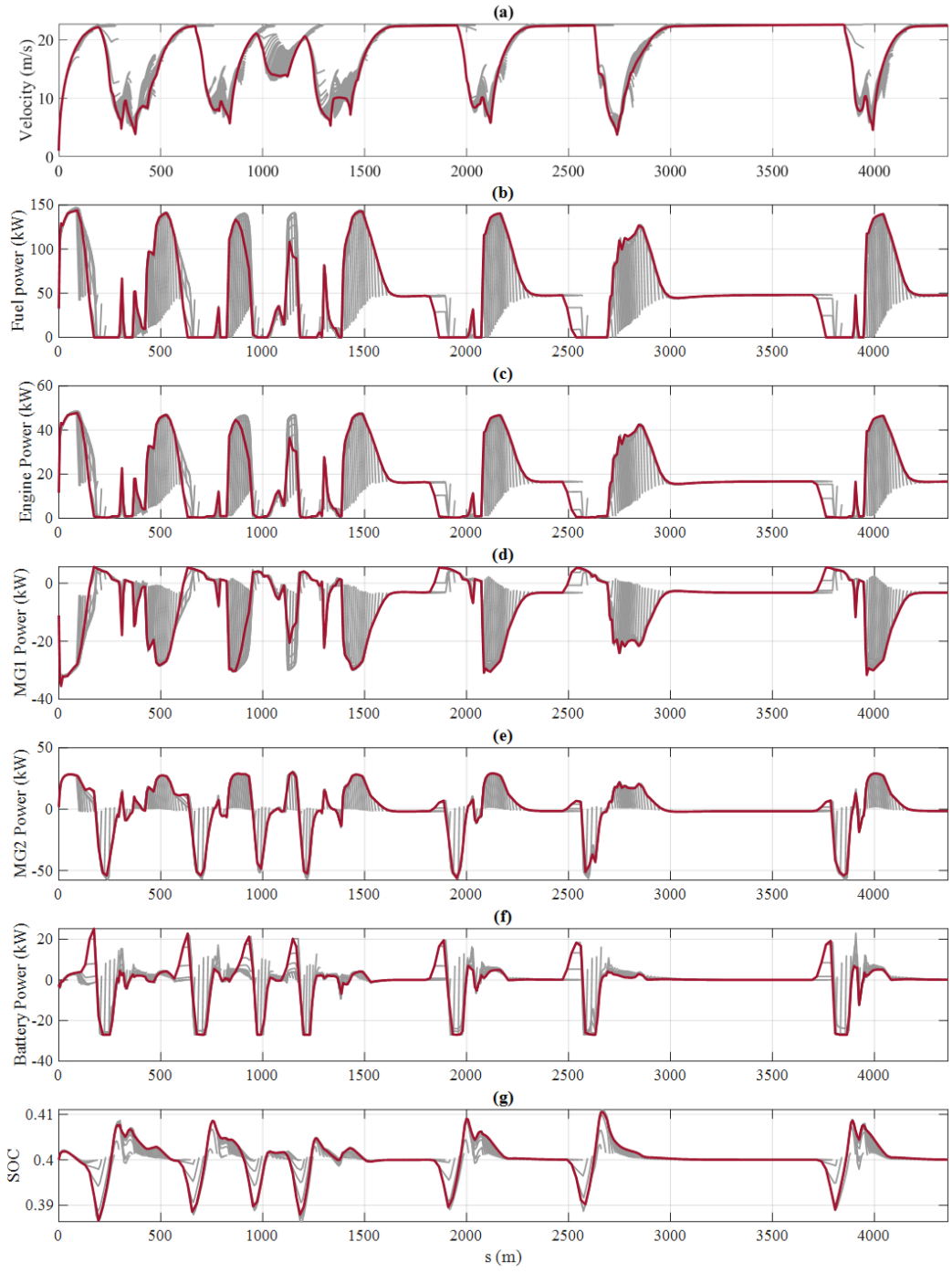

Figure 7.28: Results of trajectory and powertrain component signals for the MPC-based approach, for a lap around Gilles Villeneuve circuit with $H_d = 100\,m$.

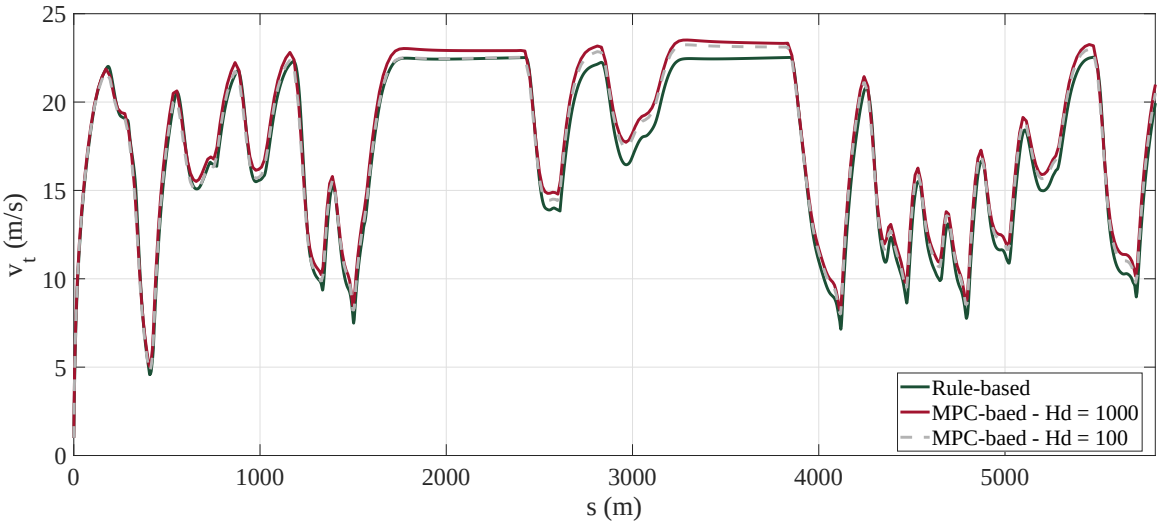

Figure 7.29: Tangential velocity profiles for rule-based and MPC-based controllers with different H_d, for Suzuka circuit.

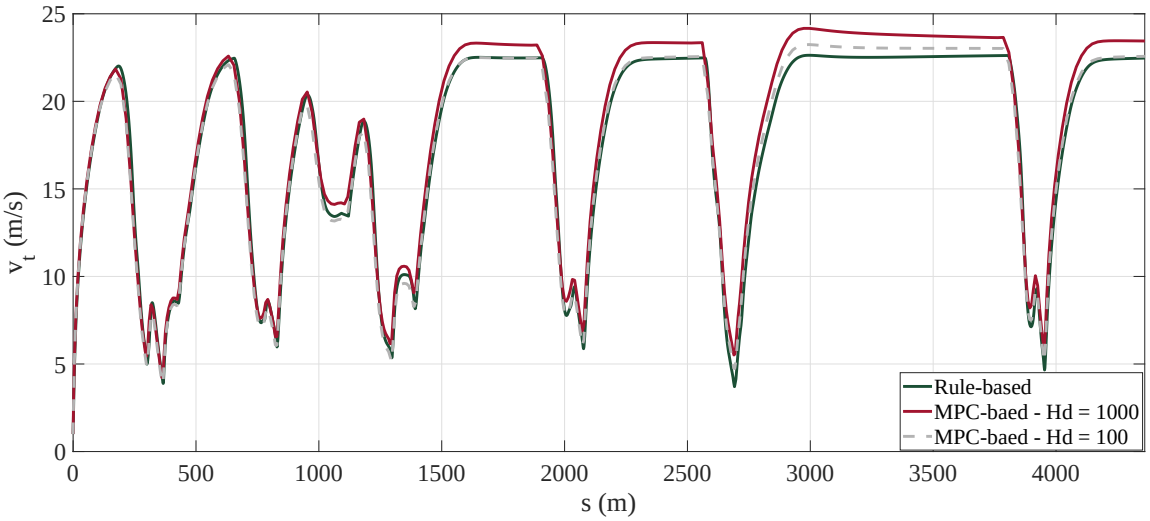

Figure 7.30: Tangential velocity profiles for rule-based and MPC-based controllers with different H_d, for Gilles Villeneuve circuit.

perfect calibration of the rule-based controller, the final SOC for this case is also very close to the initial SOC, as seen in the Figure 7.25 and 7.25. We also apply dynamic programming on the high-fidelity model for the velocity profiles of the rule-based controller, reported in Figure 7.29 and 7.30. DP results are the globally optimal results that we use as benchmarks to evaluate the developed ASEMS using MPC-based controller in the integrated model. We report the an exhaustive comparison of the fuel

consumption in Table 7.5. where we find diff. 1 and diff. 2 using following equations

Table 7.5: Fuel Consumption Comparison

Method	Suzuka Track			Gilles Villeneuve Track		
	FC (g)	diff. 1 (%)	diff. 2 (%)	FC (g)	diff. 1 (%)	diff. 2 (%)
Rule-based	381.42	0	25.08	335.47	0	22.62
DP	304.94	−20.05	0	273.58	−18.45	0
MPC-based with $H_d = 100m$	363.19	−4.78	19.01	328.68	−2.02	20.14
MPC-based with $H_d = 200m$	360.93	−5.37	18.36	324.81	−3.18	18.73
MPC-based with $H_d = 300m$	358.60	−5.98	17.60	322.08	−3.99	17.73
MPC-based with $H_d = 400m$	354.23	−7.13	16.16	318.65	−5.02	16.47
MPC-based with $H_d = 500m$	350.69	−8.06	15.00	314.87	−6.14	15.09
MPC-based with $H_d = 600m$	348.98	−8.50	14.44	312.20	−6.94	14.12
MPC-based with $H_d = 700m$	348.27	−8.69	14.21	309.11	−7.86	12.99
MPC-based with $H_d = 800m$	340.34	−10.77	11.61	302.90	−9.71	10.72
MPC-based with $H_d = 900m$	332.08	−12.94	8.90	298.55	−11.01	9.13
MPC-based with $H_d = 1000m$	327.59	−14.11	7.42	292.49	−12.81	6.91

$$\text{diff. } 1 = \frac{FC - FC_{RB}}{FC_{RB}} \times 100 \tag{7.46}$$

$$\text{diff. } 2 = \frac{FC - FC_{DP}}{FC_{DP}} \times 100 \tag{7.47}$$

Rule-based model is sub-optimal in total fuel consumption for a single lap with an average of 23.85% for two racing tracks, compared to optimal results of DP. Also, we can clearly see that even with an observable horizon of $H_d = 100\,m$, MPC-based controller outperforms the rule-based controller with an average of 3.2% less FC. Interestingly, as longer observable horizons are achievable, fuel consumption significantly getting closer to the DP results. For the ultimate case of $H_d = 1000\,m$ in our analysis, the MPC-based controller is just sub-optimal by 7.17% on average, compared to DP results. Figure 7.31 shows the trend in total fuel consumption and how the MPC-based method lays between the rule-based and optimal DP results in terms of fuel consumption.

Longer observable horizon for the MPC-based approach results in less fuel con-

sumption. However, this comes with an increased computational burden which would undermine the real-time applicability. The final decision for the observable horizon depends on the capabilities of perception modules as well as embedded hardware computational power. This also depends on the trade-off between optimality and the computational burden. As a result, allocation of significant processing resource for this approach would result in better fuel economy. Furthermore, Figure 7.32 and 7.32 show

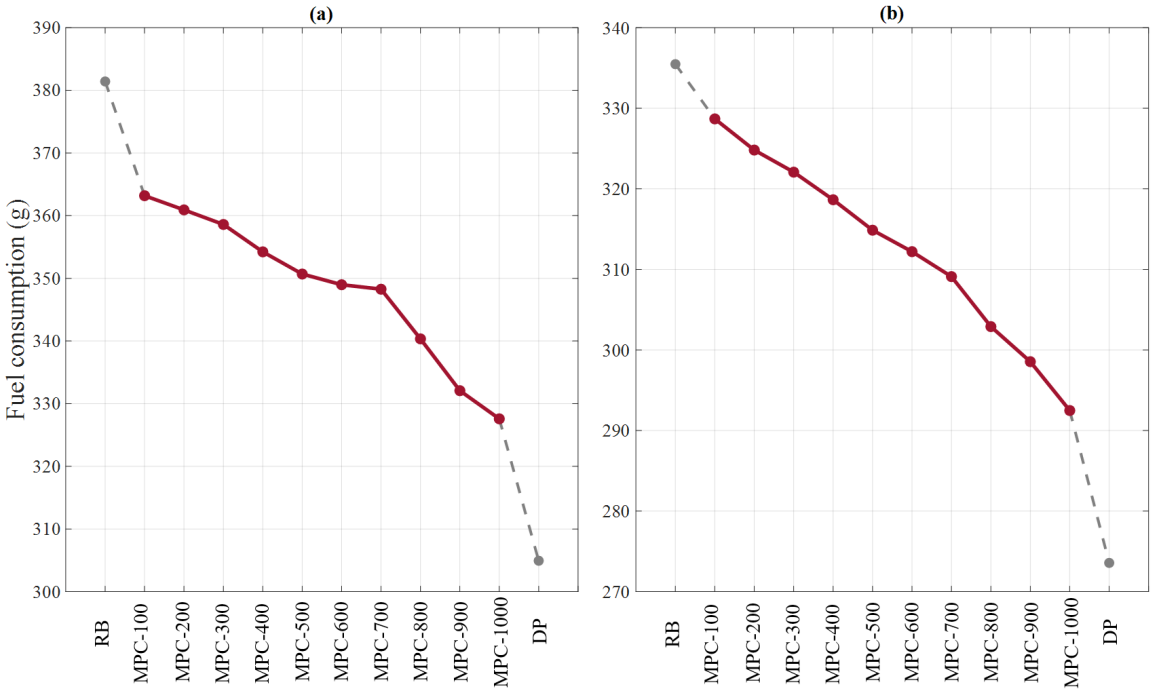

Figure 7.31: Comparison of total fuel consumption for a single lap around the (a) Suzuka and (b) Gilles Villeneuve racing tracks.

the SOC profile for two extreme cases of analyzed MPC-based controllers, compared with optimal SOC profile of DP. As observable horizon increases, tolerable SOC difference also increases. Also note that overall trend of SOC trends are completely comparable.

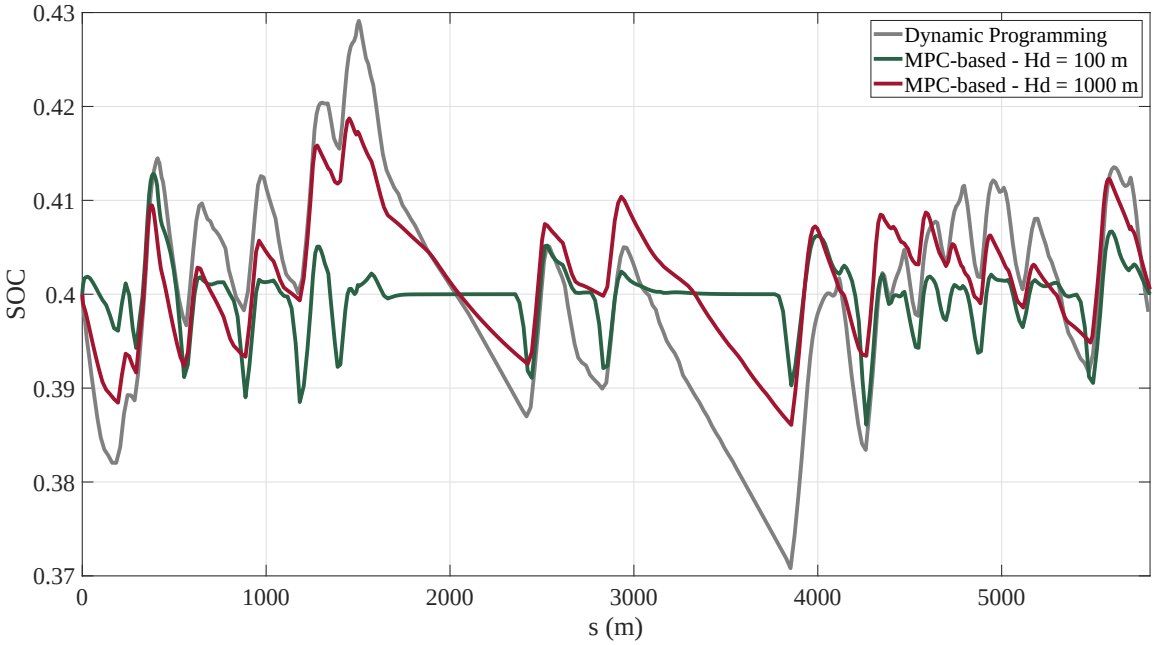

Figure 7.32: Comparison of SOC profiles for a single lap around Suzuka racing track.

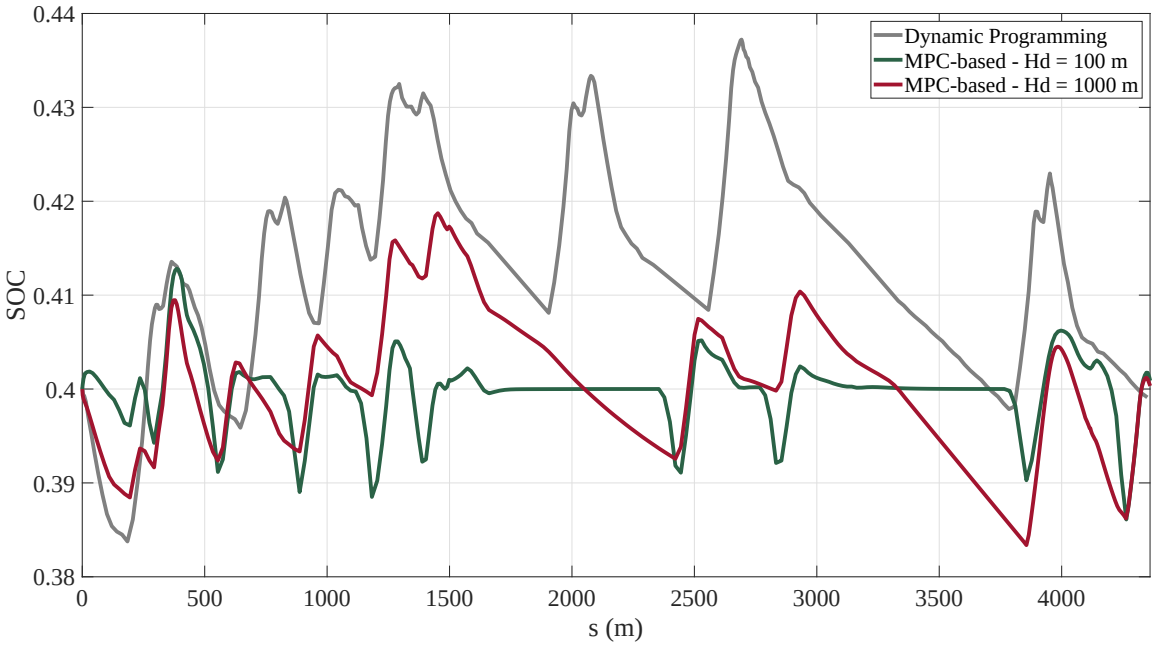

Figure 7.33: Comparison of SOC profiles for a single lap around Gilles Villeneuve racing track.

Chapter 8

Conclusions and Future Work

The automotive industry is experiencing groundbreaking transformations as a result of two mainstreams: electrification and autonomous driving. In addition to the advantages of each field individually, we discussed how intersection and interaction of them could provide new opportunities for further improvements in the vehicles of the next generation. For the case of an autonomous hybrid electric vehicle (A-HEV), we presented the idea of autonomous-specific energy management strategies (ASEMS) in this work. We investigated the idea further and also provided a proof-of-concept.

In this chapter, we collect and discuss the main conclusions of our work. We also present the potential improvements and next steps in the form of future work.

8.1 Conclusions

First, for our case study, Toyota Prius 2010, we developed a high-fidelity model using online available data. We identified the model parameters by comparing model output to the original dynamometer data. Our model is a system-level model with a focus on power flow and energy consumption. In the absence of an actual A-HEV, we used this as the plant model to make sensible judgments of different types of energy management strategies. Driver, control unit, and the vehicle are the main subsystems of the developed model, each including other subsystems. Evaluation of the high-fidelity model shows acceptable conformity with the dynamometer data. For instance, for the steady-state driving cycle, model and data engine fuel flow have an rms error of 0.091 g/s. As a result, we can ensure that any observed improvement in the results of the

model due to a new energy management strategy can be similarly obtained in the actual vehicle.

Second, we presented a novel convex model representation of the case study. We developed the convex model by representing each component (e.g., engine, motor/generator, battery, power-split) using convex functions and constraints. This helped us to reformulate the optimal control problem of energy-efficient energy management strategy within the canonical convex optimization format. The main advantage of facing a convex optimization problem (e.g., linear programming, quadratic programming, conic optimization, semidefinite programming) is having access to advanced dedicated numerical solvers. These solvers can achieve a globally optimal solution in a considerably less amount of time compared to other alternatives for solving an optimal control problem. For instance, on the convex model, results for dynamic programming are 2.40% sub-optimal on average for a few driving cycles, compared to the convex approach. Additionally, the convex approach needs 97.43% less time on average, to obtain the optimal results. However, the result should be evaluated finally on the high-fidelity model. At this point, we removed the driver and control unit out of the loop of the high-fidelity model. We applied the extracted signals from the convex approach to the vehicle model. These signals are the control inputs, torque, and speed for the powertrain components. The results of convex approach just slightly deteriorated (2.75% on average) on the nonlinear vehicle model, and showed comparable results to the dynamic programming. This is mainly due to the presented novel convex representation of the vehicle and powertrain.

Third, in the absence of having access to motion planning data of an actual self-driving car in the typical driving scenarios, we perform the ASEMS proof-of-concept by developing the optimization-based motion planning for the simplified driving scene of a racing track. We considered Suzuka and Gilles Villeneuve racing tracks as examples. We also considered that A-HEV is driving in the racing track with known boundaries and constraints and having the ability to observe up to the observable/prediction horizon. We considered comfort and travel time as our optimization objective while addressing both path and trajectory planning problems. We provided the planned path, precise geometrical coordinates (e.g., x-y coordinates, orientation, curvature) expressed as a function of arc-length variable up to the observable horizon, to the trajectory planner to obtain the velocity profile up to the observable horizon. Also, as shown, we let the vehicle to perform a lap around the track by iteratively solving the

optimization problems for the path and trajectory planning. We also analyzed the dependence of the results on the tuning parameters. Calibrating tuning parameters to emphasize on the travel time resulted in path and trajectories similar to those being used in the motorsport. On the other hand, pushing the trade-off toward comfort gives a smoother path by taking advantage of Euler spirals and comfortable trajectory due to lateral and tangential acceleration/deceleration minimization.

Fourth, we integrated the developed energy management strategy using the convex optimization approach with the motion planning module. We took a model predictive control approach and solved the energy-efficient energy management optimization problem at each step and applied the control inputs on the nonlinear vehicle model. For the chosen set of hyper-parameters, solving path, trajectory, and the energy management problem takes about $0.05s$ combined, at each step. Again, we let the A-HEV with integrated EMS to perform a lap around the track. To get a better comparison, we also tested the rule-based controller in the same condition. Even with the short observable horizon of 100 m, MPC-based controller outperformed rule-based controller by achieving 3.2% less fuel consumption on average for a lap. We implemented dynamic programming on the same condition to get the benchmark of minimum feasible fuel consumption per lap. We also observed that as a longer observable horizon is achievable, results of MPC-based controller tend to converge to the DP results, being only 7.17% sub-optimal for the observable horizon of 1000 m. Even with the horizon of 100 m, improvements as a result of using ASEMS instead of a conventional rule-based controller is extremely promising. With the conservative promise of 3.2% reduction in fuel consumption, we anticipate that ASEMS can save about 30,000,000 liters of fuel per year for the prospective Waymo (Chrysler Pacifica) and Uber (Volvo XC90) A-HEV fleets combined.

8.2 Future Work

In this section, we discuss the potential future work, as a sequel to this work, particularly regarding further investigations on the ASEMS. In this context, we are eagerly looking forward to collaborating with other researchers, engineers, tech companies, and automotive manufacturers.

8.2.1 Advanced High-Fidelity Model

High-fidelity model, presented in Chapter 5, considers mostly quasi-static equations for the components. We want to expand the model to consider the higher-order dynamics, particularly in the engine and power-split behavior. Also, we are looking to incorporate the effects of the temperature on the subsystems, such as the battery. In the vehicle subsystem, we only considered the longitudinal dynamics. Advanced 2-D or 3-D vehicle dynamics would increase the fidelity of the model. While we are working on improving the model, we are looking forward to collaborations to use already developed vehicle and powertrain models to decrease the gap between simulation and the real-life environment.

8.2.2 Convex Optimization Problem Complexity

As we achieve advanced high-fidelity models, we should also proceed to obtain more accurate convex representation to keep the gap reasonably low. Meanwhile, we would like to investigate and compare the results of different convex optimization problem representations, both in offline and real-time applications. The developed convex optimization problem in this work is in the form of semidefinite programming. While including complex convex functions empowered us to obtain a more accurate representation of the actual plant, solving the problem requires more processing time compared to the linear programming and quadratic programming. We are working on developing and testing different representations to find the trade-off between complexity and processing time for both offline and real-time application.

8.2.3 Solving Convex Optimization Problem

We have used available solvers for convex optimization problems such as SDPT3, Mosek, Gurobi, and SeDuMi. Performing a comprehensive study on the performance of each solver in path, trajectory, and energy management optimization problems would be extremely useful. We also want to consider the option of testing alternative solvers. In the final implementation, we want to remove CVX as the optimization modeling language out of the loop and interact directly with the solver's interface in C++, for instance. Ultimately, the specific numerical solver can be developed for the optimization problem to decrease the solving time substantially. This can be a

result of exploiting the particular KKT matrix structure to boost up the algebraic calculations.

8.2.4 Motion Planning Data

In the absence of actual motion planning data for the A-HEV, we considered using the optimization-based path-planner to tackle motion planning. However, it is truly intriguing to investigate the performance of ASEMS on the high-fidelity model using motion planning data from an actual A-HEV such as Chrysler Pacifica. In this context, we have asked Fiat Chrysler Automobiles, as the industrial partner of McMaster Automotive Resource Centre, and we are looking forward to collaborating with the FCA.

8.2.5 Vehicle Path Controller

To evaluate ASEMS, in Chapter 7, we let the vehicle to go around the track, and we executed the path planner at each step. However, we considered a perfect path following for the vehicle. Practically, the vehicle path is primarily controlled by the steering wheel angle. Also, we considered a simpler 2-D vehicle dynamics, basically a rectangle with known coordinates and orientation. Hence, we plan to include more complex dynamics model, bicycle model, for instance, and to use the steering controller at the same time.

8.2.6 State Estimation

In Chapter 7, as the vehicle traveled around the track, we updated the vehicle initial states (e.g., coordinates, orientation, speed, and SOC) using the open-loop model predictions. In practice, this is not exactly the case since there are always model uncertainties. We like to integrate state estimation methods such as Kalman Filtering or Extended Kalman Filtering to update the states using both model predictions and sensor outputs (e.g., GPS, battery voltage).

8.2.7 Testing on an A-HEV

Ultimate future work for us is repeating almost the same procedure and integrating the EMS with motion planning module in an A-HEV. It is intriguing for us to implement

the MPC-based ASEMS in the vehicle processing units and evaluate the results on an actual vehicle. Regarding this, we are looking forward to collaborating with research labs and self-driving car companies.

Appendices

Appendix A

Interactive Interface

To better illustrate the real-time performance of the ASEMS, we have developed an interactive interface using App Designer in MATLAB. As shown in following figures, this interface takes tunable initialization parameters as inputs and generates the results of path planning, trajectory planning, and the MPC-based energy management strategy. The initialization parameters we consider are

1. Observable Horizon (m): Portion of route (racing track) in front of the vehicle which is perceivable by the vehicle modules.

2. Index 1-10000: A number between 1 to 10000 which indicates the initial position of the vehicle in the racing track.

3. Initial Speed (m/s): Initial speed of the vehicle.

4. Max Speed (m/s): Maximum allowable speed of the vehicle.

5. Max Long Accel (m/s^2): Maximum allowable longitudinal acceleration for the vehicle. Mostly depends on the powertrain capability and drive comfort.

6. Min Long Accel (m/s^2): Minimum allowable longitudinal acceleration for the vehicle. Mostly depends on the braking capability and drive comfort.

7. Max Lat Accel (m/s^2): Maximum allowable lateral acceleration. Mostly depends on the drive comfort and tire limits.

8. Initial SOC: Initial state of charge of the battery pack.

9. Target SOC: Reference battery state of charge for the controller.

Beside these parameters, two sliders control the trade-off between travel time and comfort for path and trajectory planning. We can also select the operating racing track. Two dials at the end show the instantaneous vehicle speed and fuel consumption.

There are six different plots in this interface. Track plot shows the area of the track vehicle is operating at. Path plot shows the obtained path up to the observable horizon. Trajectory plot shows the velocity profile for the given path. Finally, SOC, Engine Power, and Battery Power plots are the results of MPC-based EMS for the given velocity profile taking fuel consumption as the main objective. Below, we have shown output of this interface for different conditions.

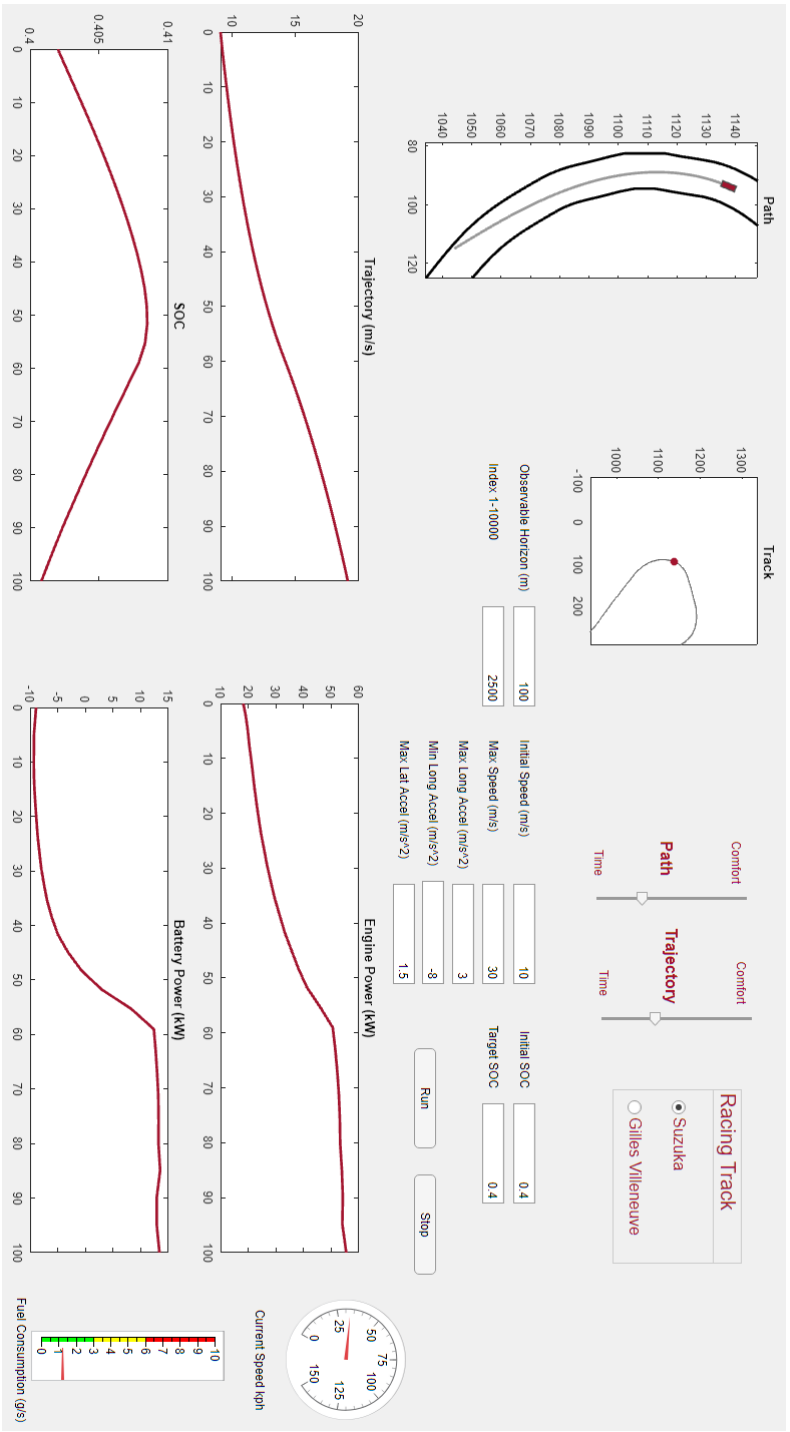

Figure A.1: Example of interactive interface output.

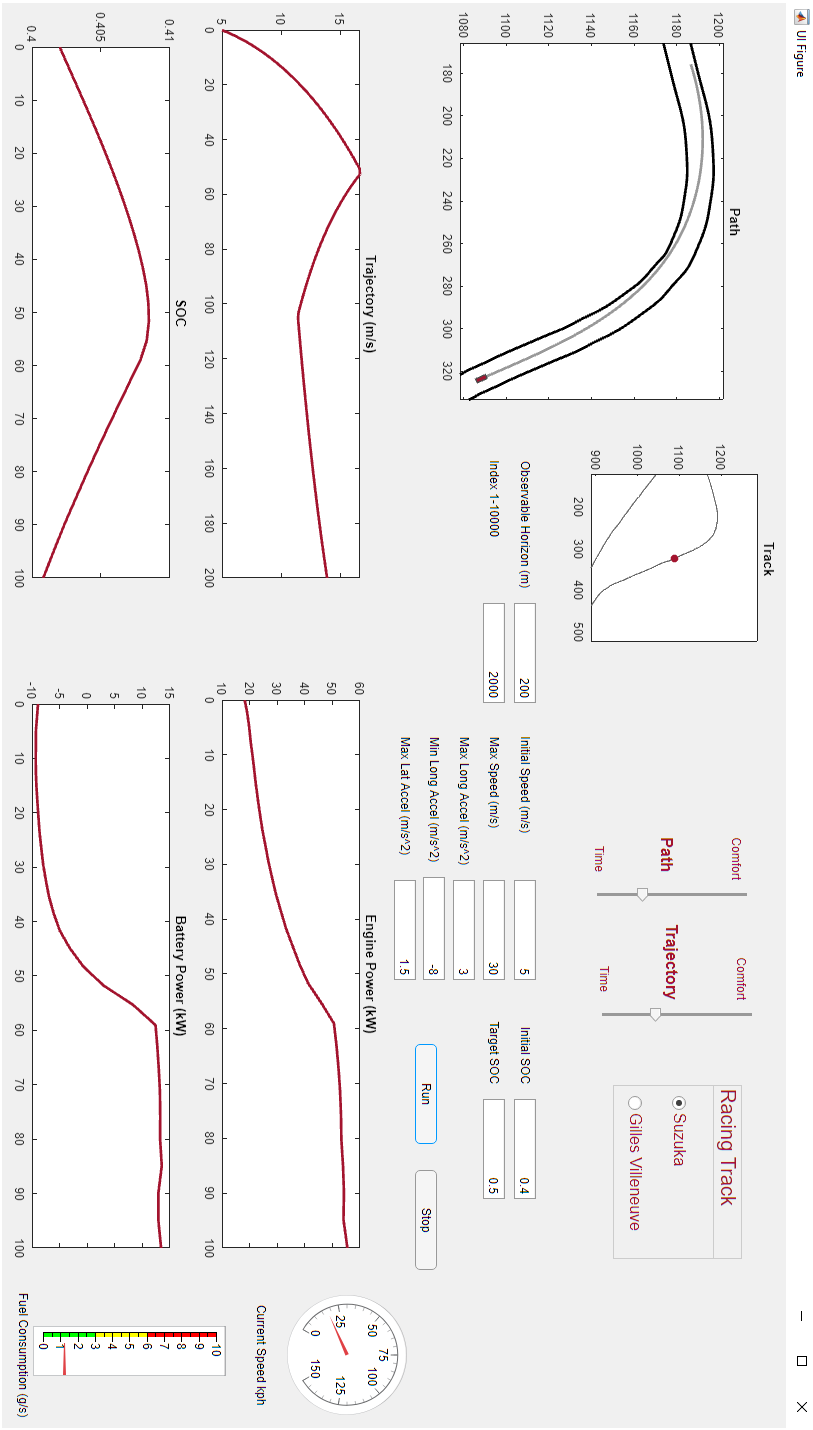

Figure A.2: Example of interactive interface output.

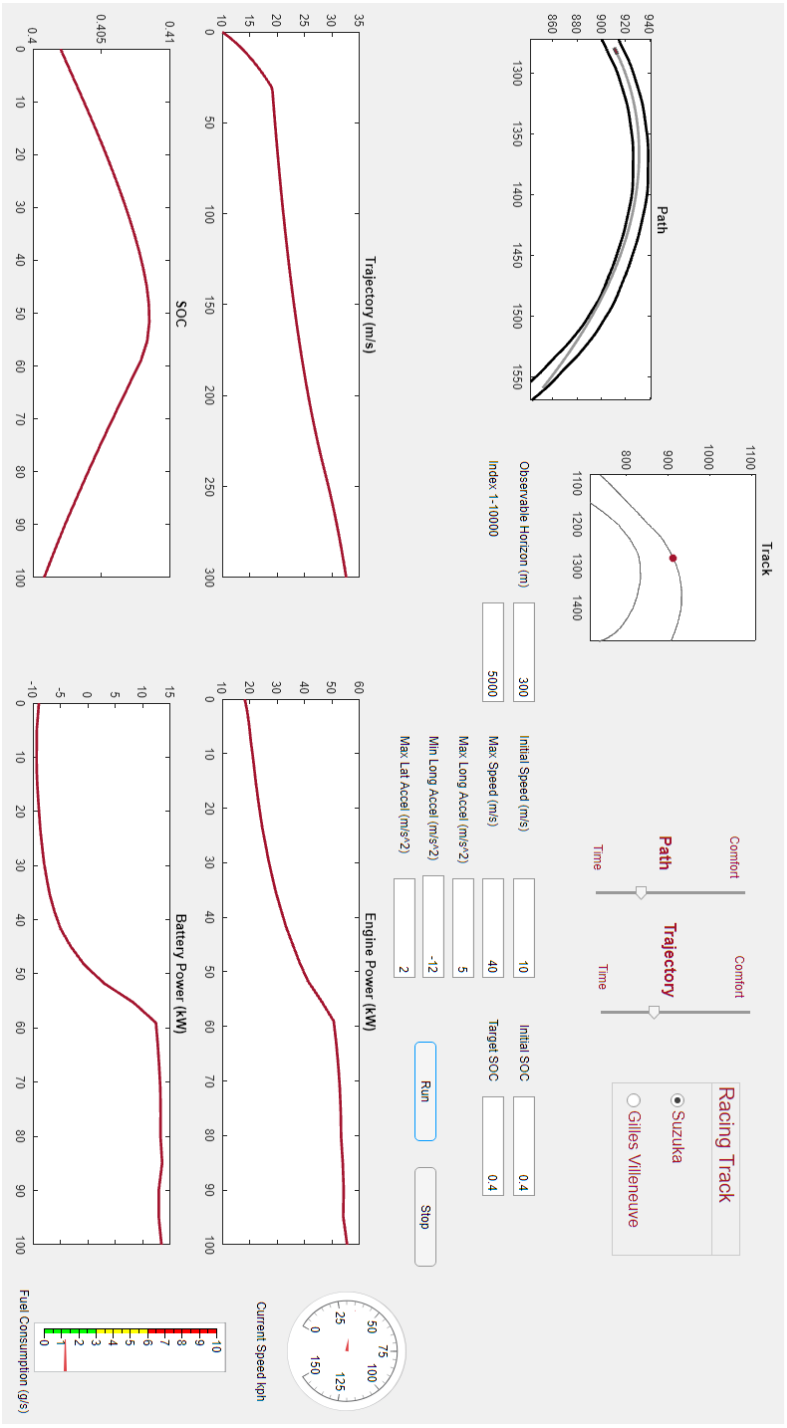

Figure A.3: Example of interactive interface output.

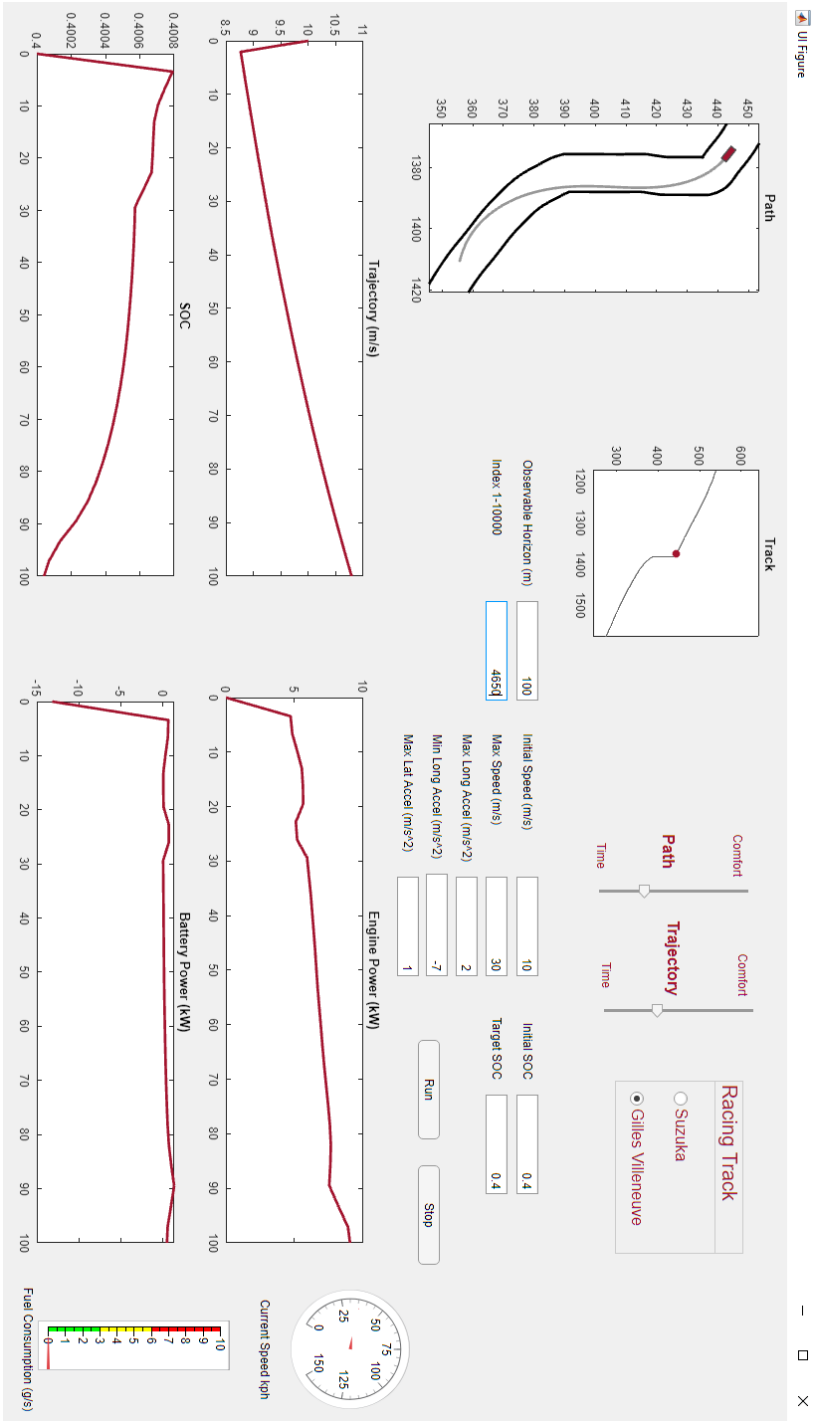

Figure A.4: Example of interactive interface output.

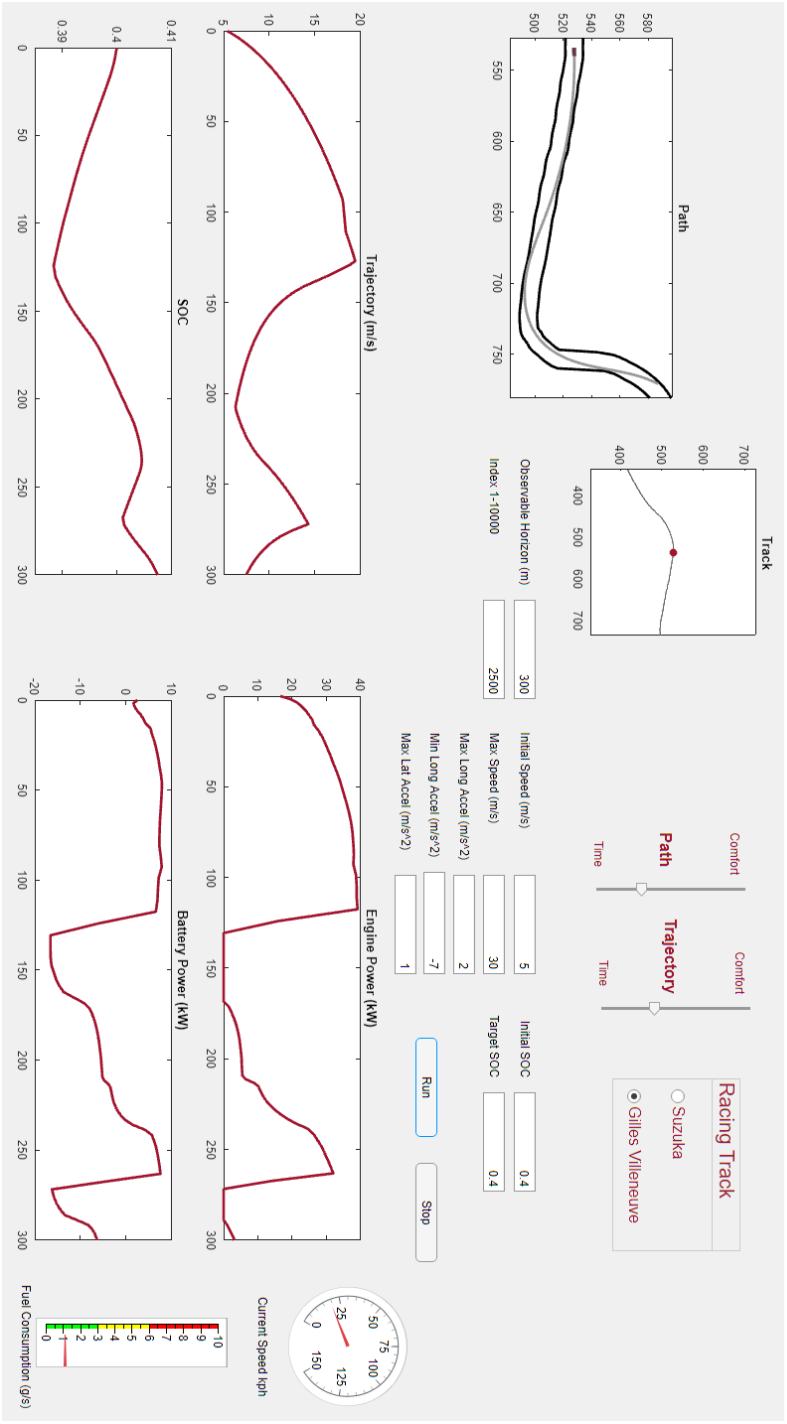

Figure A.5: Example of interactive interface output.

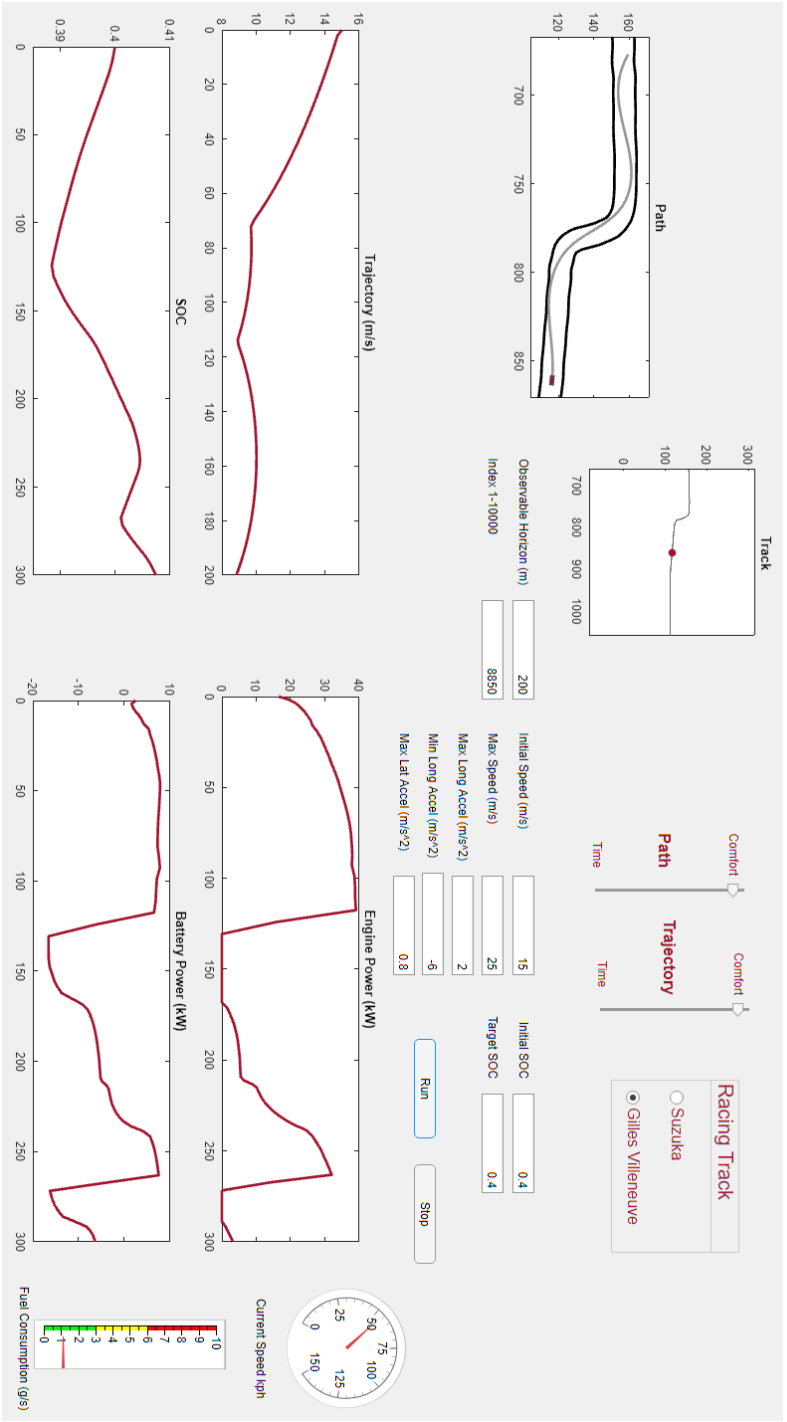

Figure A.6: Example of interactive interface output.

Bibliography

[1] *Sources of Greenhouse Gas Emissions*. URL: https://www.epa.gov/ (cit. on p. 2).

[2] *Power Electronics for Electric Drive Vehicles*. [Accessed: 2019-07-23]. URL: ecee.colorado.edu/~ecen5017/ (cit. on p. 2).

[3] Ali Emadi. "Transportation 2.0". In: *IEEE Power and Energy Magazine* 9.4 (2011), pp. 18–29 (cit. on pp. 2, 3).

[4] Berker Bilgin, James Weisheng Jiang, and Ali Emadi. *Switched Reluctance Motor Drives: Fundamentals to Applications*. CRC Press, 2019 (cit. on p. 3).

[5] Berker Bilgin, Ali Emadi, and Mahesh Krishnamurthy. "Design considerations for switched reluctance machines with a higher number of rotor poles". In: *IEEE Transactions on Industrial Electronics* 59.10 (2011), pp. 3745–3756 (cit. on p. 3).

[6] Jin Ye, Berker Bilgin, and Ali Emadi. "An extended-speed low-ripple torque control of switched reluctance motor drives". In: *IEEE Transactions on Power Electronics* 30.3 (2014), pp. 1457–1470 (cit. on p. 3).

[7] *The zero-emission vehicle (ZEV) standard*. [Accessed: 2019-07-23]. URL: http://www.environnement.gouv.qc.ca/ (cit. on p. 4).

[8] *B.C. passes law to increase sales of zero emission vehicles*. [Accessed: 2019-07-23]. URL: https://www.cbc.ca/ (cit. on p. 4).

[9] International Energy Agency. *Global EV Outlook 2019*. 2019, p. 232. DOI: https://doi.org/https://doi.org/10.1787/35fb60bd-en. URL: https://www.oecd-ilibrary.org/content/publication/35fb60bd-en (cit. on p. 4).

[10] Ching Chue Chan. "The state of the art of electric, hybrid, and fuel cell vehicles". In: *Proceedings of the IEEE* 95.4 (2007), pp. 704–718 (cit. on pp. 4, 10).

[11] *Global Autonomous Driving Market Outlook, 2018*. [Accessed: 2019-07-24]. URL: https://ww2.frost.com/ (cit. on p. 5).

[12] *Waymo's fleet of self-driving minivans is about to get 100 times bigger* (cit. on pp. 6, 27).

[13] *Uber unveils next-generation Volvo XC90 self-driving car*. [Accessed: 2019-07-24]. URL: https://www.theglobeandmail.com/ (cit. on p. 6).

[14] *Volvo XC90 Specs*. [Accessed: 2019-07-24]. URL: https://www.volvocars.com/ (cit. on p. 6).

[15] *What is the history of hybrid cars?* [Accessed: 2019-05-22]. URL: https://www.howstuffworks.com/ (cit. on p. 10).

[16] Berker Bilgin, Pierre Magne, Pawel Malysz, Yinye Yang, Vera Pantelic, Matthias Preindl, Alexandre Korobkine, Weisheng Jiang, Mark Lawford, and Ali Emadi. "Making the case for electrified transportation". In: *IEEE Transactions on Transportation Electrification* 1.1 (2015), pp. 4–17 (cit. on p. 11).

[17] *Technology Trends - Electrification*. [Accessed: 2019-07-25]. URL: https://www.continental-automotive.com/ (cit. on p. 11).

[18] *The race to improve fuel economy*. [Accessed: 2019-05-28]. URL: https://www.consumerreports.org/ (cit. on p. 14).

[19] *CAFE Public Information Center*. [Accessed: 2019-05-28]. URL: https://www.nhtsa.gov/ (cit. on p. 14).

[20] *United States Environment Protection Agency, Sources of Greenhouse Gas Emissions, Transportation Sector Emissions*. [Accessed: 2019-05-29]. URL: http://www.epa.gov/ (cit. on p. 15).

[21] James M Anderson, Kalra Nidhi, Karlyn D Stanley, Paul Sorensen, Constantine Samaras, and Oluwatobi A Oluwatola. *Autonomous vehicle technology: A guide for policymakers*. Rand Corporation, 2014 (cit. on pp. 15, 24–26).

[22] Ann Y Watson, Richard R Bates, Donald Kennedy, et al. *Air pollution, the automobile, and public health*. National Academies, 1988 (cit. on p. 15).

[23] M Williams and R Minjares. "A technical summary of Euro 6/VI vehicle emission standards". In: *International Council for Clean Transportation (ICCT), Washington, DC, accessed July* 10 (2016), p. 2017 (cit. on p. 15).

[24] Zifei Yang and Anup Bandivadekar. "Light-duty vehicle greenhouse gas and fuel economy standards". In: *ICCT report* (2017) (cit. on p. 16).

[25] Christos Keramydas, Georgios Papadopoulos, Leonidas Ntziachristos, Ting-Shek Lo, Kwok-Lam Ng, Hok-Lai Wong, and Carol Wong. "Real-World Measurement of Hybrid Buses' Fuel Consumption and Pollutant Emissions in a Metropolitan Urban Road Network". In: *Energies* 11.10 (2018), p. 2569 (cit. on p. 16).

[26] Amgad Elgowainy, J Han, L Poch, M Wang, A Vyas, M Mahalik, and A Rousseau. *Well-to-wheels analysis of energy use and greenhouse gas emissions of plug-in hybrid electric vehicles.* Tech. rep. Argonne National Lab.(ANL), Argonne, IL (United States), 2010 (cit. on p. 16).

[27] *'Electrification factor' in transportation.* [Accessed: 2019-05-29]. URL: `https://www.eetimes.com/` (cit. on p. 16).

[28] *Turbo Engine Use at Record High.* [Accessed: 2019-05-29]. URL: `https://www.wardsauto.com/` (cit. on p. 17).

[29] Tomai Katrašnik, Samuel Rodman, Ferdinand Trenc, Aleš Hribernik, and Vladimir Medica. "Improvement of the dynamic characteristic of an automotive engine by a turbocharger assisted by an electric motor". In: *Journal of engineering for gas turbines and power* 125.2 (2003), pp. 590–595 (cit. on p. 17).

[30] Michael Valentine-Urbschat, Wolfgang Bernhart, et al. "Powertrain 2020–the future drives electric". In: *Roland Berger Strategy Consultants* 9 (2009) (cit. on pp. 17, 19, 20).

[31] *F1 Explained: The Most Powerful Mercedes F1 Engine Ever Made!* [Accessed: 2019-05-29]. URL: `https://www.youtube.com/watch?v=rGDJqTDXgtg` (cit. on p. 18).

[32] *The Dream of an Automated Highway.* [Accessed: 2019-05-31]. URL: `https://www.fhwa.dot.gov/` (cit. on p. 21).

[33] *Vehicle deaths estimated at 40,000 for third straight year.* [Accessed: 2019-05-31]. URL: `https://www.nsc.org/home/` (cit. on p. 21).

[34] *Self-Driving Vehicles Will Change The World In Some Unexpected Ways*. [Accessed: 2019-05-31]. URL: https://www.forbes.com/ (cit. on p. 21).

[35] *Essential stats for justifying and comparing self-driving cars to humans at the wheel*. [Accessed: 2019-05-31]. URL: https://www.forbes.com/ (cit. on p. 22).

[36] *Programme for a european traffic system with highest efficiency and unprecedented safety*. [Accessed: 2019-05-31]. URL: https://www.eurekanetwork.org/ (cit. on p. 22).

[37] Pedro F Lima. "Optimization-based motion planning and model predictive control for autonomous driving: With experimental evaluation on a heavy-duty construction truck". PhD thesis. KTH Royal Institute of Technology, 2018 (cit. on pp. 22, 29, 96).

[38] *Canadian Motor Vehicle Traffic Collision Statistics: 2017*. [Accessed: 2019-05-31]. URL: https://www.canada.ca/ (cit. on p. 23).

[39] Azim Eskandarian. *Handbook of intelligent vehicles*. Vol. 2. Springer, 2012 (cit. on p. 23).

[40] *Waymo's self-driving car crash in Arizona reviews tough questions*. [Accessed: 2019-05-31]. URL: https://www.wired.com/ (cit. on p. 23).

[41] *National crash rate for conventional vehicles higher than crash rate of self-driving cars, report shows*. [Accessed: 2019-05-31]. URL: https://vt.edu/ (cit. on p. 23).

[42] Todd Litman. "Transportation cost and benefit analysis". In: *Victoria Transport Policy Institute* 31 (2009) (cit. on p. 24).

[43] Peter Belenky. "The value of travel time savings: departmental guidance for conducting economic evaluations, revision 2". In: *Department of Transportation* (2011) (cit. on p. 24).

[44] Felix Steck, Viktoriya Kolarova, Francisco Bahamonde-Birke, Stefan Trommer, and Barbara Lenz. "How autonomous driving may affect the value of travel time savings for commuting". In: *Transportation research record* (2018), p. 0361198118757980 (cit. on p. 24).

[45] *Blind man sets out alone in Google's driverless car*. [Accessed: 2019-06-02]. URL: https://www.washingtonpost.com/ (cit. on p. 24).

[46] Sandi Rosenbloom. "Driving cessation among older people: when does it happen and what impact does it have?" In: *Transportation Research Record* 1779.1 (2001), pp. 93–99 (cit. on p. 24).

[47] *Tesla Autonomy Day.* [Accessed: 2019-06-02]. URL: `https://www.youtube.com/` (cit. on p. 25).

[48] Pedro Fernandes and Urbano Nunes. "Platooning with IVC-enabled autonomous vehicles: Strategies to mitigate communication delays, improve safety and traffic flow". In: *IEEE Transactions on Intelligent Transportation Systems* 13.1 (2012), pp. 91–106 (cit. on p. 25).

[49] Paul Sorensen, Martin Wachs, Endy Y Min, Aaron Kofner, and Liisa Ecola. *Moving Los Angeles: Short-term policy options for improving transportation.* Rand Corporation, 2008 (cit. on p. 25).

[50] *Highlights of the Automotive Trends Report.* [Accessed: 2019-06-02]. URL: `https://www.epa.gov/` (cit. on p. 26).

[51] Tyler C Folsom. "Energy and autonomous urban land vehicles". In: *IEEE Technology and Society Magazine* 31.2 (2012), pp. 28–38 (cit. on p. 25).

[52] *Nevada State Law. AB 511 Section 8. 2011* (cit. on p. 27).

[53] SAE On-Road Automated Vehicle Standards Committee et al. "Taxonomy and definitions for terms related to on-road motor vehicle automated driving systems". In: *SAE International* (2014) (cit. on p. 27).

[54] Niclas Evestedt. "Sampling Based Motion Planning for Heavy Duty Autonomous Vehicles". PhD thesis. Linköping University Electronic Press, 2016 (cit. on p. 29).

[55] Michael Treml, José Arjona-Medina, Thomas Unterthiner, Rupesh Durgesh, Felix Friedmann, Peter Schuberth, Andreas Mayr, Martin Heusel, Markus Hofmarcher, Michael Widrich, et al. "Speeding up semantic segmentation for autonomous driving". In: *MLITS, NIPS Workshop.* 2016 (cit. on p. 30).

[56] David González, Joshué Pérez, Vicente Milanés, and Fawzi Nashashibi. "A review of motion planning techniques for automated vehicles". In: *IEEE Transactions on Intelligent Transportation Systems* 17.4 (2015), pp. 1135–1145 (cit. on p. 30).

[57] A. Biswas and A. Emadi. "Energy Management Systems for Electrified Powertrains: State-of-the-Art Review and Future Trends". In: *IEEE Transactions on Vehicular Technology* 68.7 (2019-07), pp. 6453–6467. ISSN: 0018-9545. DOI: 10.1109/TVT.2019.2914457 (cit. on p. 32).

[58] Pier Giuseppe Anselma, Giovanni Belingardi, Alessandro Falai, Claudio Maino, Federico Miretti, Daniela Misul, and Ezio Spessa. "Comparing Parallel Hybrid Electric Vehicle Powertrains for Real-world Driving". In: *2019 AEIT International Conference of Electrical and Electronic Technologies for Automotive (AEIT AUTOMOTIVE)*. IEEE. 2019, pp. 1–6 (cit. on p. 32).

[59] Lucas Bruck, Ali Emadi, and Kavya P Divakarla. "A review of the relevance of driving condition mapping and vehicle simulation for energy management system design". In: *International Journal of Powertrains* 8.3 (2019), pp. 224–251 (cit. on p. 32).

[60] Brahmadevan V Padmarajan, Andrew McGordon, and Paul A Jennings. "Blended rule-based energy management for PHEV: System structure and strategy". In: *IEEE Transactions on Vehicular Technology* 65.10 (2015), pp. 8757–8762 (cit. on p. 33).

[61] Stephanie Stockar, Vincenzo Marano, Marcello Canova, Giorgio Rizzoni, and Lino Guzzella. "Energy-optimal control of plug-in hybrid electric vehicles for real-world driving cycles". In: *IEEE Transactions on Vehicular Technology* 60.7 (2011), pp. 2949–2962 (cit. on p. 33).

[62] Souleman Njoya Motapon, Louis-A Dessaint, and Kamal Al-Haddad. "A comparative study of energy management schemes for a fuel-cell hybrid emergency power system of more-electric aircraft". In: *IEEE transactions on industrial electronics* 61.3 (2013), pp. 1320–1334 (cit. on p. 34).

[63] Gino Paganelli, Sebastien Delprat, Thierry-Marie Guerra, Janette Rimaux, and Jean-Jacques Santin. "Equivalent consumption minimization strategy for parallel hybrid powertrains". In: *Vehicular Technology Conference. IEEE 55th Vehicular Technology Conference. VTC Spring 2002 (Cat. No. 02CH37367)*. Vol. 4. IEEE. 2002, pp. 2076–2081 (cit. on p. 34).

[64] Cristian Musardo, Giorgio Rizzoni, Yann Guezennec, and Benedetto Staccia. "A-ECMS: An adaptive algorithm for hybrid electric vehicle energy management". In: *European Journal of Control* 11.4-5 (2005), pp. 509–524 (cit. on p. 34).

[65] Pier Giuseppe Anselma, Yi Huo, Joel Roeleveld, Giovanni Belingardi, and Ali Emadi. "Slope-weighted energy-based rapid control analysis for hybrid electric vehicles". In: *IEEE Transactions on Vehicular Technology* 68.5 (2019), pp. 4458–4466 (cit. on p. 34).

[66] R. Bellman. *Dynamic Programming*. 1st ed. Princeton, NJ, USA: Princeton University Press, 1957 (cit. on p. 35).

[67] Jiankun Peng, Hongwen He, and Rui Xiong. "Rule based energy management strategy for a series–parallel plug-in hybrid electric bus optimized by dynamic programming". In: *Applied Energy* 185 (2017), pp. 1633–1643 (cit. on p. 35).

[68] Avra Brahma, Yann Guezennec, and Giorgio Rizzoni. "Optimal energy management in series hybrid electric vehicles". In: *Proceedings of the 2000 American Control Conference. ACC (IEEE Cat. No. 00CH36334)*. Vol. 1. 6. IEEE. 2000, pp. 60–64 (cit. on p. 35).

[69] Jeremy Lempert, Brynn Vadala, Kamran Arshad-Aliy, Joel Roeleveld, and Ali Emadi. "Practical considerations for the implementation of dynamic programming for HEV powertrains". In: *2018 IEEE Transportation Electrification Conference and Expo (ITEC)*. IEEE. 2018, pp. 755–760 (cit. on p. 35).

[70] L.S. Pontryagin. *Mathematical Theory of Optimal Processes*. Classics of Soviet Mathematics. Taylor & Francis, 1987. ISBN: 9782881240775 (cit. on p. 35).

[71] Lorenzo Serrao, Simona Onori, and Giorgio Rizzoni. "ECMS as a realization of Pontryagin's minimum principle for HEV control". In: *2009 American control conference*. IEEE. 2009, pp. 3964–3969 (cit. on p. 36).

[72] S. Boyd and L. Vandenberghe. *Convex optimization*. Cambridge university press, 2004 (cit. on pp. 36, 70, 77).

[73] Diederik Verscheure, Bram Demeulenaere, Jan Swevers, Joris De Schutter, and Moritz Diehl. "Time-optimal path tracking for robots: A convex optimization approach". In: *IEEE Transactions on Automatic Control* 54.10 (2009), pp. 2318–2327 (cit. on p. 37).

[74] Yuping Zeng, Jing Sheng, and Ming Li. "Adaptive Real-Time Energy Management Strategy for Plug-In Hybrid Electric Vehicle Based on Simplified-ECMS and a Novel Driving Pattern Recognition Method". In: *Mathematical Problems in Engineering* 2018 (2018-10), pp. 1–12. DOI: 10.1155/2018/5816861 (cit. on p. 37).

[75] Nikolce Murgovski, Lars Mårdh Johannesson, and Jonas Sjöberg. "Engine on/off control for dimensioning hybrid electric powertrains via convex optimization". In: *IEEE Transactions on Vehicular Technology* 62.7 (2013), pp. 2949–2962 (cit. on p. 37).

[76] Soren Ebbesen, Mauro Salazar, Philipp Elbert, Carlo Bussi, and Christopher H Onder. "Time-optimal control strategies for a hybrid electric race car". In: *IEEE Transactions on Control Systems Technology* 26.1 (2017), pp. 233–247 (cit. on p. 37).

[77] Reza Takapoui, Nicholas Moehle, Stephen Boyd, and Alberto Bemporad. "A simple effective heuristic for embedded mixed-integer quadratic programming". In: *International Journal of Control* (2017), pp. 1–11 (cit. on p. 37).

[78] Jaehyun Park and Stephen Boyd. "A semidefinite programming method for integer convex quadratic minimization". In: *Optimization Letters* 12.3 (2018), pp. 499–518 (cit. on p. 37).

[79] Basil Kouvaritakis and Mark Cannon. "Model predictive control". In: *Switzerland: Springer International Publishing* (2016) (cit. on p. 38).

[80] Lorenzo Serrao, Simona Onori, and Giorgio Rizzoni. "A comparative analysis of energy management strategies for hybrid electric vehicles". In: *Journal of Dynamic Systems, Measurement, and Control* 133.3 (2011), p. 031012 (cit. on p. 39).

[81] Emilia Silvas, Theo Hofman, Nikolce Murgovski, LF Pascal Etman, and Maarten Steinbuch. "Review of optimization strategies for system-level design in hybrid electric vehicles". In: *IEEE Transactions on Vehicular Technology* 66.1 (2016), pp. 57–70 (cit. on p. 39).

[82] Argonne National Laboratory. *Downloadable Dynamometer Database*. [Accessed: 2018-03-17]. URL: https://www.anl.gov/es/downloadable-dynamometer-database (cit. on pp. 41, 53, 54, 59, 71).

[83] *Power Rankings: We rank the teams ahead of Australia.* [Accessed: 2019-07-22]. URL: https://www.formula1.com/ (cit. on p. 52).

[84] Timothy A Burress, Steven L Campbell, Chester Coomer, Curtis William Ayers, Andrew A Wereszczak, Joseph Philip Cunningham, Laura D Marlino, Larry Eugene Seiber, and Hua-Tay Lin. *Evaluation of the 2010 Toyota Prius hybrid synergy drive system.* Tech. rep. Oak Ridge National Lab.(ORNL), Oak Ridge, TN (United States). Power ..., 2011 (cit. on p. 54).

[85] Namwook Kim, Jongryeol Jeong, Aymeric Rousseau, and Henning Lohse-Busch. "Control Analysis and Thermal Model Development for Plug-In Hybrid Electric Vehicles". In: *SAE International Journal of Alternative Powertrains* 4 (2015-05). DOI: 10.4271/2015-01-1157 (cit. on p. 54).

[86] Namwook Kim, Aymeric Rousseau, and Eric Rask. "Vehicle-level control analysis of 2010 Toyota Prius based on test data". In: *Proceedings of the Institution of Mechanical Engineers, Part D: Journal of Automobile Engineering* 226.11 (2012), pp. 1483–1494. DOI: 10.1177/0954407012445955. eprint: https://doi.org/10.1177/0954407012445955. URL: https://doi.org/10.1177/0954407012445955 (cit. on p. 54).

[87] Yi Lu Murphey, Jungme Park, Zhihang Chen, Ming L Kuang, M Abul Masrur, and Anthony M Phillips. "Intelligent hybrid vehicle power control—Part I: Machine learning of optimal vehicle power". In: *IEEE Transactions on Vehicular Technology* 61.8 (2012), pp. 3519–3530 (cit. on p. 64).

[88] Chan-Chiao Lin, Jun-Mo Kang, JW Grizzle, and Huei Peng. "Energy management strategy for a parallel hybrid electric truck". In: *Proceedings of the 2001 American Control Conference.(Cat. No. 01CH37148).* Vol. 4. IEEE. 2001, pp. 2878–2883 (cit. on p. 65).

[89] Guangming Tan, Ninghui Sun, and Guang R Gao. "Improving performance of dynamic programming via parallelism and locality on multicore architectures". In: *IEEE Transactions on Parallel and Distributed Systems* 20.2 (2008), pp. 261–274 (cit. on p. 65).

[90] Shucai Xiao, Ashwin M Aji, and Wu-chun Feng. "On the robust mapping of dynamic programming onto a graphics processing unit". In: *2009 15th*

International Conference on Parallel and Distributed Systems. IEEE. 2009, pp. 26–33 (cit. on p. 65).

[91] Olle Sundström, Daniel Ambühl, and Lino Guzzella. "On implementation of dynamic programming for optimal control problems with final state constraints". In: *Oil & Gas Science and Technology–Revue de l'Institut Français du Pétrole* 65.1 (2010), pp. 91–102 (cit. on pp. 65, 83).

[92] SJ Pachernegg. *A closer look at the Willans-line*. Tech. rep. SAE Technical Paper, 1969 (cit. on p. 68).

[93] M. Grant and S. Boyd. "CVX: Matlab Software for Disciplined Convex Programming, version 2.1". In: (2014-03) (cit. on pp. 71, 81, 103, 111).

[94] MOSEK ApS. *The MOSEK optimization toolbox for MATLAB manual. Version 8.1.* 2017. URL: `http://docs.mosek.com/8.1/toolbox/index.html` (cit. on pp. 71, 81, 111).

[95] Tobias Nüesch, Philipp Elbert, Michael Flankl, Christopher Onder, and Lino Guzzella. "Convex optimization for the energy management of hybrid electric vehicles considering engine start and gearshift costs". In: *Energies* 7.2 (2014), pp. 834–856 (cit. on p. 73).

[96] Nikolce Murgovski, Lars Johannesson, Xiaosong Hu, Bo Egardt, and Jonas Sjöberg. "Convex relaxations in the optimal control of electrified vehicles". In: *2015 American Control Conference (ACC)*. IEEE. 2015, pp. 2292–2298 (cit. on p. 73).

[97] Nikolce Murgovski, Lars Johannesson, and Jonas Sjöberg. "Convex modeling of energy buffers in power control applications". In: *IFAC Proceedings Volumes* 45.30 (2012), pp. 92–99 (cit. on p. 75).

[98] Philipp Elbert, Tobias Nüesch, Andreas Ritter, Nikolce Murgovski, and Lino Guzzella. "Engine on/off control for the energy management of a serial hybrid electric bus via convex optimization". In: *IEEE Transactions on Vehicular Technology* 63.8 (2014), pp. 3549–3559 (cit. on p. 75).

[99] Kim-Chuan Toh, Michael J Todd, and Reha H Tütüncü. "SDPT3—a MATLAB software package for semidefinite programming, version 1.3". In: *Optimization methods and software* 11.1-4 (1999), pp. 545–581 (cit. on pp. 81, 103, 111).

[100] LLC Gurobi Optimization. *Gurobi Optimizer Reference Manual*. 2019. URL: http://www.gurobi.com (cit. on p. 81).

[101] Olle Sundstrom and Lino Guzzella. "A generic dynamic programming Matlab function". In: *2009 IEEE Control Applications,(CCA) & Intelligent Control,(ISIC)*. IEEE. 2009, pp. 1625–1630 (cit. on p. 83).

[102] *Fiat Chrysler partners with Aurora to develop self-driving commercial vans*. [Accessed: 2019-06-18]. URL: https://techcrunch.com/ (cit. on p. 93).

[103] Matthias Gerdts and Björn Martens. "Optimization-based motion planning in virtual driving scenarios with application to communicating autonomous vehicles". In: *arXiv preprint arXiv:1801.07612* (2018) (cit. on p. 96).

[104] Pedro Lima. "Predictive control for autonomous driving: With experimental evaluation on a heavy-duty construction truck". PhD thesis. KTH Royal Institute of Technology, 2016 (cit. on p. 96).

[105] Arthur Newell Talbot. *The railway transition spiral*. Engineering News Publishing Company, 1904 (cit. on p. 101).

[106] Jin Xu, Kui Yang, YiMing Shao, and GongYuan Lu. "An experimental study on lateral acceleration of cars in different environments in Sichuan, Southwest China". In: *Discrete Dynamics in nature and Society* 2015 (2015) (cit. on p. 126).